Naval Research Laboratory
Monterey, CA 93943-5502

AD-A274 596

NRL/PU/7530--93-0008

Leadex Environmental Phenomena and Effects Observed by DMSP, NOAA, and ERS-1 Satellites

ROBERT W. FETT

Consultant Meteorologist
Science Applications International Corp.
Monterey, CA

DTIC
ELECTE
JAN 0 5 1994
S D
E

Prepared for:

Forecast Support Branch
Marine Meteorology Division

Contract No. N00014-92-C-6018

November 1993

93-31432

Approved for public release; distribution unlimited.

93 12 28 010

REPORT DOCUMENTATION PAGE

Form Approved
OMB No. 0704-0188

Public reporting burden for this collection of information is estimated to average 1 hour per response, including the time for reviewing instructions, searching existing data sources, gathering and maintaining the data needed, and completing and reviewing the collection of information. Send comments regarding this burden or any other aspect of this collection of information, including suggestions for reducing this burden, to Washington Headquarters Services, Directorate for information Operations and Reports, 1215 Jefferson Davis Highway, Suite 1204, Arlington, VA 22202-4302, and to the Office of Management and Budget, Paperwork Reduction Project (0704-0188), Washington, DC 20503.

1. Agency Use Only *(Leave blank).*	2. Report Date.	3. Report Type and Dates Covered.
	November 1993	Final 25 Mar-24 Apr 92

4. Title and Subtitle.
Leadex Environmental Phenomena and Effects Observed by DMSP, NOAA, and ERS-1 Satellites

5. Funding Numbers.
PE 0601153N
PN 30103-3B0
AN DN153074
CN N00014-92-C-6018

6. Author(s).
Robert W. Fett

7. Performing Organization Name(s) and Address(es).
Science Applications International Corporation (SAIC) Monterey, CA 93940; and Naval Research Laboratory, Marine Meteorology Division, Monterey, CA 93943-5502

8. Performing Organization Report Number.
NRL/PU/7530--93-0008

9. Sponsoring/Monitoring Agency Name(s) and Address(es).
Naval Research Laboratory
Washington, DC 20375-5320

10. Sponsoring/Monitoring Agency Report Number.

11. Supplementary Notes.

12a. Distribution/Availability Statement.
Approved for public release; distribution unlimited.

12b. Distribution Code.

13. Abstract *(Maximum 200 words).*

This report examines notable atmospheric and cryospheric conditions observed by satellites over the Beaufort Sea region surrounding the Leadex ice camp position. DMSP and NOAA direct readout high resolution data include visible and infrared scenes in a variety of discrete channels. The special sensor microwave imager (SSM/I) data of DMSP and the synthetic aperture radar (SAR) data of the European ERS-1 satellite are of special interest and value in evaluating changes in ice appearance and configuration noted during the period of Leadex from 25 March to 24 April 1992. Multi-channel comparisons of the various data types over the same location and correlation with available ground truth data yield significant insights into the nature and state of the phenomena observed.

14. Subject Terms.
Leadex, DMSP data, Cryospheric conditions
Arctic leads, SSM/I data, SAR data

15. Number of Pages.
104

16. Price Code.

17. Security Classification of Report.	18. Security Classification of This Page.	19. Security Classification of Abstract.	20. Limitation of Abstract.
UNCLASSIFIED	UNCLASSIFIED	UNCLASSIFIED	Same as report

CONTENTS

DTIC QUALITY INSPECTED 5

Accesion For	
NTIS CRA&I	☒
DTIC TAB	☐
Unannounced	☐
Justification	
By	
Distribution /	
Availability Codes	
Dist	Avail and / or Special
A-1	

ACKNOWLEDGEMENTS

The support of the sponsor, Office of Naval Research Program, Element 61153N, is gratefully acknowledged. DMSP and NOAA satellite data utilized in this report were processed at Anchorage, Alaska, by LT Warren W. Rodie, USN, and Thomas F. Lee, Naval Research Laboratory, Monterey, CA, specifically for Leadex support. Additional assistance was provided by Maureen Thompson, Computer Sciences Corporation, Monterey. The weather analyses and forecast products are presented as developed by the model originators, Dr. Stephen Burk and William Thompson, NRL, Monterey. Significant discussions concerning the nature and causes of some of the phenomena presented in this report were held with Dr. Burk, Mr. Thompson, and Ronald E. Englebretson of Science Applications International Corp., Monterey. Use of buoy (ice station) data gathered during Leadex was made possible through the efforts of Dr. James Overland, Pacific Marine Environmental Laboratory/NOAA, and Dr. Kenneth Davidson, Naval Postgraduate School, Monterey. Synthetic Aperture Radar (SAR) data used in this report are through the courtesy of the European Space Agency (ESA); further publication of these data without the permission of ESA is prohibited.

LEADEX ENVIRONMENTAL PHENOMENA AND EFFECTS OBSERVED BY DMSP, NOAA, AND ERS-1 SATELLITES

1. INTRODUCTION

Leadex is the first Arctic experiment in which the highest quality direct readout satellite data from both the NOAA and DMSP satellite systems were continuously archived for later research while also being utilized through immediate processing for operational use. The DMSP data retrieval, made possible courtesy of the United States Air Force, Air Weather Service, also include the Special Sensor Microwave Imager (SSM/I) data. This data set is further embellished by the availability of Synthetic Aperture Radar (SAR) data over the Leadex area of operations. These data, acquired from the European Space Agency's satellite ERS-1, are especially important in yielding information relating to ice type, age, and movement. The combined data forms provide an unparalleled opportunity for multi-channel comparisons useful in resolving ambiguities inherent in one data type alone.

Leadex, being a month-long experiment in the spring of the year, provided a many-faceted weather scenario, ranging from clear, calm conditions, to those of a full-blown blizzard. Ice, which had few open leads in the early phase of the program, was literally "torn apart" at a later stage, creating hundreds of leads in only a few hours. From an atmospheric perspective, weather systems moved across the Beaufort Sea from all directions including a tropical-like movement from the east. The strong low level inversion over the ice often seemed to de-couple low level systems from those aloft and to preserve low level cloud forms moving independently from those aloft. The Navy Operational Regional Atmospheric Prediction System (NORAPS) model was run as a mesoscale model having 20 km grid spacing and using second-order closure physics. This version of NORAPS -- called SOCMM in this report, for Second Order Closure Mesoscale Model -- was found to produce quite accurate forecasts of the positioning of highs, lows, troughs etc., a fact that helped ease the forecast burden, except for the important parameters of low level ceilings and visibilities.

This preliminary report is intended to focus on some of the salient events noted during Leadex, and to report on early implications of the uniquely-acquired satellite data set; a full investigation of many additional aspects, particularly related to ice camp operations and the unique buoy (ice station) data set, will be the subject of research by many investigators in coming months.

THIS PAGE DELIBERATELY LEFT BLANK

2. DMSP/NOAA/ERS-1 DATA INTERCOMPARISONS

One of the first notable discoveries in the intercomparison of SAR data with DMSP and NOAA visible and infrared data was that the larger ice floes and leads apparent in the SAR data could also be seen in the larger scale weather satellite images. Fig 1 (below) is a portion of an ERS-1 image just north of the ice camp position on 29 March 1992 at 0649 UTC. Two features, one resembling a "tadpole" and the other a "steer's head" are evident in this image. The "tadpole" shape is formed by a large floe of multiyear ice surrounded by darker areas of first-year ice and a long "tail" of first-year ice stretching to the south. The shape of a "steer's head" is formed by a large area of first-year ice surrounded by multiyear floes.

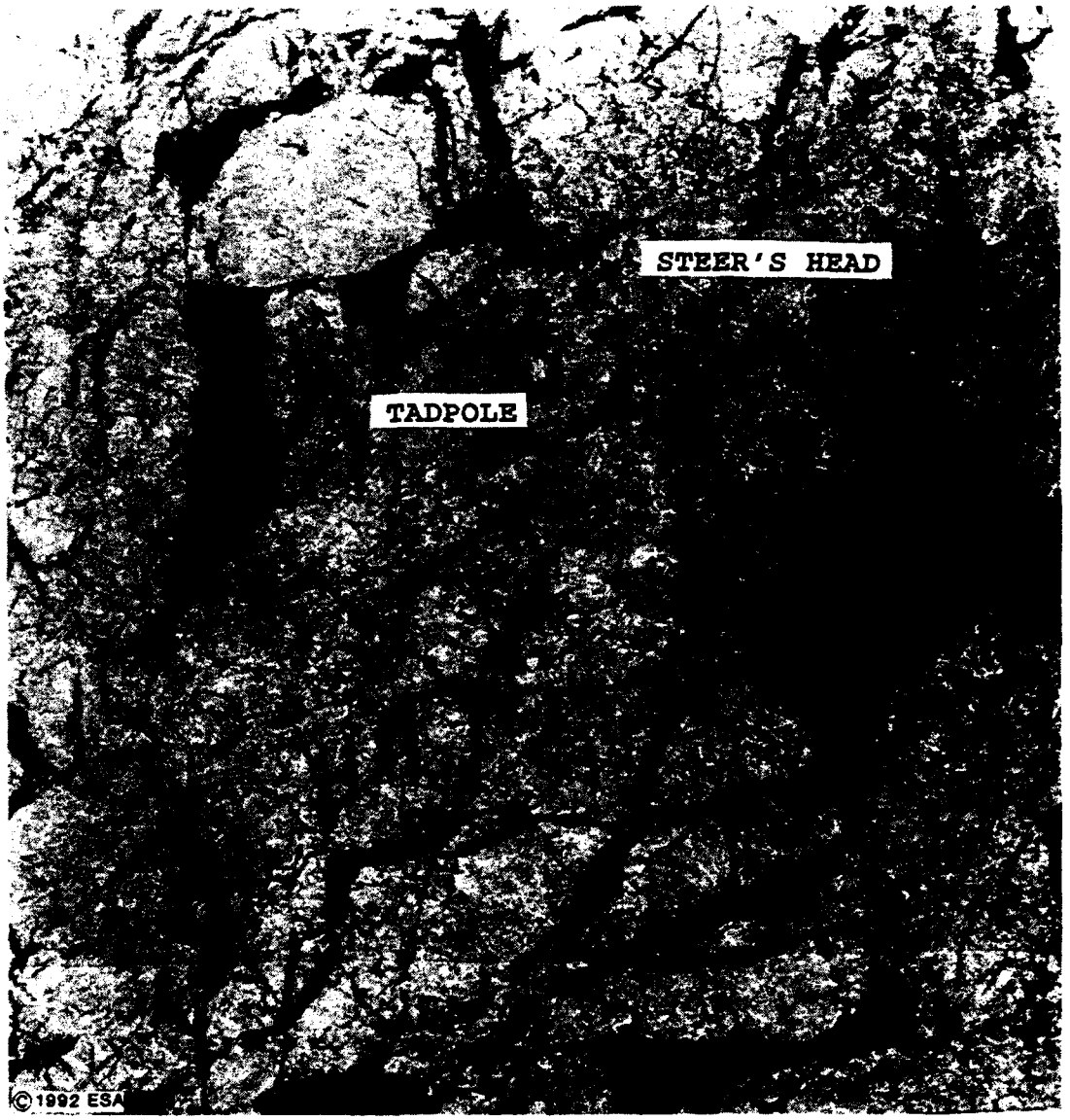

FIG 1. ERS-1 Synthetic Aperture Radar (SAR) low resolution (240m) data. 29 March 1992, 0649 UTC.©1992 ESA; used by permission.

These same features (and many of the other intervening features of leads and floes) can easily be detected in weather satellite visible and infrared images. Fig 2 (below) is a DMSP infrared example acquired a day earlier (28 March at 0459 UTC). The multiyear floes radiate at a much colder temperature than the thinner adjacent first-year ice forms and therefore preserve the same light (cold) and dark (warm) gray shade relationship exhibited in the SAR data. The "tadpole" form and the "steer's head" are readily apparent in this image, implying a clear sky condition over the area.

Temperature profiles were obtained in transects through the "tail" of the tadpole along line AB; through the "head" of the tadpole along line CD; and through the "steer's head" along line EF. The profile through the "tail" of the tadpole is shown in Fig 3a. This profile shows that the first year ice forming the "tail" is 4.5 to 6 deg C warmer than the adjacent multiyear ice. The profile along line CD through the "head" of the tadpole (Fig 3b) across the multiyear floes, conversely, is 4.5 to 5.5 deg C colder than adjacent first year ice. Profile EF through the "steer's head" (Fig 3c) again shows that the first year ice is on the order of 4.4 to 5.5 deg C warmer than the adjacent cold multiyear floes.

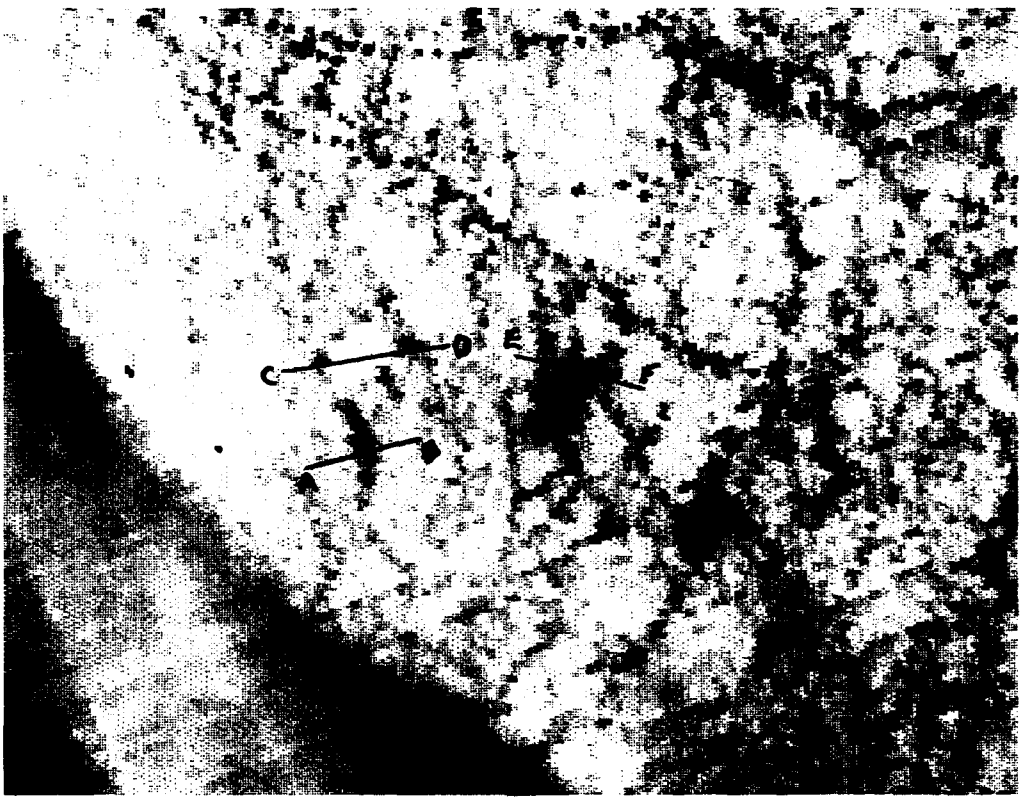

FIG 2. DMSP infrared data. 28 March 1992, 0459 UTC.

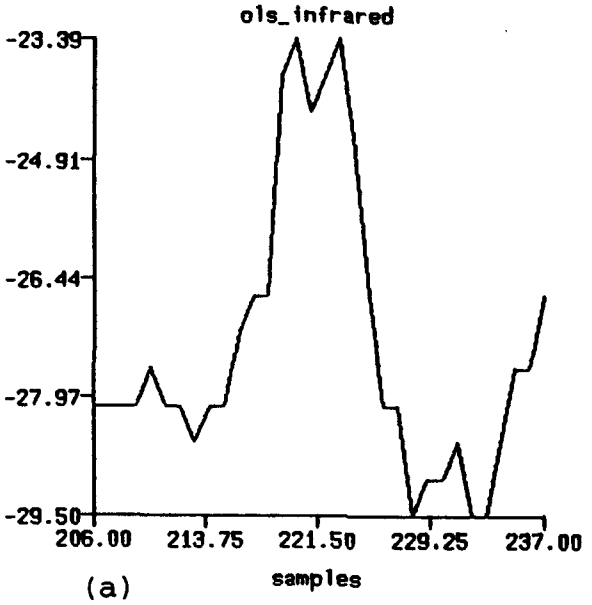

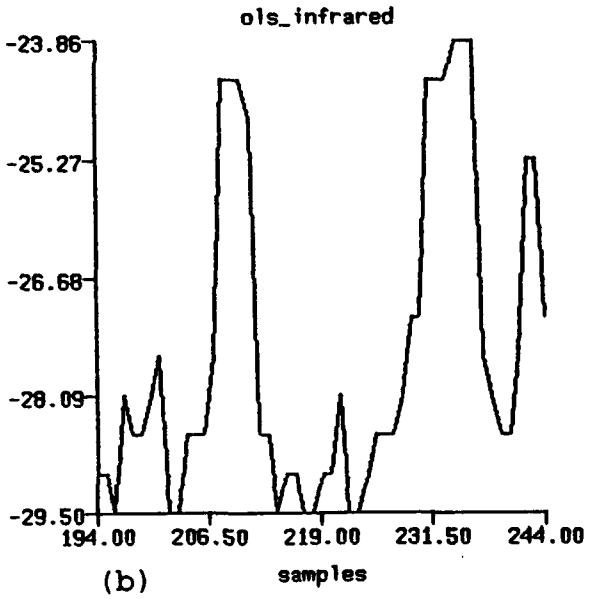

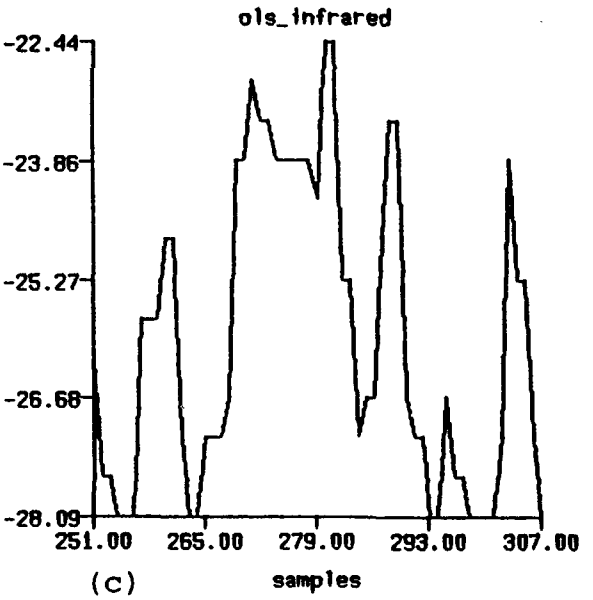

FIG 3. (a) Temperature profile through "tail " of tadpole along line AB.
(b) Temperature profile through "head" of tadpole along line CD.
(c) Temperature profile through "steer's head" along line EF.

Fig 4 (below) shows DMSP visible data on 29 March 1992 at 1941 UTC. These data also reveal the "tadpole" and "steer's head" ice formations. The albedo of a lead not covered by snow is always darker than the adjacent drift ice, being composed of various combinations of dark open water, and light, or dark, gray ice. Figs 5 and 6 are examples of typical aerial views of lead appearance during spring 1991 in the Beaufort Sea.

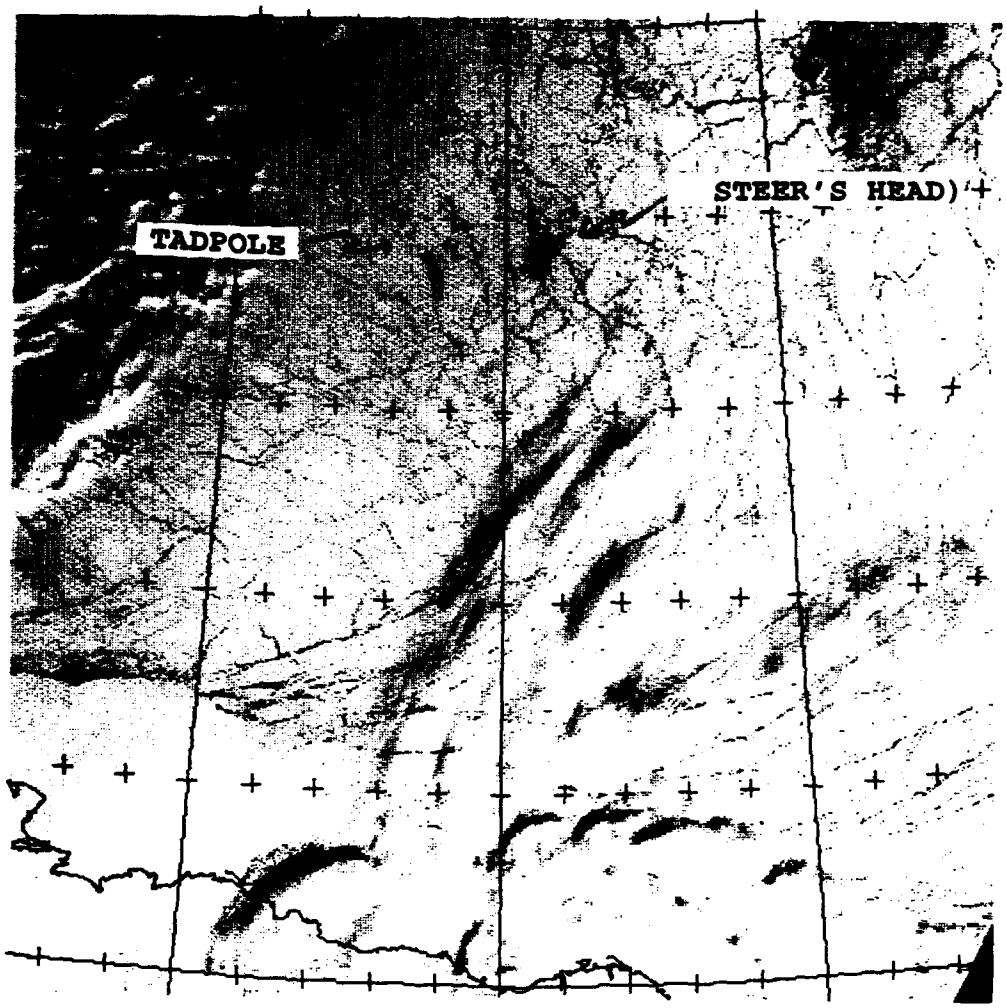

FIG 4. DMSP visible data. 29 March 1992, 1941 UTC.

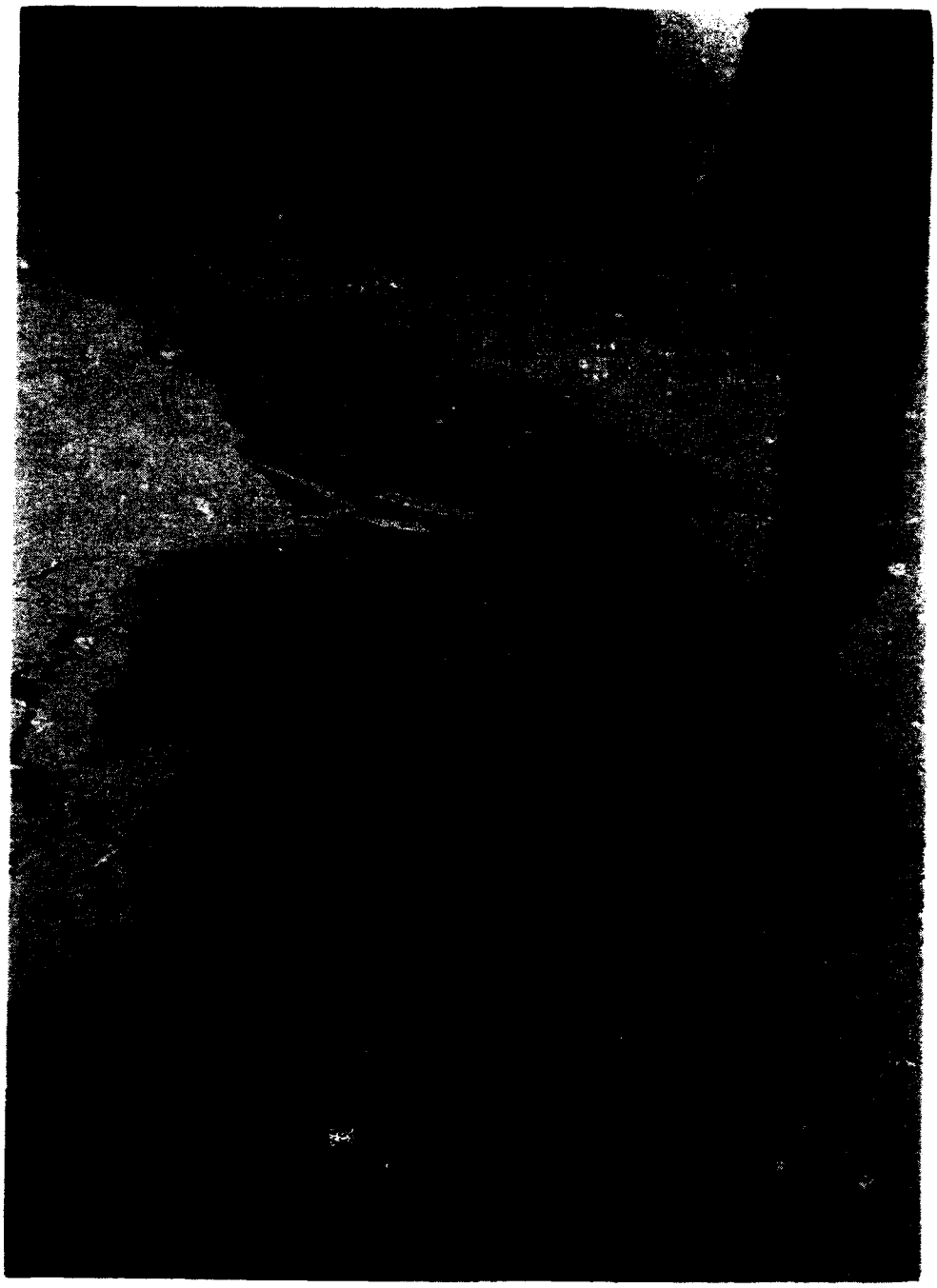

FIG 5. Aerial view of lead in the central Beaufort Sea during March 1991. View is toward the east.

FIG 6. Aerial view of lead in the central Beaufort Sea during March 1991. View is toward the northeast.

In addition to the normally darker albedo, frozen leads have a smoother surface than the rougher multiyear floes which they surround. At low sun angles these smoother surfaces reflect most of the incident solar rays away from the spacecraft sensor. By contrast the rough multiyear floes have many reflective facets to divert incident solar radiation to the satellite. This adds to the brighter appearance of the multiyear floes. Fig 7 (below) shows some of the rougher ice features near the base camp on a multiyear floe during the pilot Leadex operation in spring 1991.

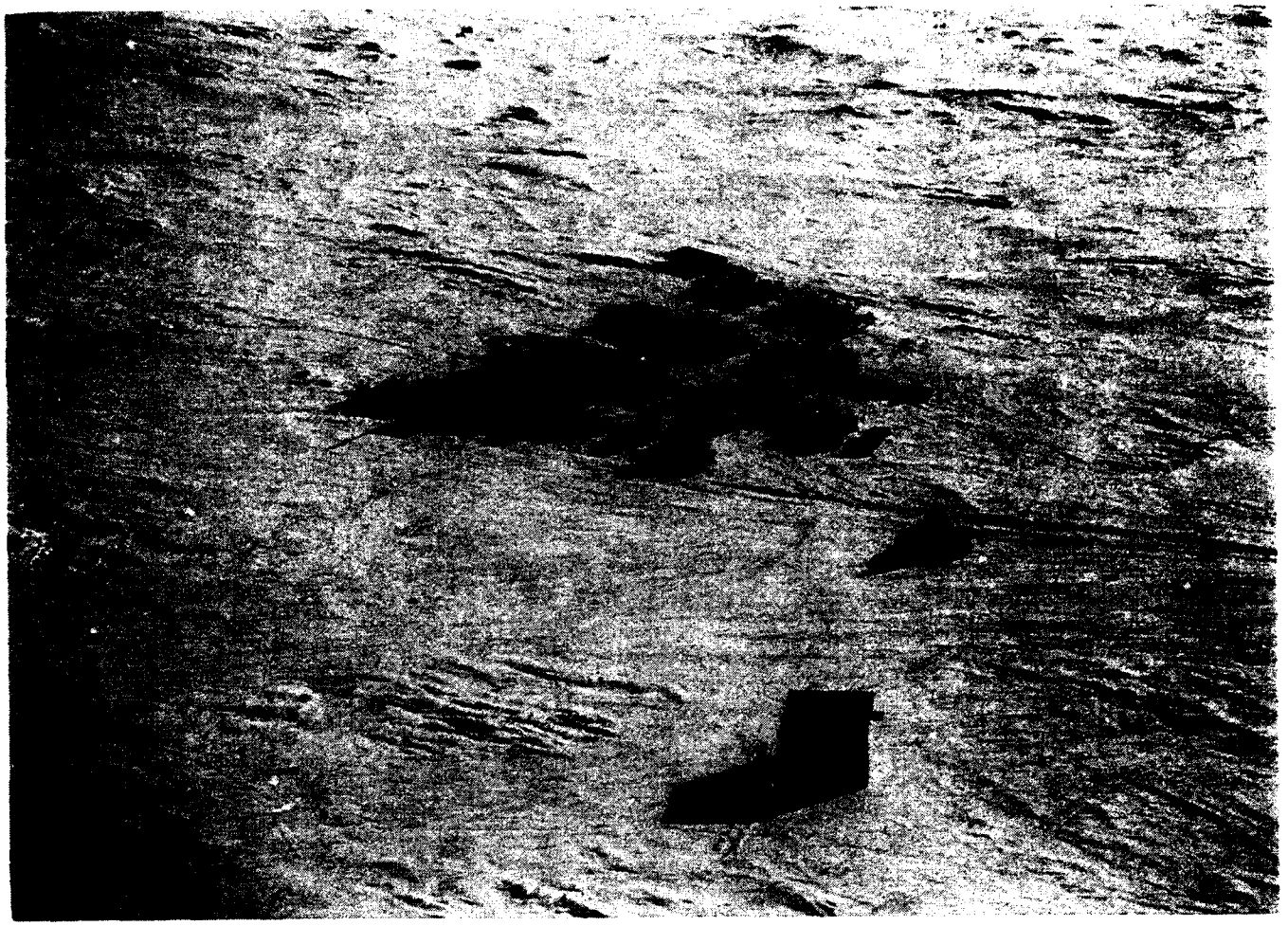

FIG 7. Aerial view of Leadex ice camp during March 1991.

The companion DMSP infrared view to the visible data shown in Fig 4 is shown in Fig 8. This image also shows the "tadpole" and "steer's head" as well as other leads and first year ice features. It is desirable to relate such features observed in DMSP visible and IR data to the microwave imager (SSM/I) data of DMSP, which were acquired simultaneously over the same area. The 85.5 GHz channel has a swath width of 1394 km and an effective field of view (resolution) of 15x13 km. This, of course, is much cruder than the 2.7 km resolution DMSP visible and IR data shown earlier (higher resolution DMSP data were not available for this study). Nevertheless, one should expect that larger, more homogeneous, features appearing in the DMSP visible and IR data should also show some unique response in the corresponding SSM/I data.

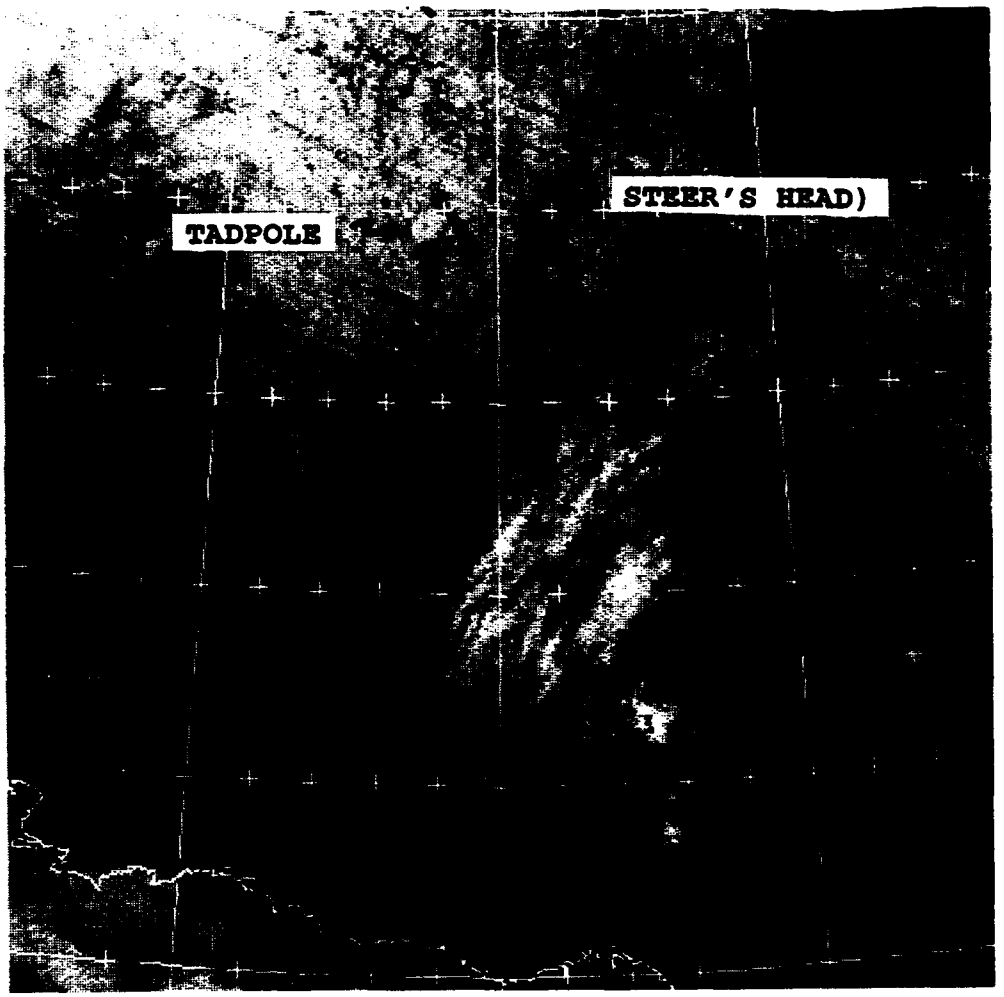

FIG 8. DMSP infrared data. 29 March 1992, 1941 UTC.

Fig 9 is a large scale SSM/I 85 GHz, horizontally polarized, view of the Beaufort Sea region, obtained simultaneously with the visible and IR data of Figs 4 and 8. In this image pixels have been averaged to provide a large scale view. Thinner first year ice south and southeast of Banks Island appears bright (white), in contrast to the darker tonality of the multiyear ice, which is the dominant ice form over the rest of the Beaufort Sea. Embedded in the multiyear ice region are small white areas that indicate the presence of first year ice forms at those locations. One might expect that a large first year ice region such as the "steer's head" could be related to one of the small white areas appearing in the SSM/I data of Fig 9. In fact, a careful comparison of this image with figures 4 and 8 reveals the position of the steer's head as shown in Fig 9.

FIG 9. DMSP large-scale SSM/I data. 29 March 1992, 1941 UTC.

Full resolution SSM/I 85 GHz, horizontally polarized, data for the same area and time as the visible and IR data of Figs 4 and 8 are shown in Fig 10 (below). Individual pixels revealed in this rendition produce a "smeared" effect. Nevertheless, bright responses corresponding to the first year ice of the "tadpole tail", the "steer's head", and an unnamed adjacent region of first year ice are clearly evident, and can be related on a one-to-one basis with these same features in Figs 4 and 8. Note also the bright response corresponding to the lead feature north of Barrow near 71.5N and the similarly bright response of first year ice adjacent to the shoreline and extending out to near 71.5N along the North Slope. This correlation implies that such features, once identified, can be tracked on a day-to-day basis using SSM/I data even when the region is largely cloud covered. The latter conclusion relates to the fact that the microwave 85 GHz date are transmitted to the passive microwave sensor with relatively little attenuation by non-precipitating cloud forms in the region, i.e., clouds are relatively "transparent" to this sensor.

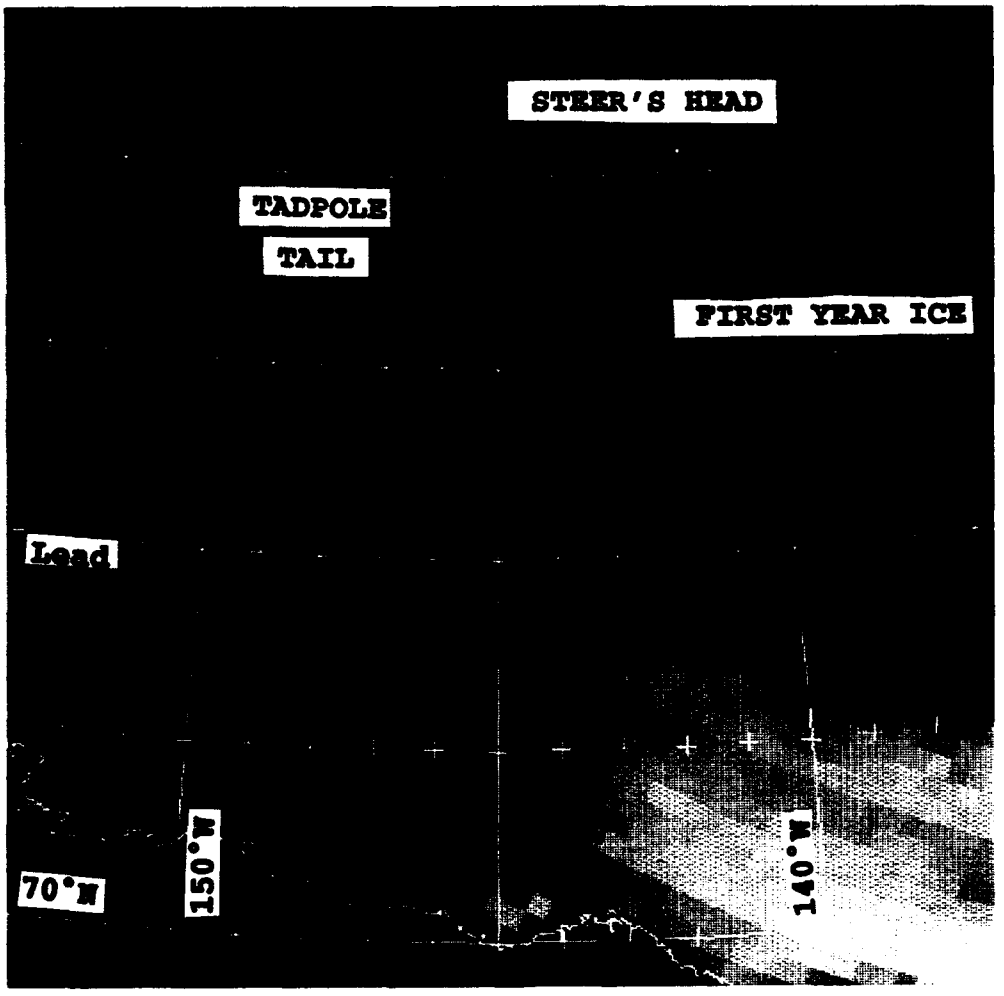

FIG 10. DMSP full-resolution SSM/I data. 29 March 1992, 1941 UTC.

Some important implications of the above observations may be summarized:

1. The temperature of frozen first year ice as sensed by satellite (DMSP or NOAA for example) is warmer than the temperature of adjacent multiyear floes.

2. The warmer the temperature of a lead the more likely it is to contain some open water. During Leadex a lead temperature of -5°C seemed to indicate a lead with high potential for open water.

3. Lead surfaces are generally smoother than the drift ice through which they run.

4. Large scale high resolution satellite data can be useful in tracking ice features also visible in SAR data.

5. Microwave imager data such as that derived from the SSM/I sensor of the DMSP system are useful in detecting leads and first year ice features embedded in a region of multiyear floes.

6. Item #5 makes possible a day-to-day monitoring of the position of known first year ice features and, potentially, the opening of new lead formations even in the presence of significant cloud cover.

THIS PAGE DELIBERATELY LEFT BLANK

3. THE SEVERE STORM OF 5-7 APRIL 1992 AND INFLUENCE ON LEAD FORMATION

During 5-7 April 1992 a small but very intense low pressure system moved eastward between the North Slope and the ice camp. The low produced 30-40 kt westerly winds at coastal locations while ice camp winds, on the north side of the low, remained quite light. The effect of the strong winds created great stress in the near shore fast ice, eventually breaking it into gigantic floes, and creating numerous new lead openings between the North Slope and the ice camp. This study documents that storm event, showing the changes that occurred as viewed by satellite.

On 5 April 1992 at 0000 UTC a ridge extended southward into the Beaufort Sea from a high pressure cell centered approximately 250 nm NW of Prince Patrick Island. Winds were very light northeasterly at the ice camp and in the process of veering from westerly to easterly at Deadhorse and Prudhoe Bay, as a mesoscale E-W oriented trough moved south over the North Slope. Further to the west Barrow was reporting light easterly winds in advance of an intense low centered well to the west of Wrangel Island.

Fig 1 is a DMSP visible image showing the Leadex region on 5 April at 0010 UTC. A major lead is apparent stretching generally ENE from near Barrow, passing just south of the ice camp. A branch of the lead near 144W was termed "Husky 1" by visiting research crews on helicopter flights to the lead. Numerous other leads are evident north of Barrow and to the north and west of the ice camp.

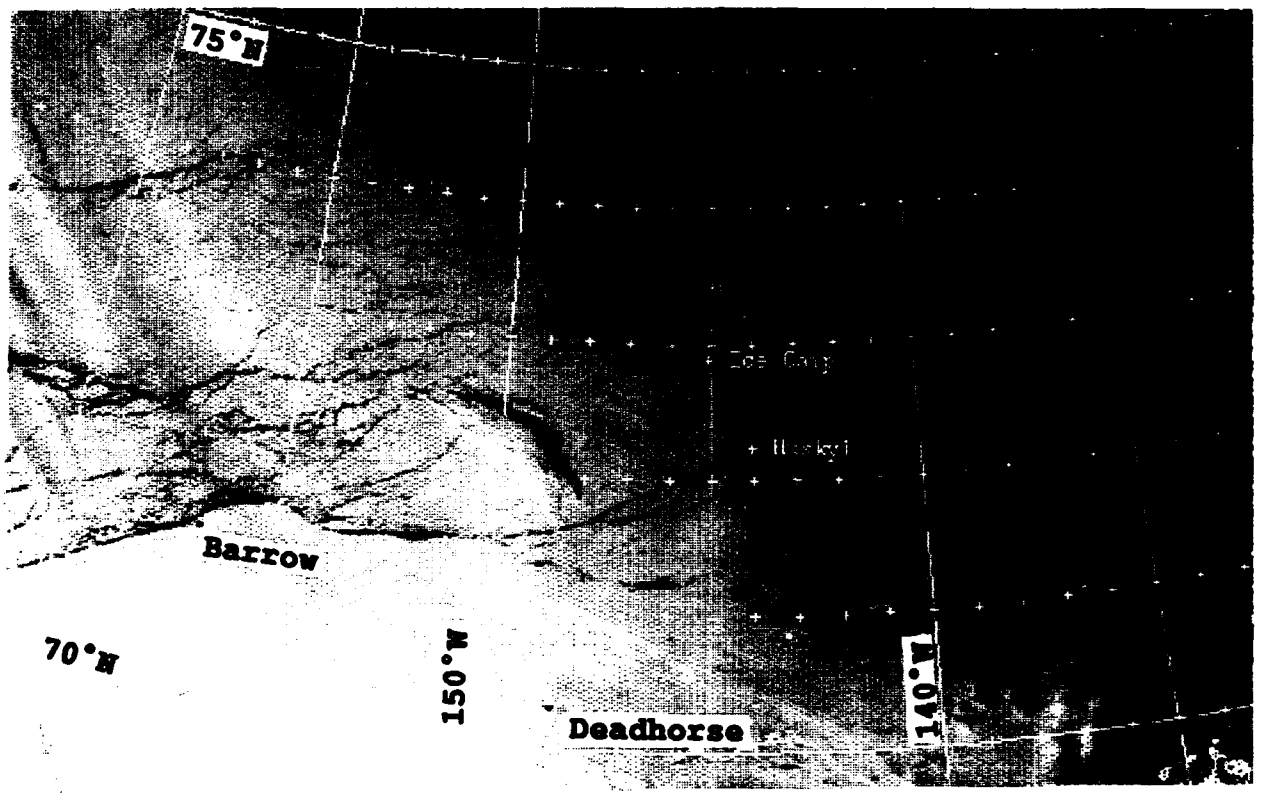

FIG 1. A DMSP visible image. 5 April 1992, 0010 UTC.

Evidence from this image and other images on preceding days shows fewer leads south of the "Husky 1" lead over the fast ice toward Prudhoe Bay. The fast ice itself seems fairly solid based on this image, although some thin obscuration over the fast ice is present in some areas.

Barrow's pressure started falling quite rapidly due to an approaching front, and by 1200 UTC on 5 April winds increased to 20 kts from the southeast, with visibility dropping to 1 1/2 miles in blowing snow. The rawinsonde for Barrow at this time (Fig 2) shows conditions prior to frontal passage. A strong low level inversion is shown with a surface temperature of -23.9°C (-11°F). Winds were from 110° at 20 kts. A veering of the wind to southwesterly and westerly aloft was an indication of the warm air advection ahead of the front.

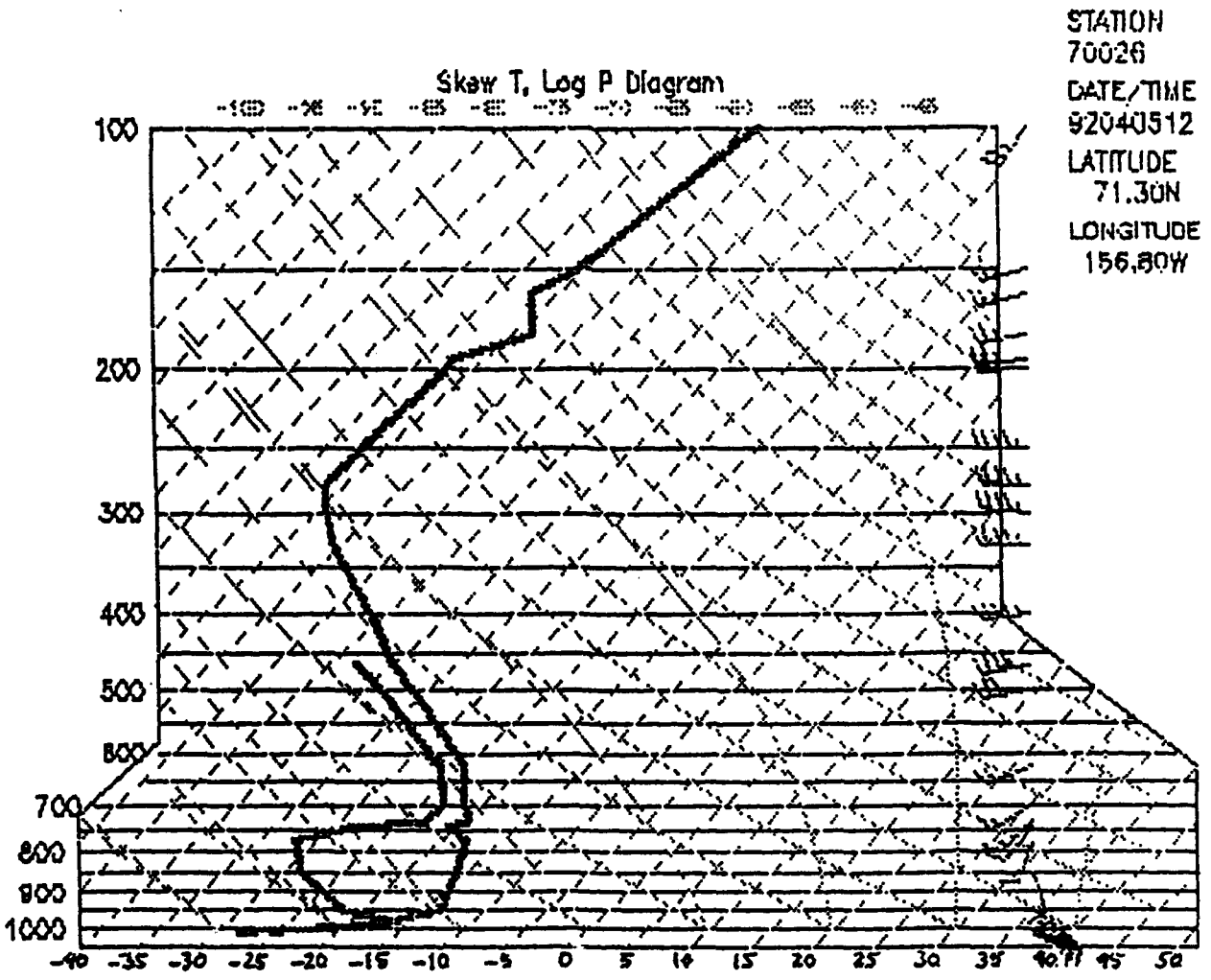

FIG 2. A Skew T, Log P diagram of rawinsonde data for Barrow, Alaska. 5 April 1992, 0000 UTC.

A NOAA channel 4 IR image acquired on 5 April at 1353 UTC and processed at National Weather Service (NWS), Anchorage, is shown in Fig 3. High overcast cirrus striations from the approaching storm are seen in this image passing southeastward over the western portion of the North Slope. Barrow's winds had increased to 25 kts, gusting to 29 kts from the southsoutheast at this time (05/1400 UTC), as the visibility dropped further to 1/2 mile in light snow and blowing snow. Deadhorse at the same time was still in the clear, with a visibility of three miles in ice fog, while winds were 10 kts from 080°.

Winds at Barrow continued to increase from the southeast with gusts to 29 kts until 05/2145 UTC when winds suddenly shifted to SW with diminishing speeds. Frontal passage was reported at 05/2200 UTC with SW winds of only 15 kts. Sixteen minutes later (05/2216 UTC) winds shifted to westerly at 32 kts with gusts to 39 as visibility diminished to 1/4 mile in light snow and blowing snow.

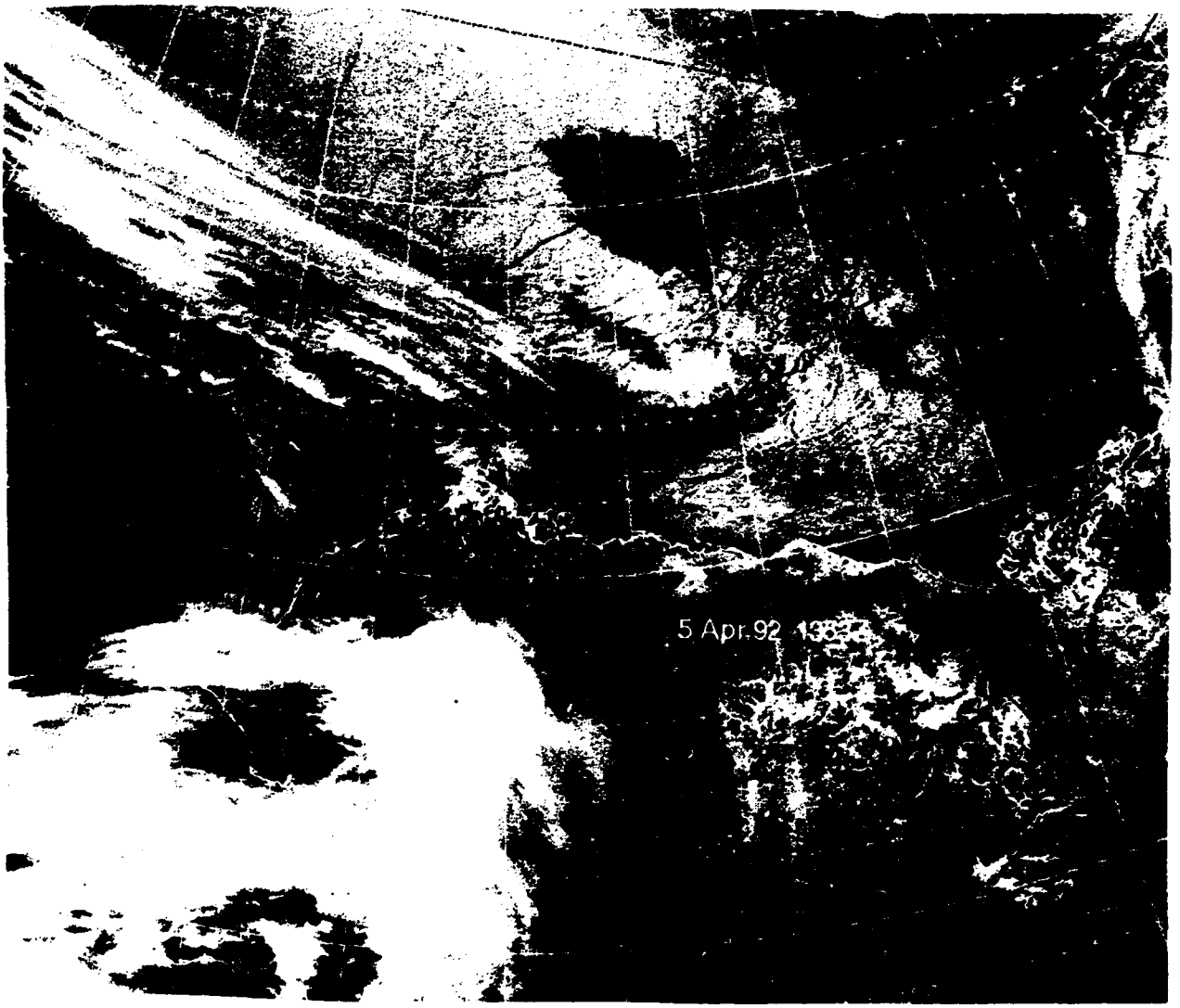

FIG 3. NOAA infrared (Ch 4) imagery. 5 April 1992, 1353 UTC.

The 6 April 1992, 0000 UTC, sounding for Barrow (Fig 4) shows the strong low level wind speeds behind the front, destruction of the low level inversion previously noted, and increase in thickness of the moist layer to at least 800 mb, with very dry air above 700 mb. The moist layer was very likely thicker between observation times as the front moved over the area.

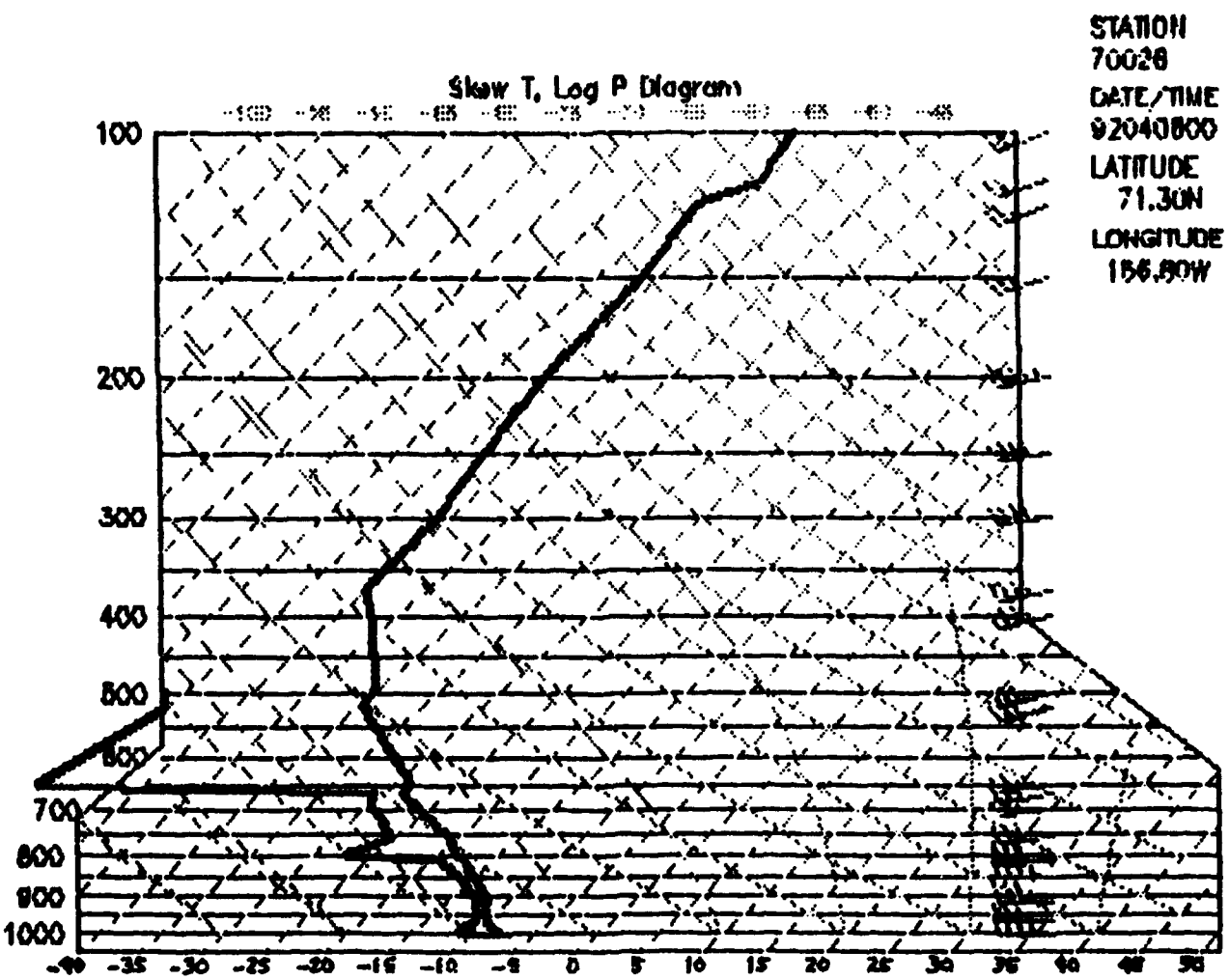

FIG 4. A Skew T. Log P diagram of rawinsonde data for Barrow, Alaska. 6 April 1992, 0000 UTC.

A NOAA infrared image acquired shortly after frontal passage at Barrow, processed at NWS, is shown in Fig 5. This 05/2210 UTC image shows the frontal band approaching Prudhoe Bay with the northern portion of the band bent back strongly toward the west. The "bent back" appearance of the system suggests that winds were much stronger near the coast and diminished rapidly, probably becoming easterly, just a short distance to the north (near 72N).

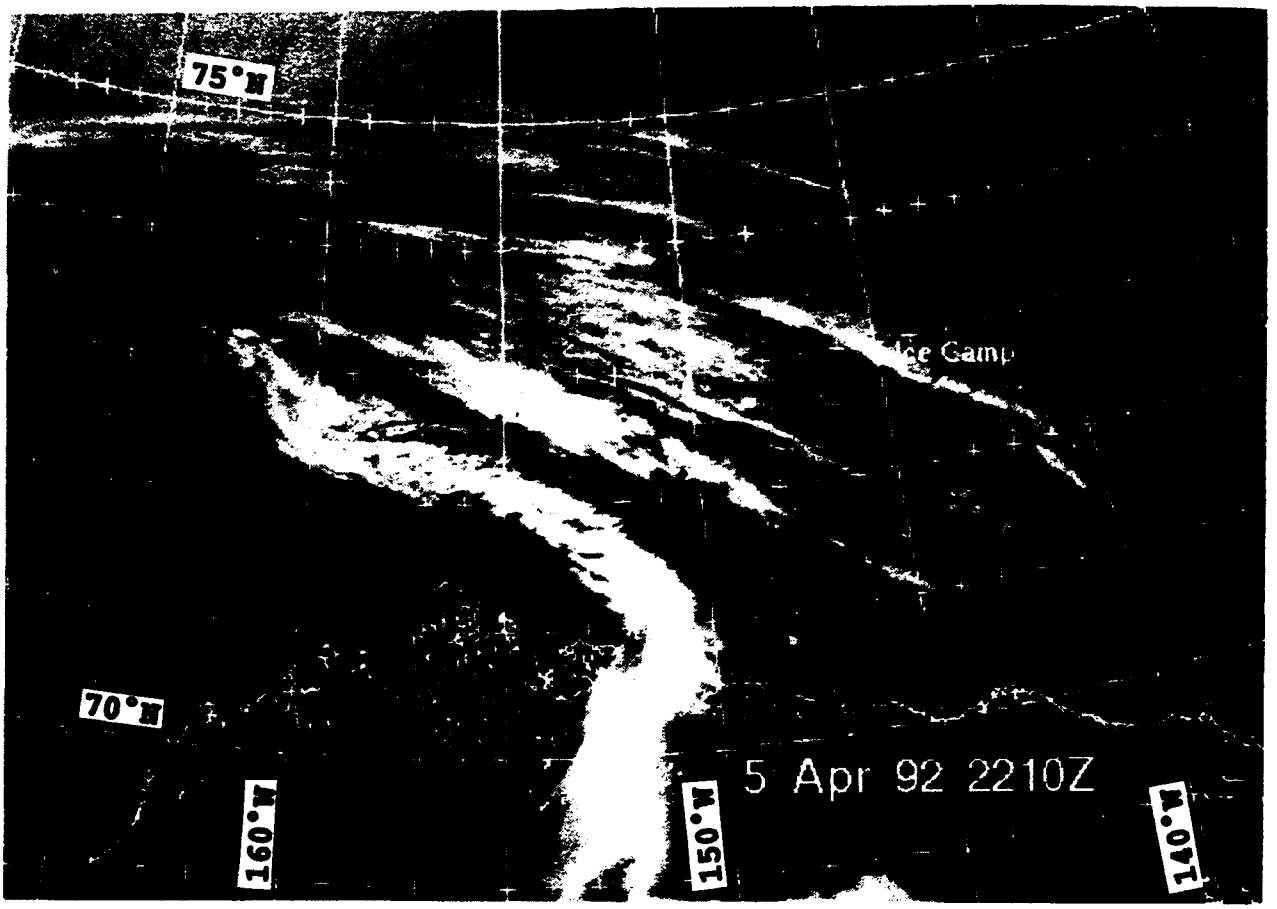

FIG 5. NOAA infrared (Ch 4) imagery. 5 April 1992, 2210 UTC.

Evidence supporting this hypothesis is provided by the Navy's Second Order Closure Mesoscale Model (SOCMM) analysis for 6 April at 0000 UTC (Fig 6). The analysis shows strong easterly winds meeting westerly winds in a narrow zone stretching NW from Barrow. This convergent zone would logically correspond to the band of cloudiness in that region shown in Fig 5.

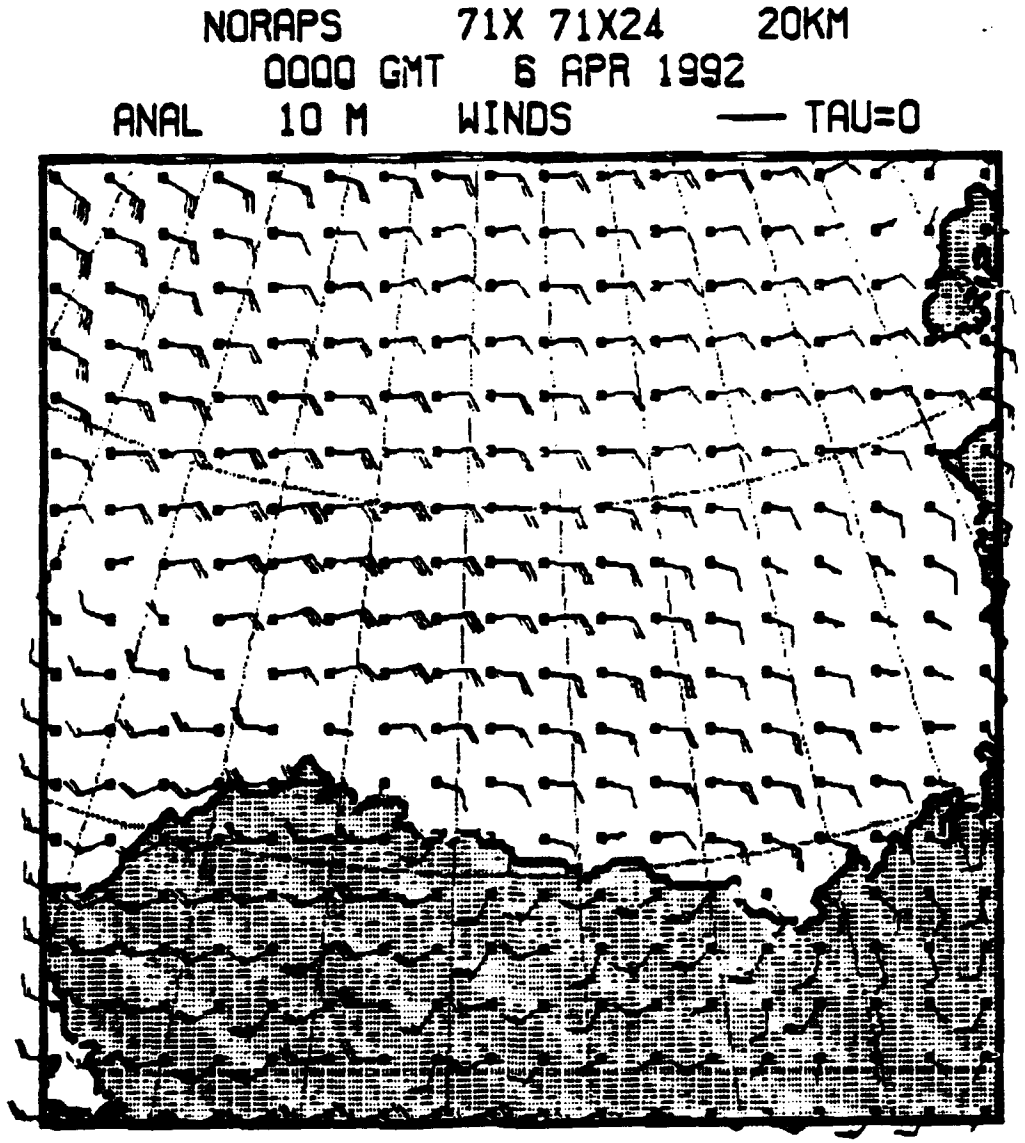

FIG 6. Navy Second Order Closure Model (SOCMM) 10 meter analysis (20 km resolution). 6 April 1992, 0000 UTC.

The NWS analysis for 6 April at 0000 UTC is shown in Fig 7. This analysis indicates the movement of a small low pressure center into the region just north of Barrow. Both the model and NWS analysis imply strong easterly winds near the ice camp; however, the 06/0000 UTC ice camp sounding data reveal easterly winds at only 17 kts, consistent with surrounding ice station data (reports plotted on the NWS analysis, Fig 7).

Deadhorse remained under easterly to southeasterly flow conditions until 05/2300 UTC, when winds suddenly shifted to 210 degrees with speed increasing to 17 kts. Pressure, however, continued falling with temperature rising to a high of +23 deg F at 06/0100 UTC. A pressure minimum of 1008.3 mb was also noted at this time as winds became gusty to 27 kts. An additional shift in winds to 270 degrees at 06/0200 UTC with speed of 27 kts gusting to 34 kts completed the scenario of frontal passage at that location.

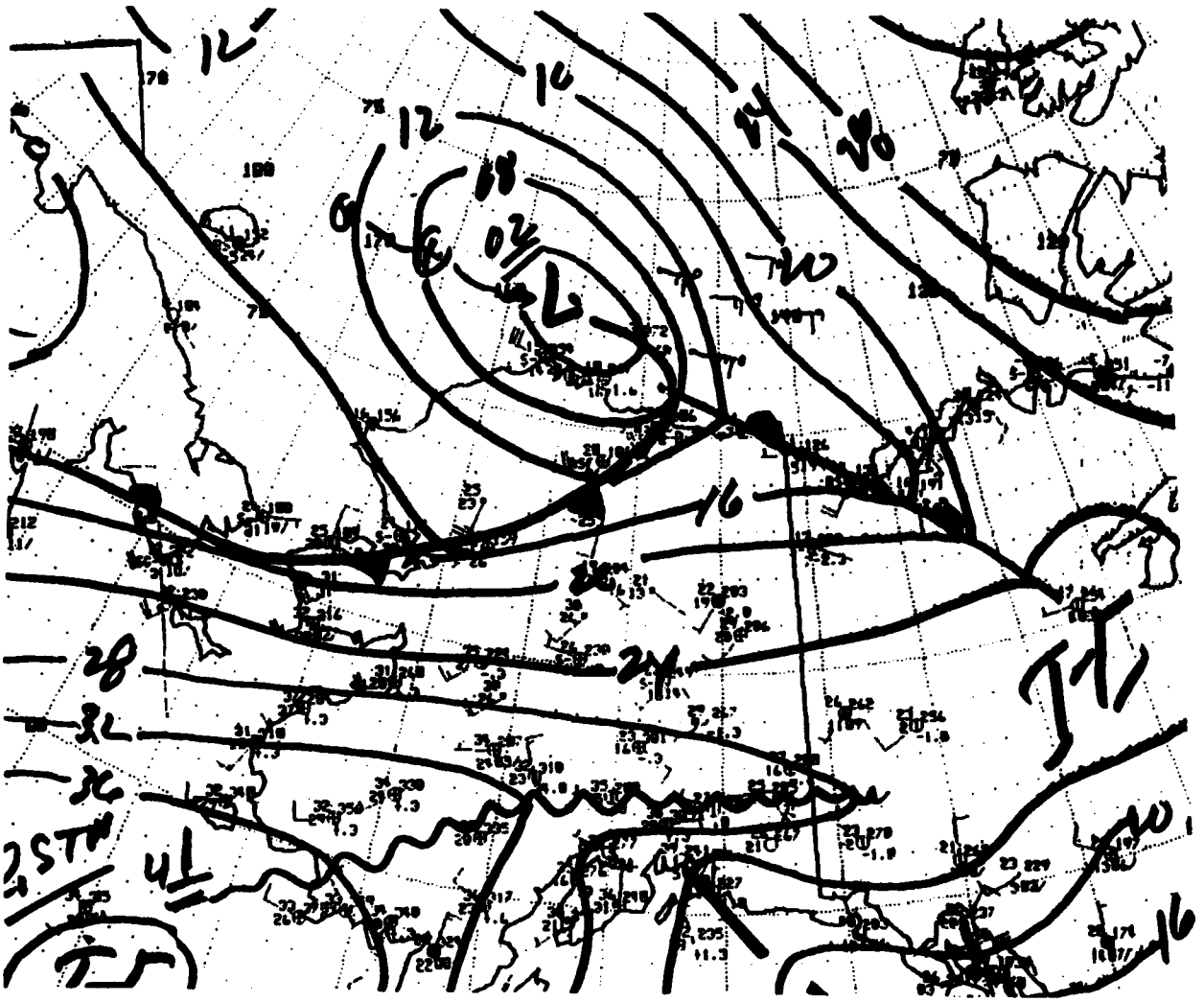

FIG 7. A National Weather Service (NWS) (Anchorage) surface analysis. 6 April 1992, 0000 UTC.

A DMSP IR view at 06/0235 UTC (Fig 8) shows the frontal band and bent-back occlusion of the system shortly after passing Deadhorse. The temperature rise at Deadhorse from -24°F at 05/1200 UTC to +23°F at 06/0100 UTC, a swing of +47°F in thirteen hours was notable, to say the least!

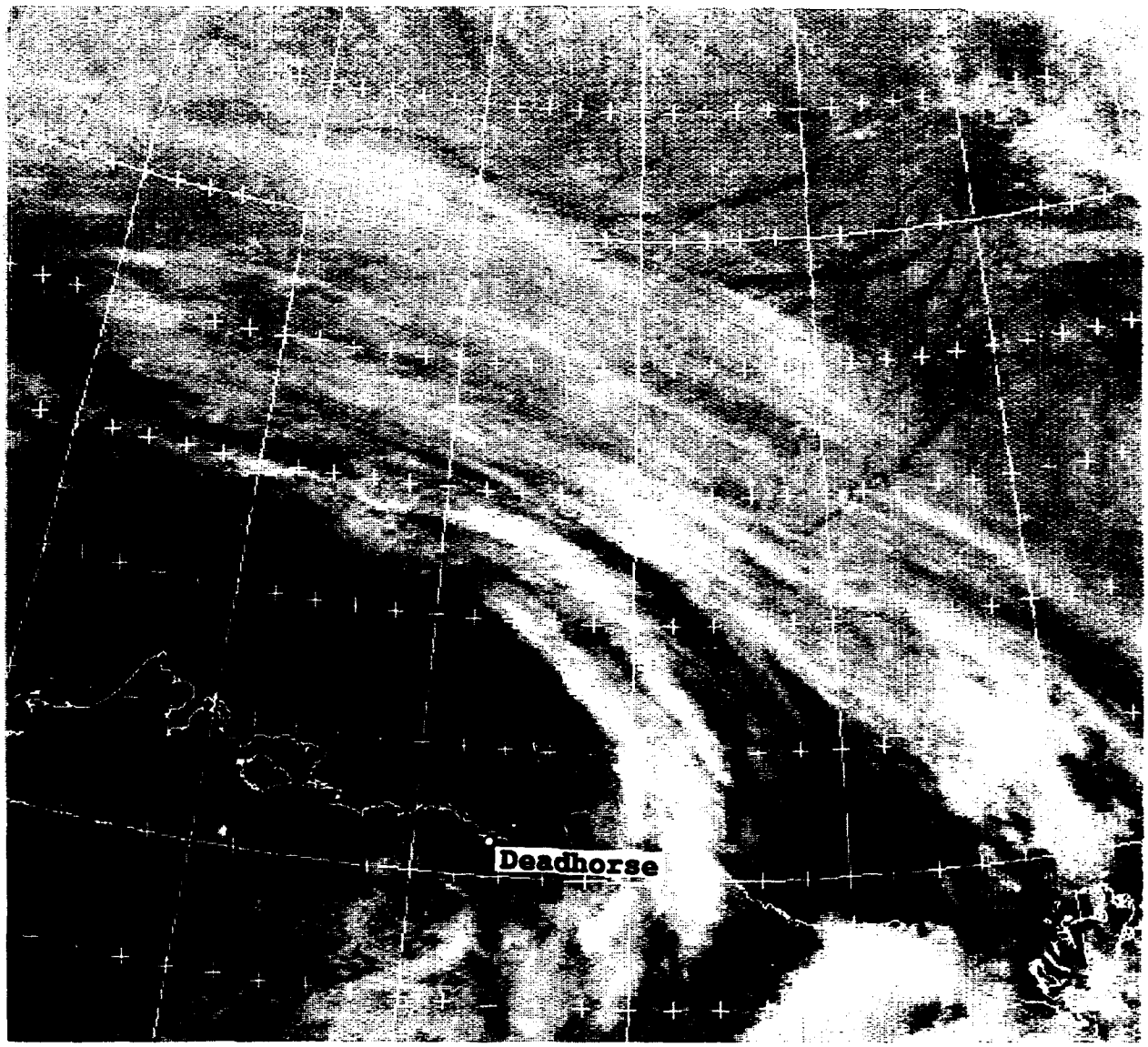

FIG 8. A DMSP infrared image. 6 April 1992, 0235 UTC.

The system moved rapidly eastward on 6 April with little abatement in wind intensity along North Slope locations. Fig 9 is the NWS surface analysis for 06/1200 UTC. The analysis shows the cold front approaching the Mackenzie River Delta area with a small low center near 71.5N, 135 W. Ice camp and buoy winds plotted on this analysis continue to show weaker easterlies north of the trough and low pressure center, with stronger winds south of the trough along the North Slope.

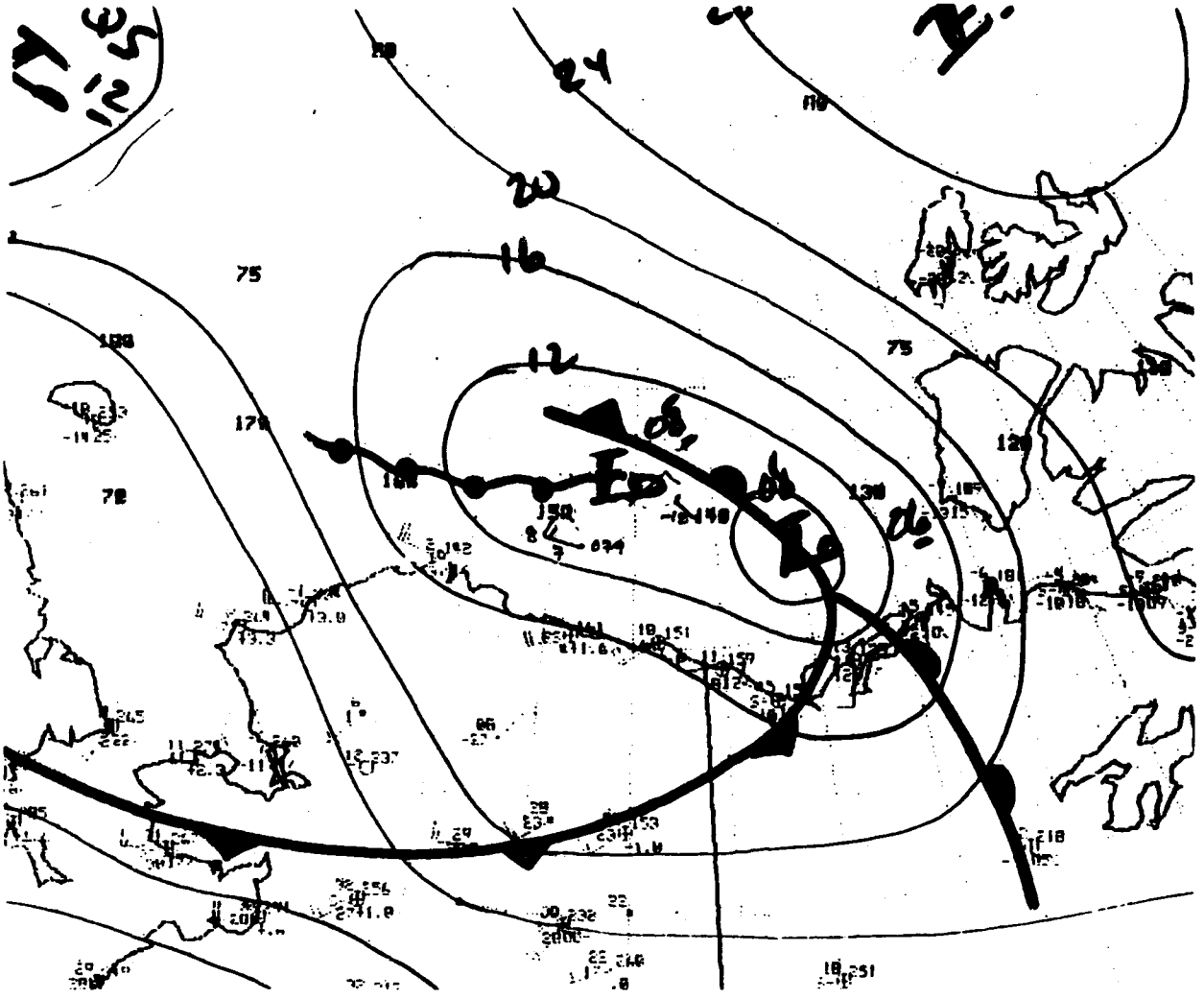

Fig 9. A NWS (Anchorage) surface analysis. 6 April 1992, 1200 UTC.

A NOAA-11 IR view at 06/1344 UTC (Fig 10) shows that leads are now beginning to open south of the ice camp and north of Barrow. Strong westerly winds and blowing snow were undoubtedly contributing to the mainly low overcast conditions suggested by the satellite data along the North Slope.

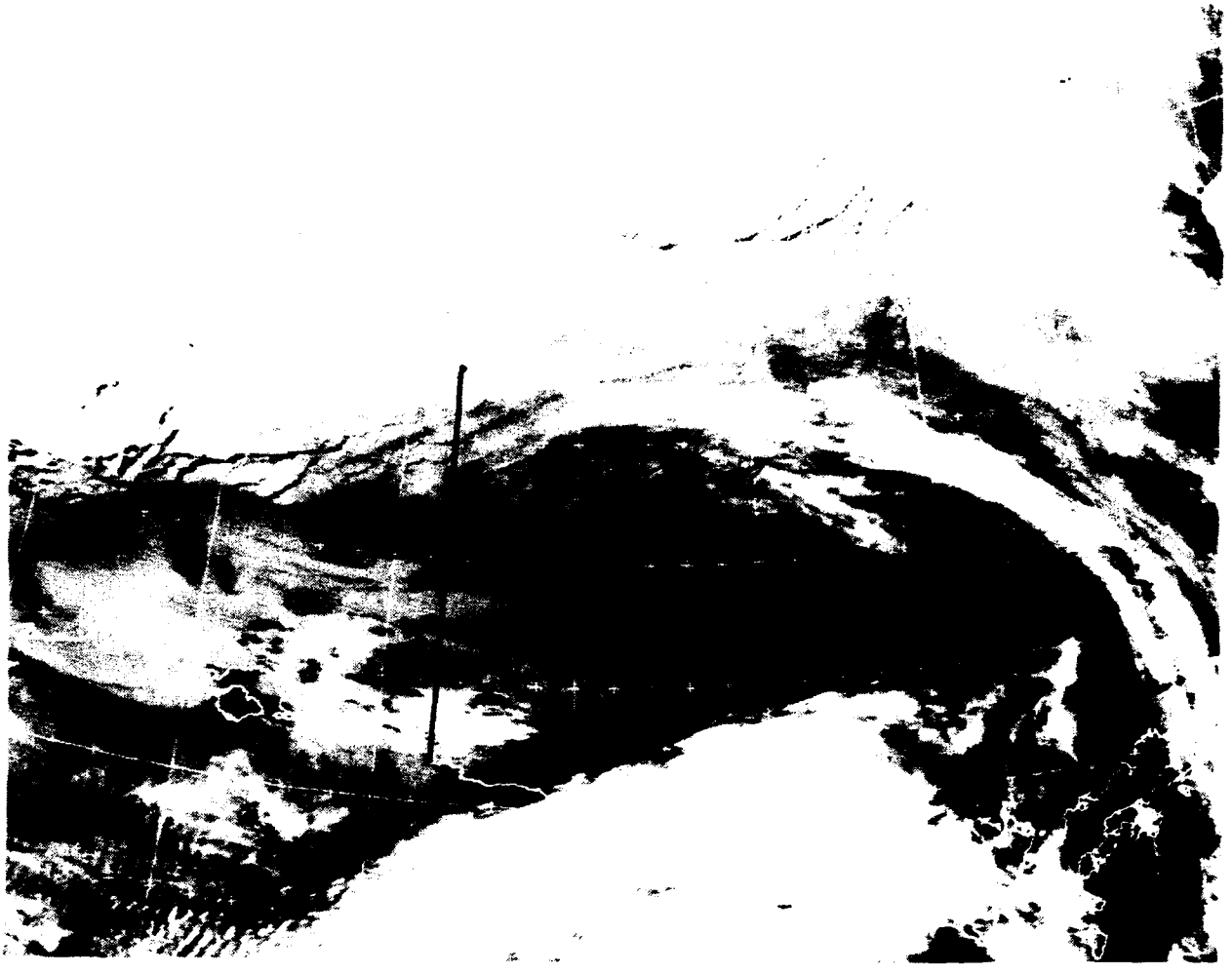

FIG 10. A NOAA-11 infrared (Ch 4) image. (N-S line from 70.3°N, 148.6°W to 73.6°N, 148.6°W represents cross section discussed with reference to FIG. 13).

The comma-like shape of the cloud mass SE of the ice camp suggests maximized vorticity in this region consistent with an E-W oriented trough shown through that region on the SOCMM analysis for 06/1200 UTC (Fig 11). Wind speeds north of the trough axis, however, shown as northeasterly at about 20 kts, as indicated earlier, are probably too high. The ice camp sounding for 06/1200 UTC (located on the north side of the trough axis) also shows light northeasterlies at no more than 10 kts.

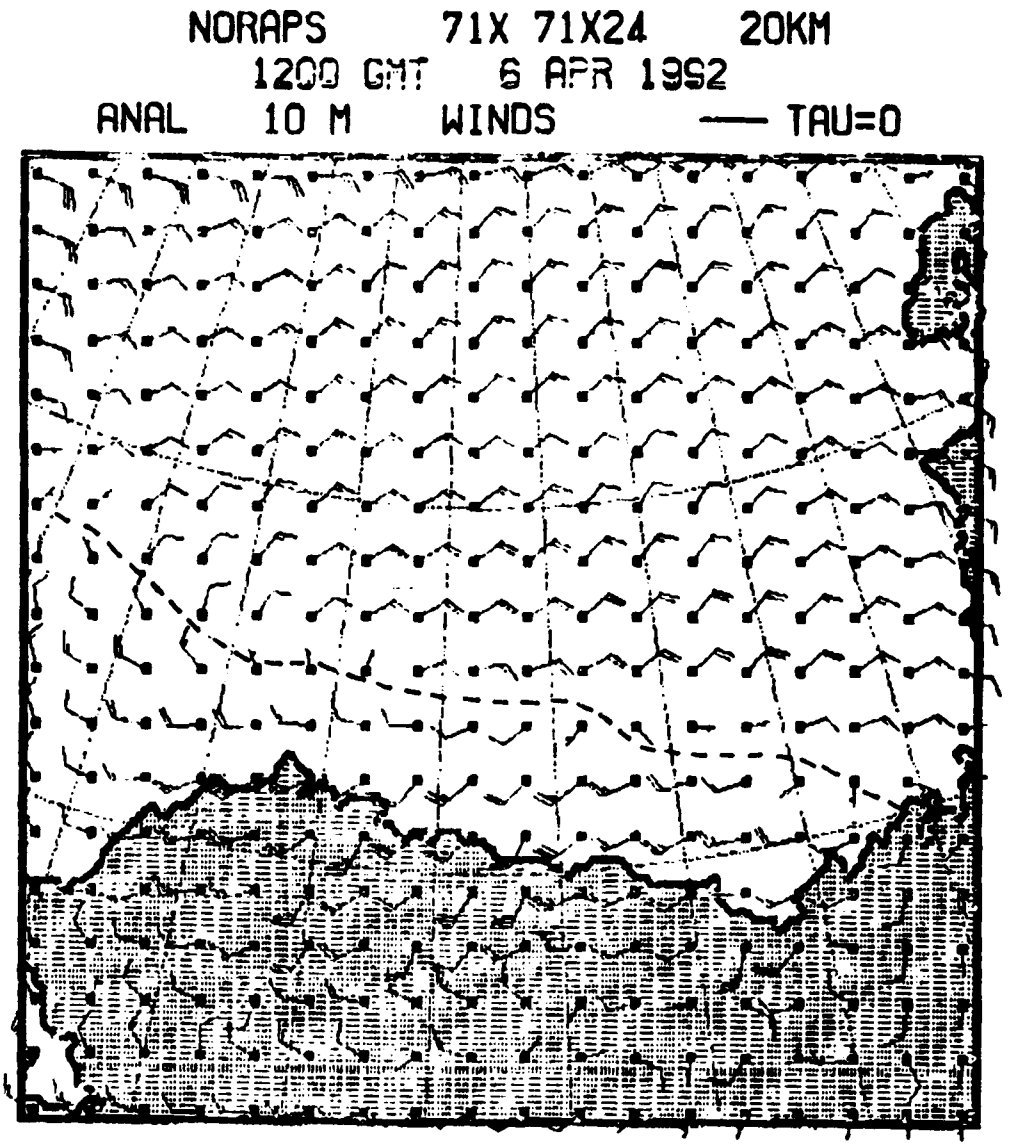

FIG 11. Navy SOCMM (20 km resolution) 10 meter analysis. 6 April 1992, 1200 UTC.

The strong westerly winds at Barrow apparently resulted in turbulence which lifted the inversion to a base near 900 mb as revealed in the 6 April, 1200 UTC sounding for that station (Fig 12). This sounding reveals very moist conditions within the inversion layer.

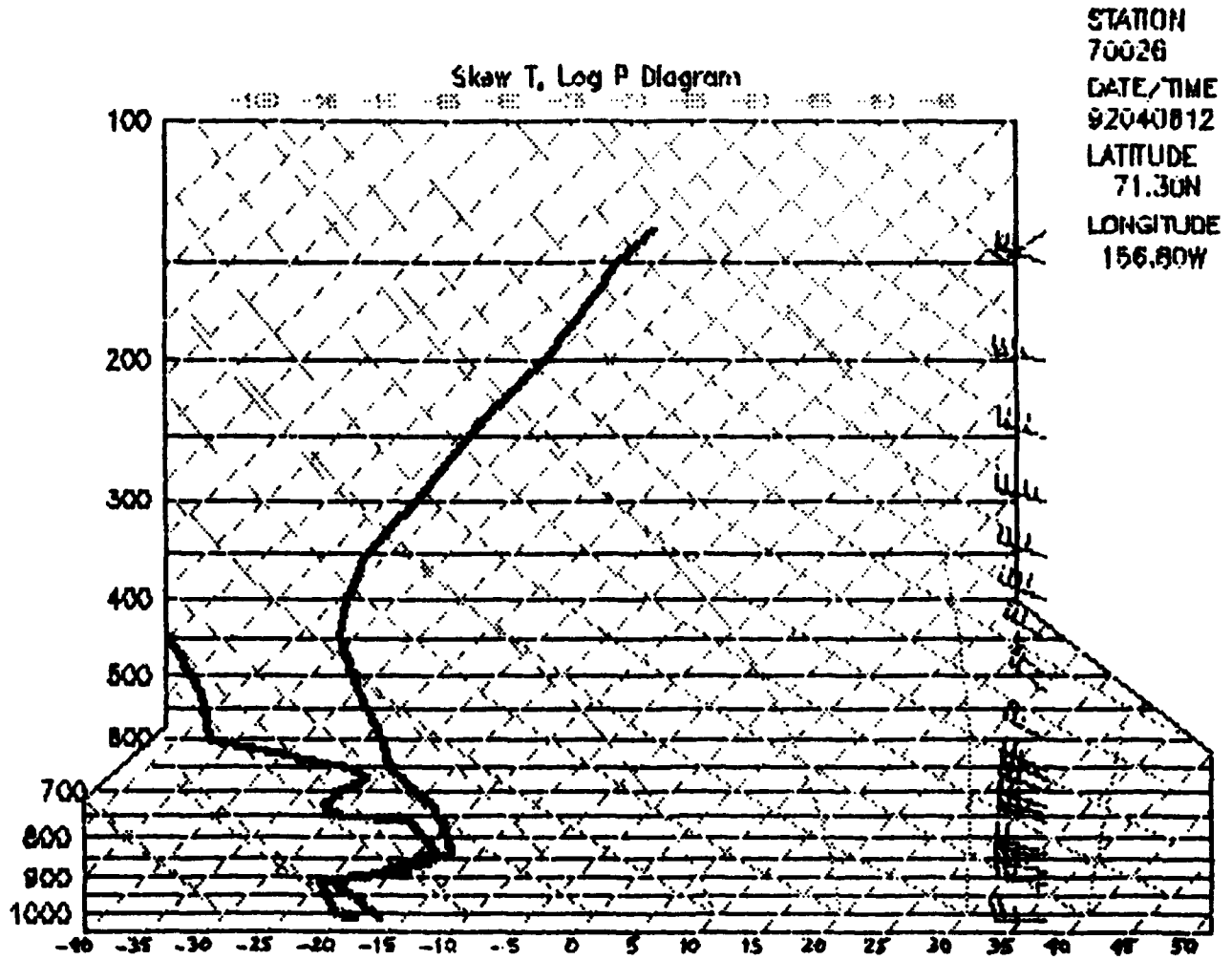

FIG 12. A Skew T, Log P diagram of rawinsonde data for Barrow, Alaska. 6 April 1992, 1200 UTC.

A north-south cross section from 70.3°N, 148.6°W to 73.6°N, 148.6°W (Fig 13), shows a 6 April 1200 UTC forecast of potential temperature (thin lines) and relative humidity (thick lines) from the surface to 845 mb. This cross-section, derived from the mesoscale model (SOCMM), can be directly related to implications of cloud cover and moisture shown in the AVHRR data (Fig 10), and to changes in the height and moisture content of the inversion following frontal passage at Barrow (Fig 12). Specifically, note that the relatively dry conditions implied by the satellite data over land and north of 72°N are reflected in low relative humidities on the cross section with a very sharp moisture gradient near 72°N. An elevated inversion is implied by the packing of potential temperature lines on the cross section near 72°N, 147.6°W. The cross section also reveals the very moist conditions within the inversion (also shown on the Barrow sounding, Fig 12), with relative humidities approaching 100%.

FIG 13. A SOCMM 6 April 1992, 1200 UTC, north-south cross section forecast of potential temperature (thin lines) and relative humidity (thick lines). Cross section extends from 70.3°N, 148.5°W to 73.6°N, 148.6°W.

Vertical time sections of potential temperature (°K) and winds (kts) for Barrow from 4 through 7 April 1992 are shown in Figs 14a and 14b, respectively. The sections confirm passage of the front at Barrow by 6 April, 0000 UTC. Note the elevated inversion occurring after frontal passage and the indications of the low pressure associated with the front existing in a deep layer from the surface through 400 mbs.

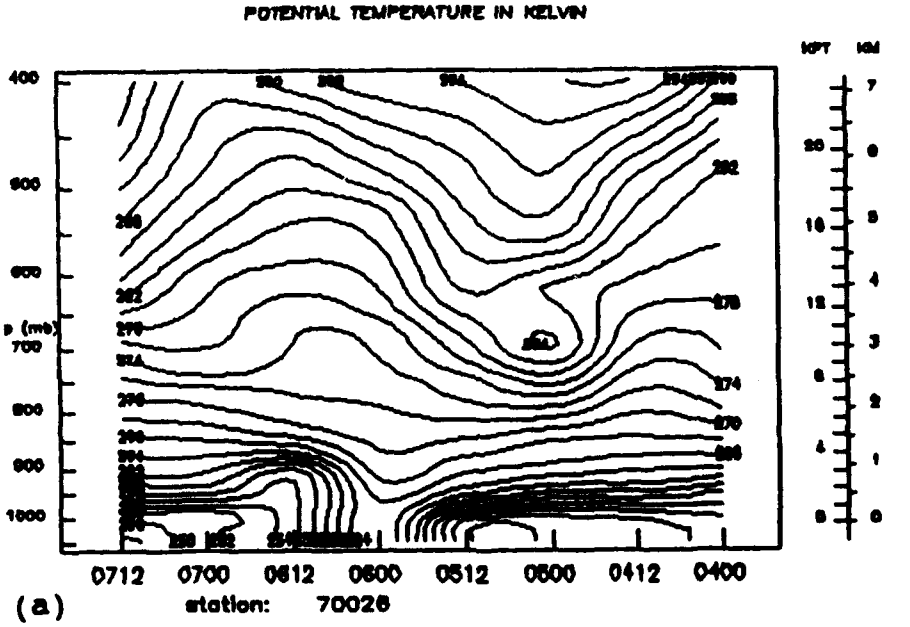

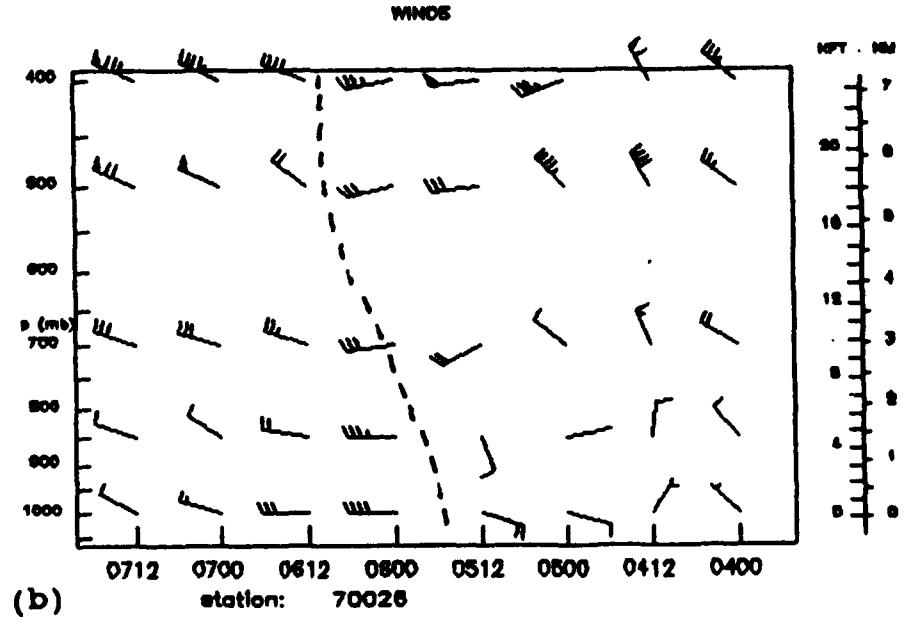

FIG 14. (a) Vertical time section of potential temperature at Barrow, Alaska. 4-7 April 1992.
(b) Vertical time section of winds (speed in kts) at Barrow, Alaska. 4-7 April 1992.

A DMSP visible image on 6 April at 2034 UTC (Fig 15) shows the massive breaks beginning to occur in the ice shelf adjacent to the North Slope. Large floes of ice have broken loose just east of Barrow while the main "Husky" lead formation south and east of the ice camp appears to have suddenly broadened (compare Fig 15 with Fig 1, an image acquired less than 2 days earlier). Additionally, many new leads appear to have formed southwest of the ice camp.

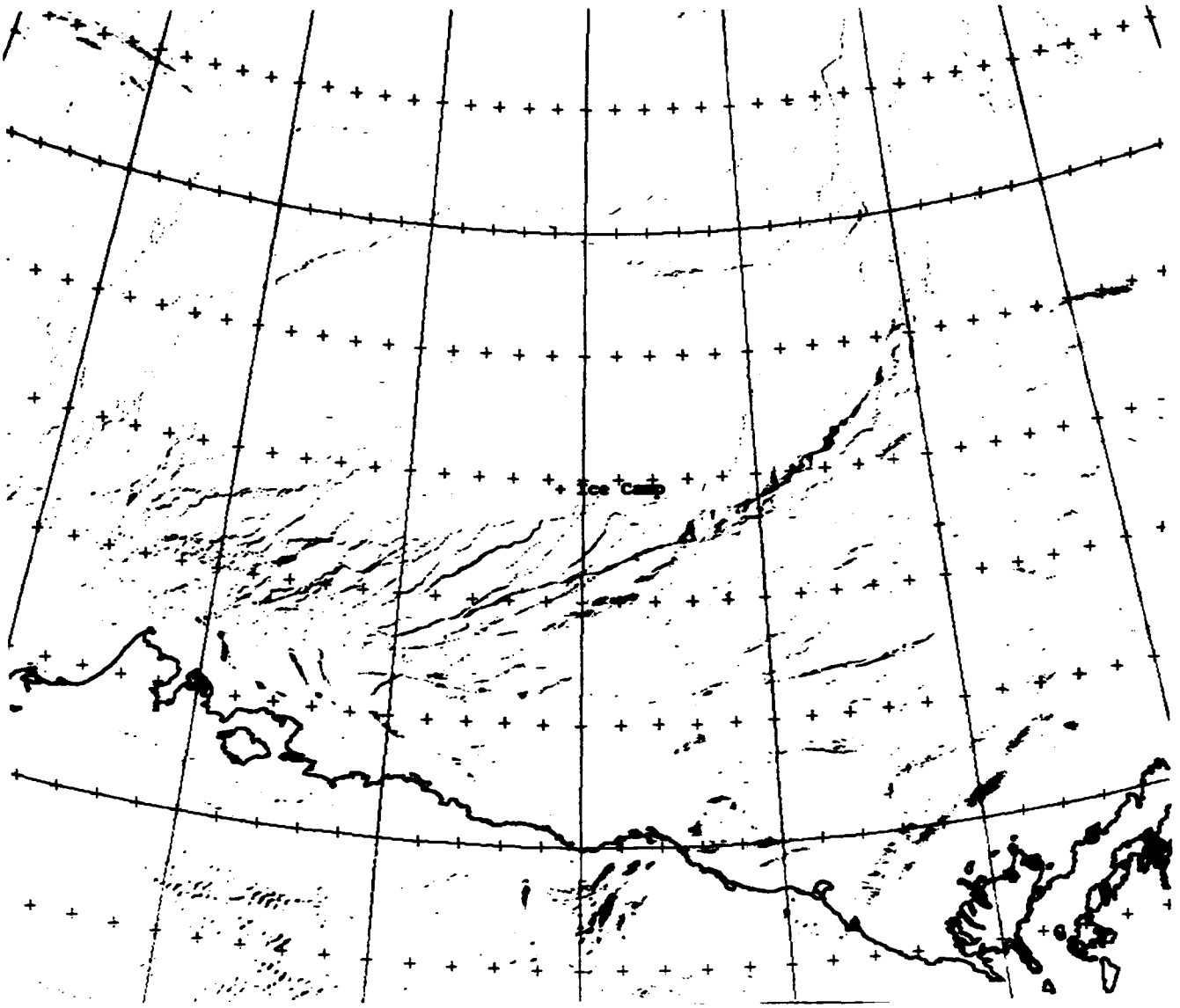

FIG 15. A DMSP visible image. 6 April 1992, 2034 UTC.

Fig 16 is the NWS surface analysis for 7 April at 0000 UTC. Strongest reported winds are now shown as westerly at 40 kts at Komakuk Beach near 140 W. The low pressure center has now moved to the eastern Beaufort Sea just west of Banks Island.

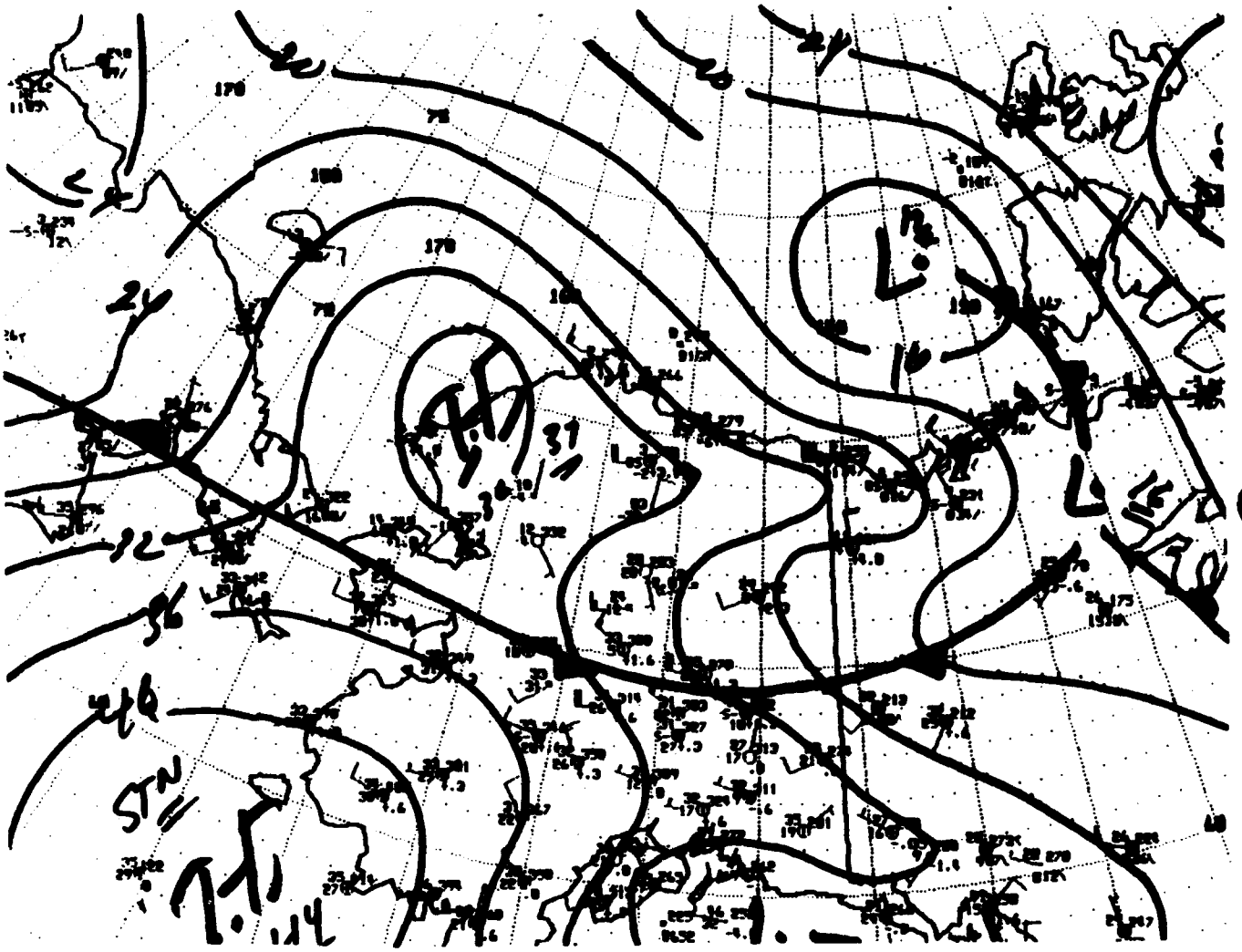

FIG 16. A NWS (Anchorage) surface analysis. 7 April 1992, 0000 UTC.

The position relates well to a NOAA IR image (Fig 17) which shows a comma-shaped cloud mass indicating a vorticity center just southwest of that location. This image also continues to show the massive floes created in the formerly solid ice shelf adjacent to the North Slope.

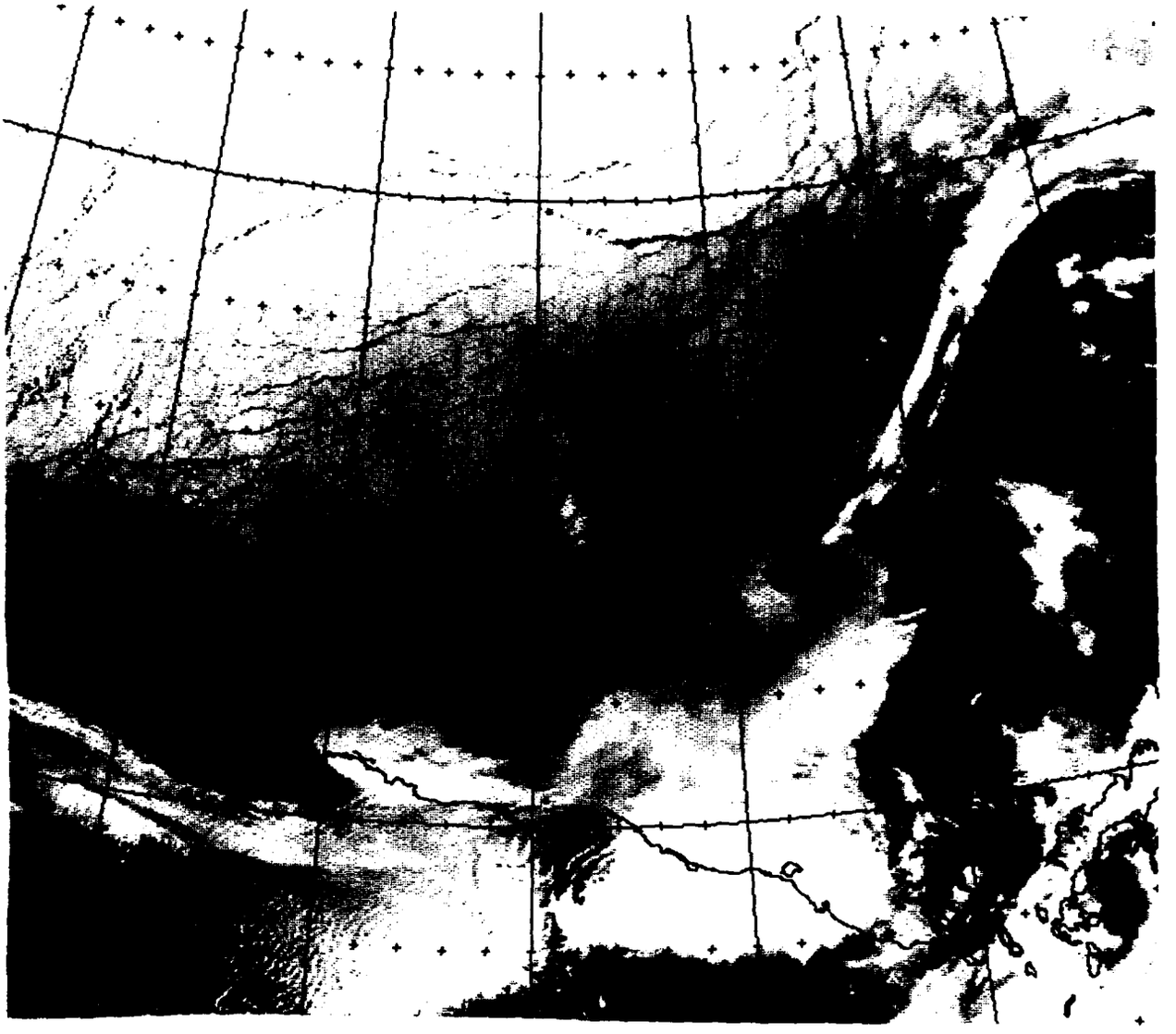

FIG 17. A NOAA infrared (Ch4) image. 6 April 1992, 2346 UTC.

A final NOAA infrared image, acquired on 7 April at 1329 UTC (Fig 18), shows the region from Barrow to the ice camp under clear conditions. Various features including the ice formations and leads identified variously as "Tadpole", "Jamie 1", "Jamie 2", and "Husky 1", are easily identified as well as the reasonably precise position of the ice camp. A comparison of this image with that of Fig 1 emphasizes the power of one single storm to significantly influence the opening of leads in a near shore high wind speed environment.

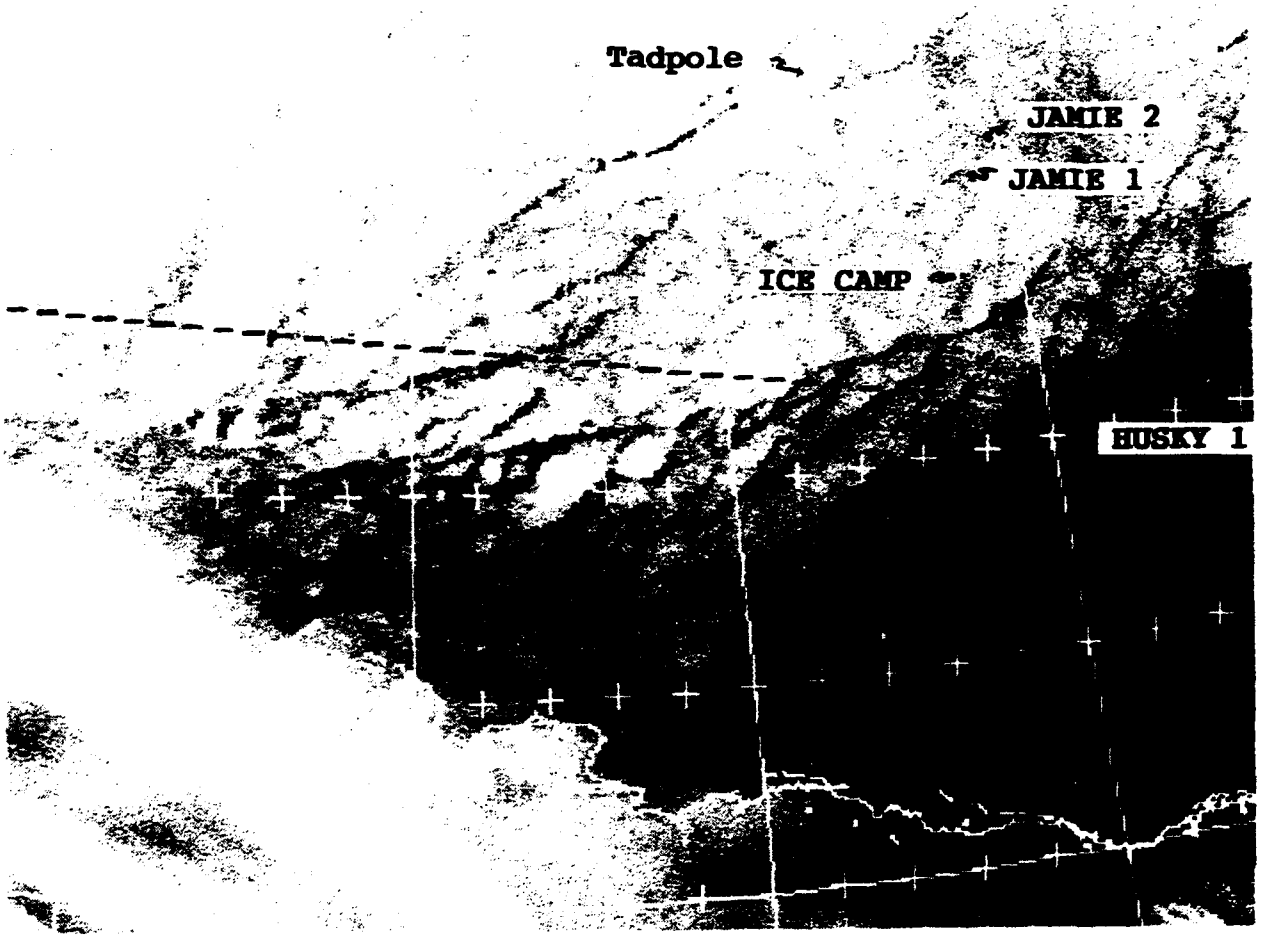

FIG 18. A NOAA infrared (Ch4) image. 7 April 1992, 1329 UTC.

Some important conclusions may be derived from this study:

1. High speed winds in a relatively narrow band can occur along the North Slope of Alaska.

2. Such winds can cause massive breaks creating giant floes of formerly "fast ice" or "near-shore" ice, and in the process open previously frozen leads to the north, as well as create numerous new leads.

3. Under such storm conditions little or no change may occur in ice drifting under lighter wind conditions to the north.

4. Satellite visible and IR data acquired on a frequent basis are excellent tools for monitoring lead development under storm conditions.

5. Individual leads and ice formations can be identified and followed on a day-to-day basis, providing an excellent method for detecting, tracking, and computing ice motion.

THIS PAGE DELIBERATELY LEFT BLANK

4. OPENING AND CLOSING OF THE "HUSKY 1" LEAD COMPLEX. 21 - 27 MARCH 1992

Synthetic Aperture Radar (SAR) data were collected over the central Beaufort Sea during the Leadex experiment which extended from early March to the end of April 1992. The data revealed no evidence of a lead on 21 March, followed by a significant lead opening in the same region on 24 March. The lead, again, was virtually closed by 27 March. Fracture of identifiable multiyear floes on each of the days permitted precise location of the opening and closing effects. Opening of the lead coincided with the onset of moderate east-southeasterly winds in advance of a low pressure system moving through the area. The highly reflective nature of portions of the lead region as it appeared in the SAR data cannot be precisely determined. Potential causes are: (1) Bragg scattering from wind-roughened water; (2) reflection of radar return from jagged edges of rafted ice; and (3) radar return from "frost flowers", small stem-like protuberances which grow rapidly on thin ice in open lead conditions. Closing of the lead occurred as the low pressure system moved northeastward past the area, bringing northerly flow on the western side. The study is documented with ice station surface observations, high resolution satellite data, and conventional analyses.

On 21 March 1992 at 2129 UTC SAR data (Fig 1) revealed a region of multiyear floes just north of the fast ice between Deadhorse and the ice camp. Center point of this image is 71.63°N, 147.52°W. Scale of the image is such that 1" equals approximately 15 km. Dashed lines drawn on this figure indicate the approximate positions where leads were destined to form a few days later (24 March). Features A, B, C, D, and E are labeled to aid in comparison with subsequent SAR images. By coincidence ice station

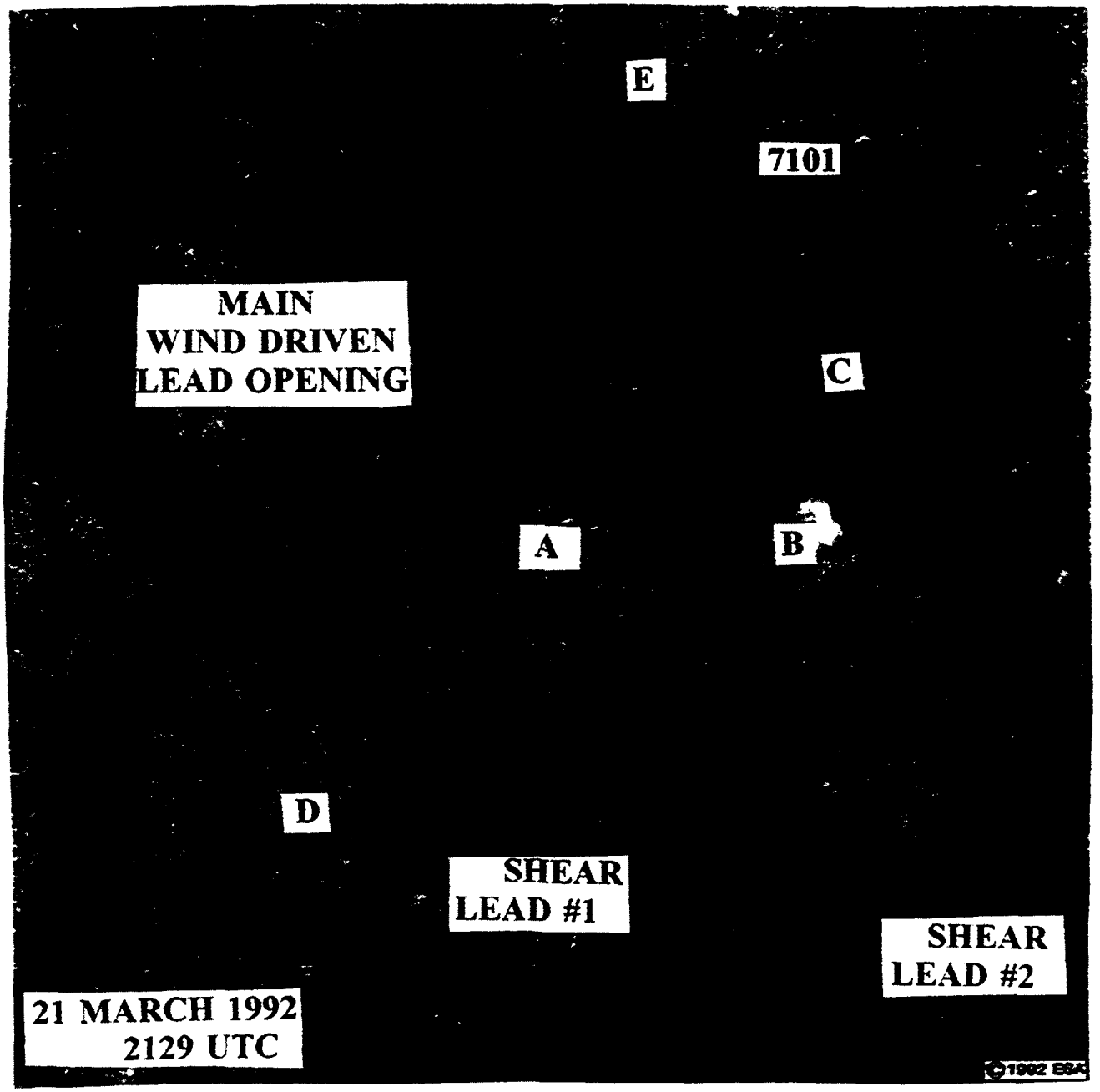

FIG 1. Synthetic Aperture Radar (SAR) data. 21 March 1992, 2129 UTC.©1992 ESA; used by permission.

(buoy) 7101 had been placed on the ice just north of the northernmost lead. Its approximate position is also shown on this figure.

Winds were very light northwesterly at 2-3 kts as indicated by buoy reports in the region at the time of these data. The light wind speeds in westerly to northwesterly flow prevailed with little change until 23 March when the direction changed to a more easterly flow in response to a developing inverted trough from the west. By 0000 UTC on 24 March wind speeds had increased to 10 kts from the southeast.

A DMSP visible image acquired at 0158 UTC (Fig 2) shows satellite-observed features at this time. Weather appears disturbed in the Barrow region with no definite indication of a low center or cloud vortex. Note that the region between Deadhorse and the ice camp shows no strong evidence of lead features. A pronounced lead is evident, however, west of the ice camp extending northeastward from Barrow.

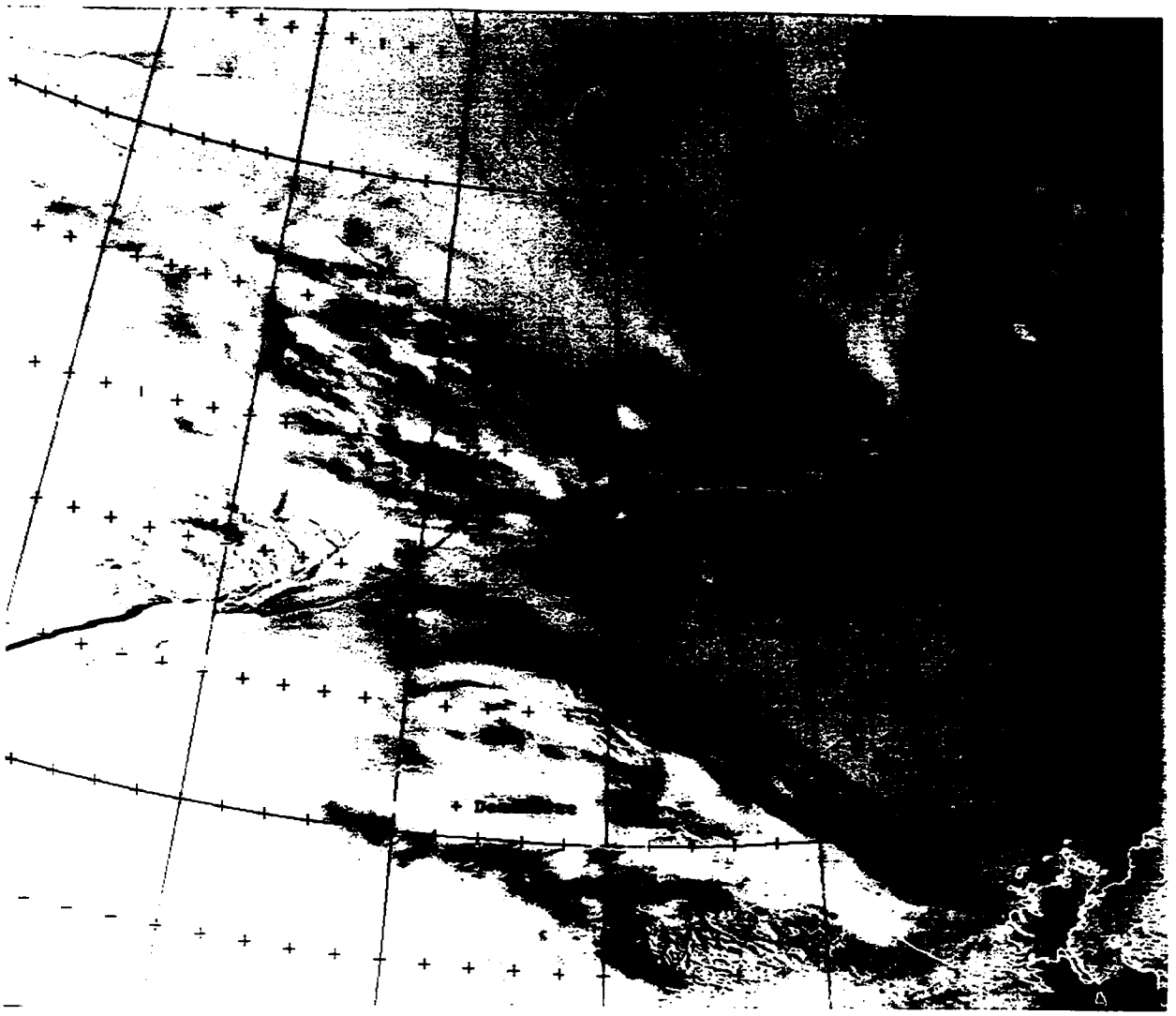

FIG 2. DMSP visible data. 24 March 1992, 0158 UTC.

Wind speeds continued to increase during the day reaching 15 to 20 kts by 1200 UTC. Fig 3 shows the National Weather Service (NWS)(Anchorage) analysis for 24 March at 1200 UTC (buoy reports plotted subsequent to the analysis). A cyclonic wind shift between the buoys and Barrow indicates the position of the inverted trough.

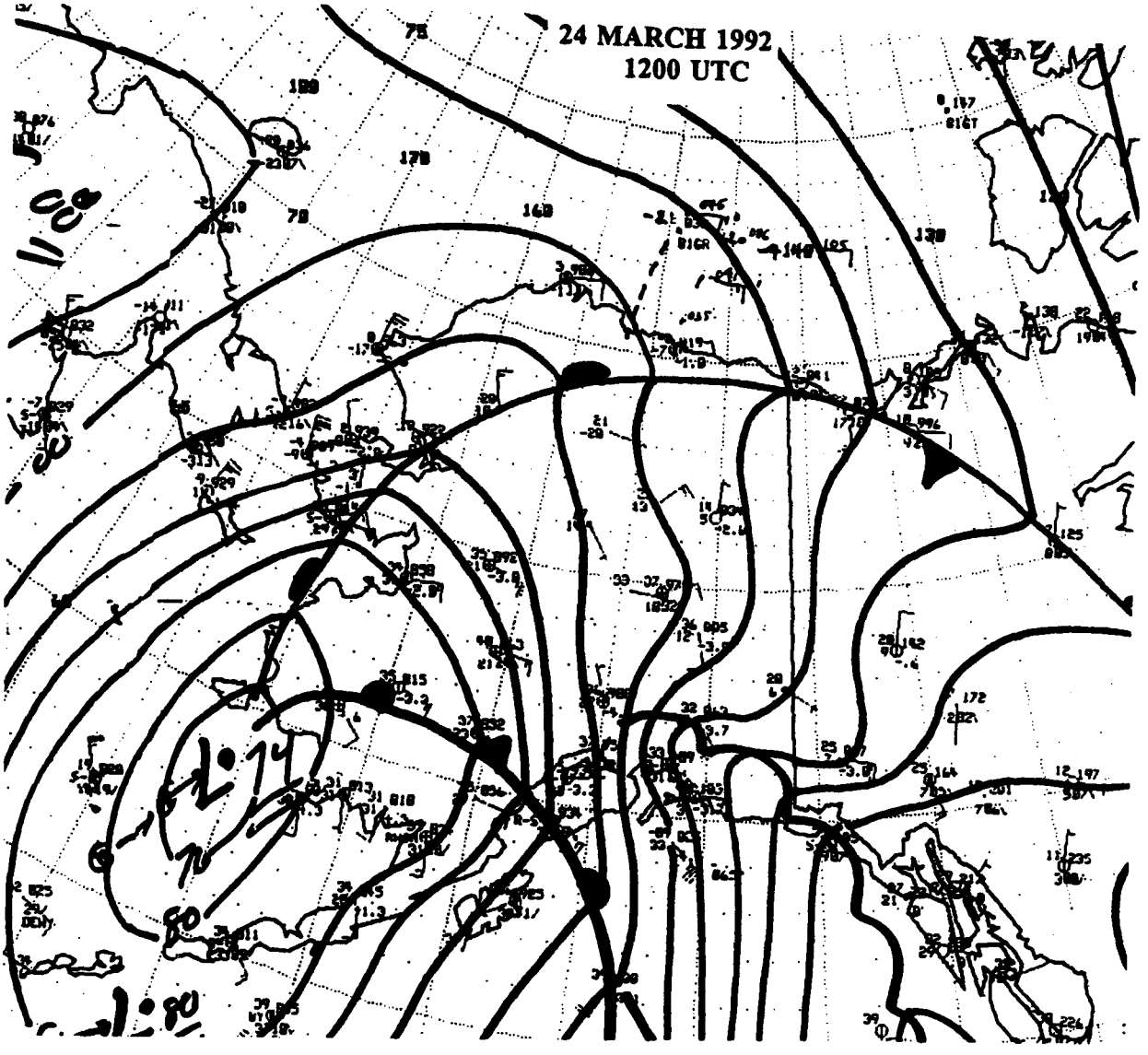

FIG 3. NWS (Anchorage) surface analysis. 24 March 1992, 1200 UTC.

Fig 4 shows an additional DMSP visible image acquired on 24 March at 1723 UTC. In comparing this image with the preceding view in Fig 2 it is apparent that the data have captured a new lead formation between 71° and 72°N, immediately north of Deadhorse. Although the Fig 2 view is partially obscured in that region the thinness of the cloud cover is such that this lead would have been visible if it had been open at an earlier time. (Note that the lead extending northeast of Barrow is visible through similarly thin obscuring cloudiness). The implication is that the lead opened dramatically within the 15 hour interval between the two views.

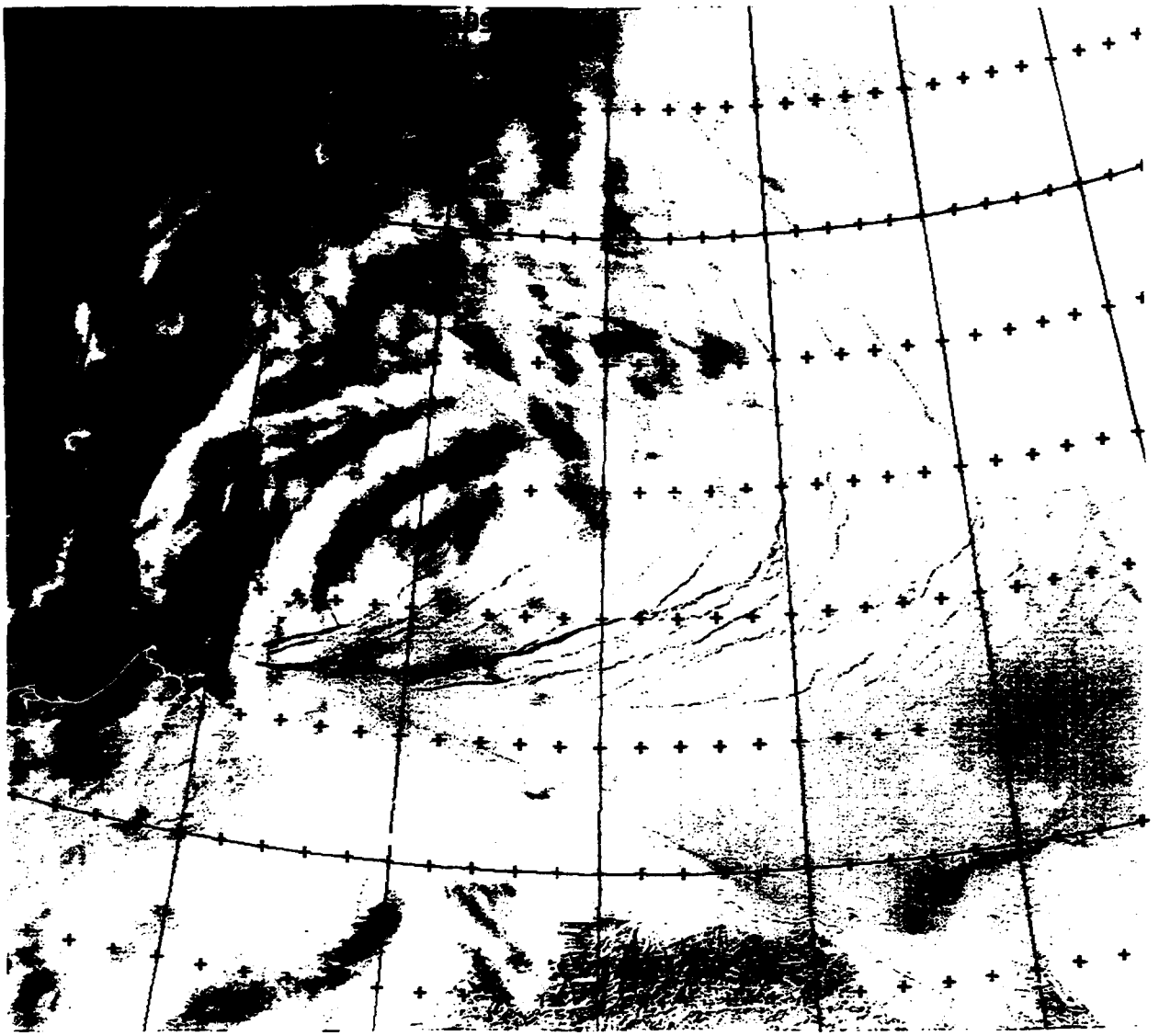

FIG 4. DMSP visible data. 24 March 1992, 1723 UTC.

Cyclonic activity is evident as implied by the cloud band curvature in Fig 4. Such cyclonic activity is also verified on the NORAPS 925 mb analysis for 25 March at 0000 UTC (Fig 5). This analysis shows a low pressure trough extending north of Barrow and eastward along the North Slope. Note the strong southeasterly winds east of the trough on this analysis.

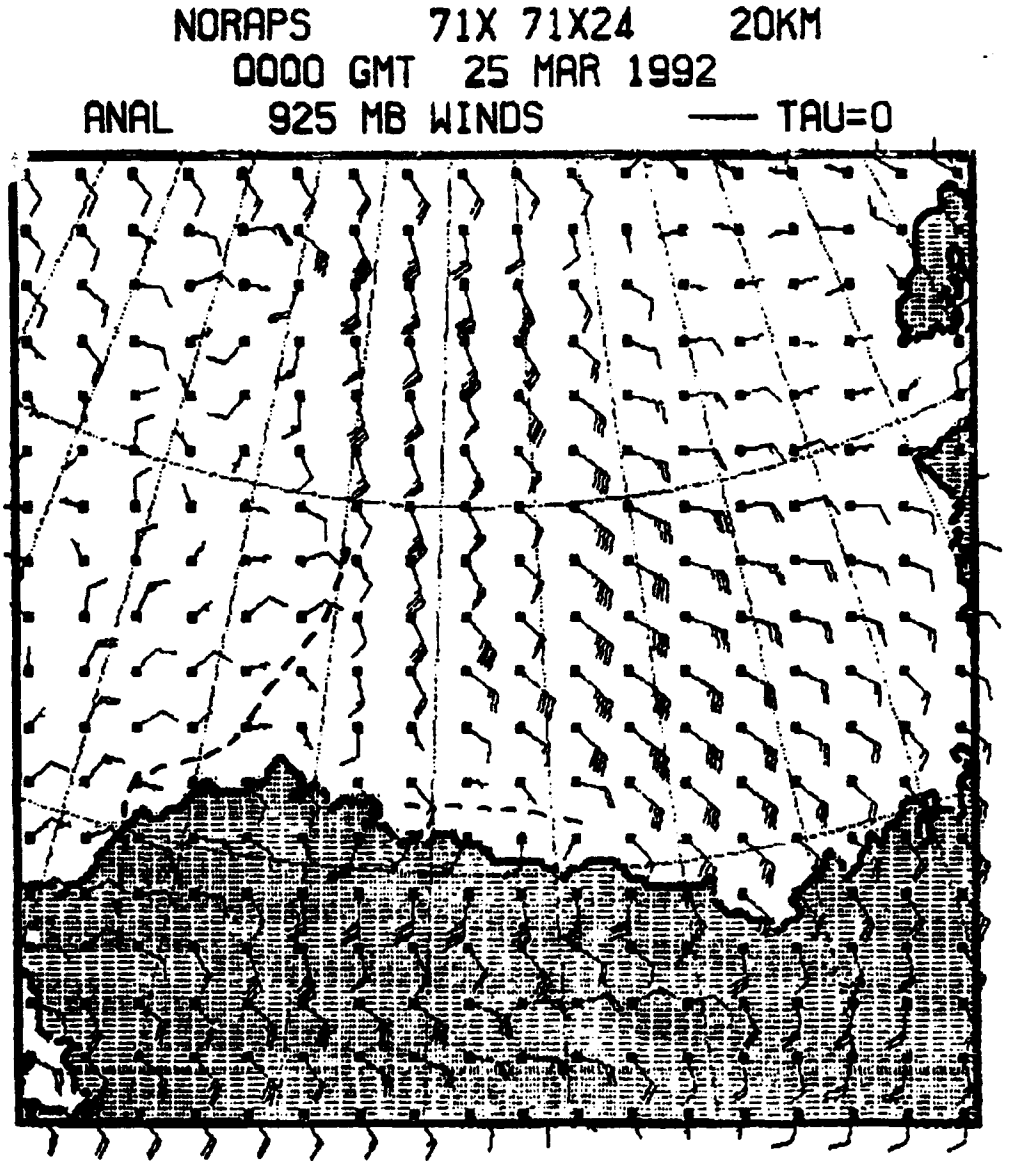

FIG 5. Navy SOCMM 925 mb analysis. 25 March 1992, 0000 UTC.

Fig 6 shows SAR data received on 24 March at 2129 UTC. These data are centered near 71.6°N, 147°W, and show the major lead openings in that region. The three leads shown in the SAR data are visible in the DMSP data (Fig 4) diverging from one another toward the east, as they do in the SAR imagery.

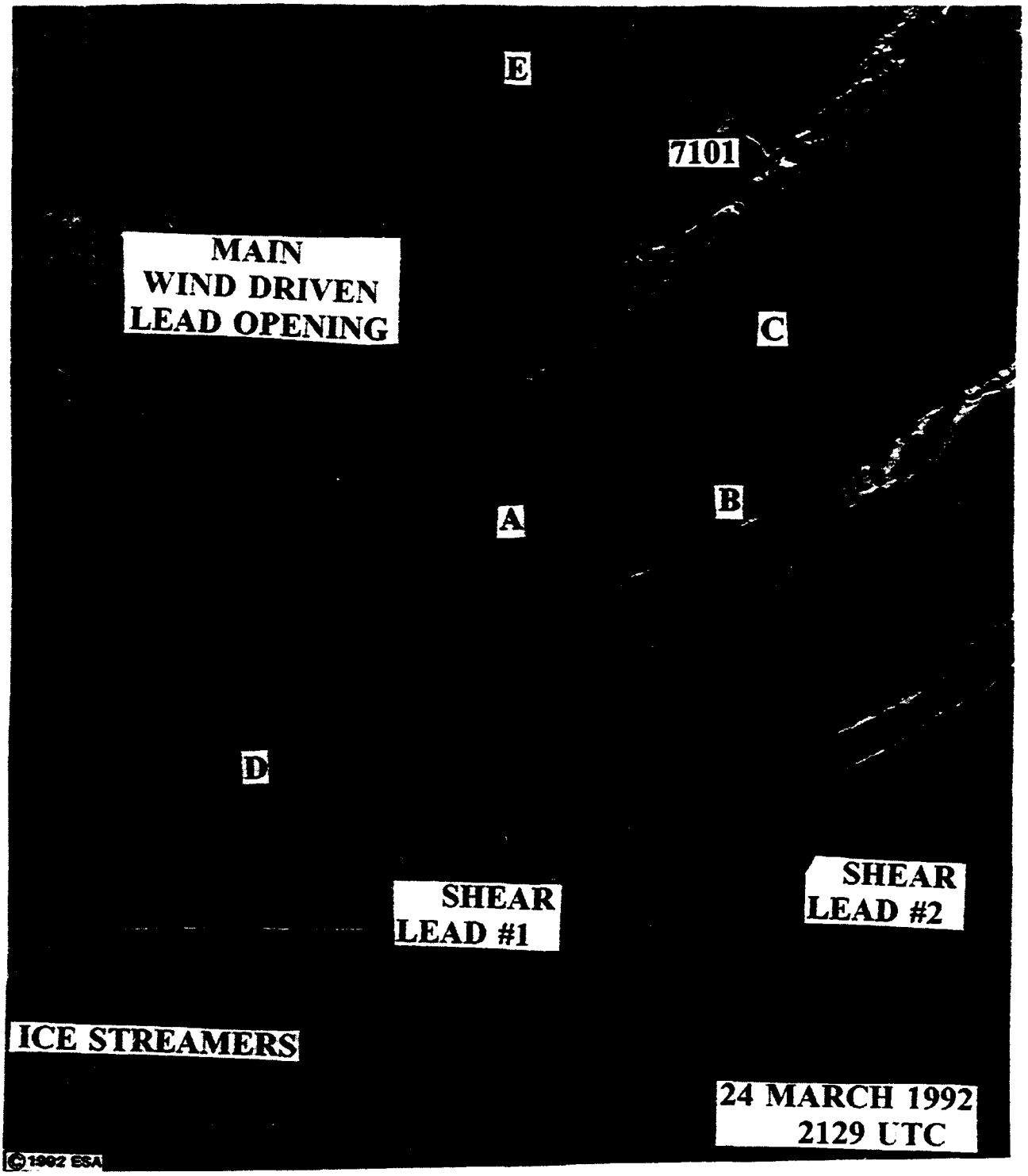

FIG 6. SAR data. 24 March 1992, 2129 UTC.
© 1992 ESA; used by permission.

In comparing the SAR data of Fig 6 with that of Fig 1 it can be seen that the leads have formed roughly along the dashed lines as earlier indicated in Fig 1; however, the nature of the lead formations south of the larger lead appears to have been shear - induced rather than wind driven. In particular the southern portions of multiyear floes A, B, C, and D, have all sheared off and moved eastward without moving appreciably southward to permit a larger lead opening. The ability of the leads to separate further was undoubtedly prevented by the strong wind stress from the SE existing at this time and the apparent inability of floes to the north to move further northward. Some grounding of floes A, B, C, and D, north of the shear leads may have been involved.

In contrast to the shear leads, the major lead to the north has opened significantly, and, in the process, has caused a fracture and northwestward movement of the northern portion of multiyear floe A of approximately 3 km. Further to the southwest the opening of the lead reaches a maximum width of about 5 km. This lead was later investigated by Leadex research personnel who named the lead "Husky 1".

The question immediately arises as to the cause for the heightened reflectivity of features of the leads in the northeast region. It has been suggested that such heightened reflectivity may be the result of Bragg scattering of wind roughened water in a relatively high wind speed area. Since ice station 7101 was reporting SE winds at about 15 kts the hypothesis of Bragg scattering as a cause for the heightened reflectivity does not seem unreasonable. Open water regions in SAR imagery which, under calm conditions appear black, would reverse tonality and appear very bright. It is important to realize, however, that leads, once open in below freezing conditions, refreeze very rapidly. Refrozen areas in the -16°C temperature which prevailed at the time, also would appear brighter in the SAR data, making it difficult to isolate a specific cause, lacking in-situ observations. The eastern portions of shear lead #1 and shear lead #2 show a consistent bright return which may be related to Bragg scattering or return from areas of refrozen ice. The main lead near buoy 7101 shows a much more complicated pattern of brighter and darker tones. It is possible and even probable that additional factors are influencing the radar return in that region. A rafting of ice floes within the lead and ridging of ice along the northern and southern boundaries are potential causes for heightened reflectivity.

Fig 7 (opposite page)is an aerial photograph of a lead extending eastward in the southern Beaufort during spring 1991 (the early test phase of Leadex), in which some jagged edges of ice floes in a rafted condition are shown. Note also the pressure ridges and shadows apparent on the north and south side of this lead indicating a ridge height of at least a meter or more, judging from the 7000 ft altitude from which the photo was taken. Such features would cause a very bright SAR return of the type and intensity shown in Fig 6.

One final possibility should be mentioned that has a demonstrated effect on a heightened SAR signal. "Frost flowers" have been identified as a cause of heightened SAR reflectivity. Such features develop over refrozen leads when the ice is generally greater than 10 cm thick in temperatures of -18°C or less. The "flowers" consist of low salinity water and rise out of the ice in stems extending to as much as 3 cm. Supercooled cloud plumes generated from open portions of a lead may contribute to rapid frost flower development.

It is likely that one or more of the above mentioned factors were involved in the heightened reflectivity noted in the leads of Fig 6. Obviously more research is required to ferret-out the predominant cause or causes.

FIG 7. Aerial photograph of a refrozen lead in the south-central Beaufort Sea. Spring 1992.

The tonality of the main wind driven lead in figure 6 changes from almost black on the south side (left of ice floe A) to a light gray shade on its northern border. This change in tonality suggests open (non-roughened) water on the south edge giving way to thin nilas and gray ice on the north side. Such an arrangement is typical of ice formation in a lead under persistent light flow from the southern quadrant. Fig 8 is an aerial photograph of what is believed to be a similar type of ice formation over a southwest-northeast oriented lead, observed over the southern Beaufort during spring of 1991. The ice streamers in the center portion of the photograph are aligned with the wind flow coming from the left (south) side of the image.

FIG 8. An aerial photograph of a SW-NE oriented lead in the south-central Beaufort Sea. Spring 1991.

Using the above "ice streamer" concept to infer wind direction from imagery data, and testing its application to SAR data, a feature of great interest appears in the lower left corner of Fig 6. In this region what appears to be ice streamers have formed as resolved by the SAR data. The SAR data are much coarser resolution (100 m) than the aerial photographic view so that individual lines of ice are not resolved; However, the pattern and configuration of the SAR view is very suggestive of this effect. (Higher 10 m resolution SAR dat have clearly revealed such streamers in other areas). The streamers at this time according to the above interpretation indicate a light north-northwesterly wind flow over the ice at that location. At about the same time ice station 7101 was recording southeast winds at 15 kts. The separate indications imply a low pressure center located very near the left center portion of the SAR image.

The center was analyzed on the NWS surface analysis for 25 March at 1200 UTC (Fig 9), approximately 15 hours after the time of the SAR data (NWS did not have real-time access to the buoy data and constructed this analysis without the buoy reports which have

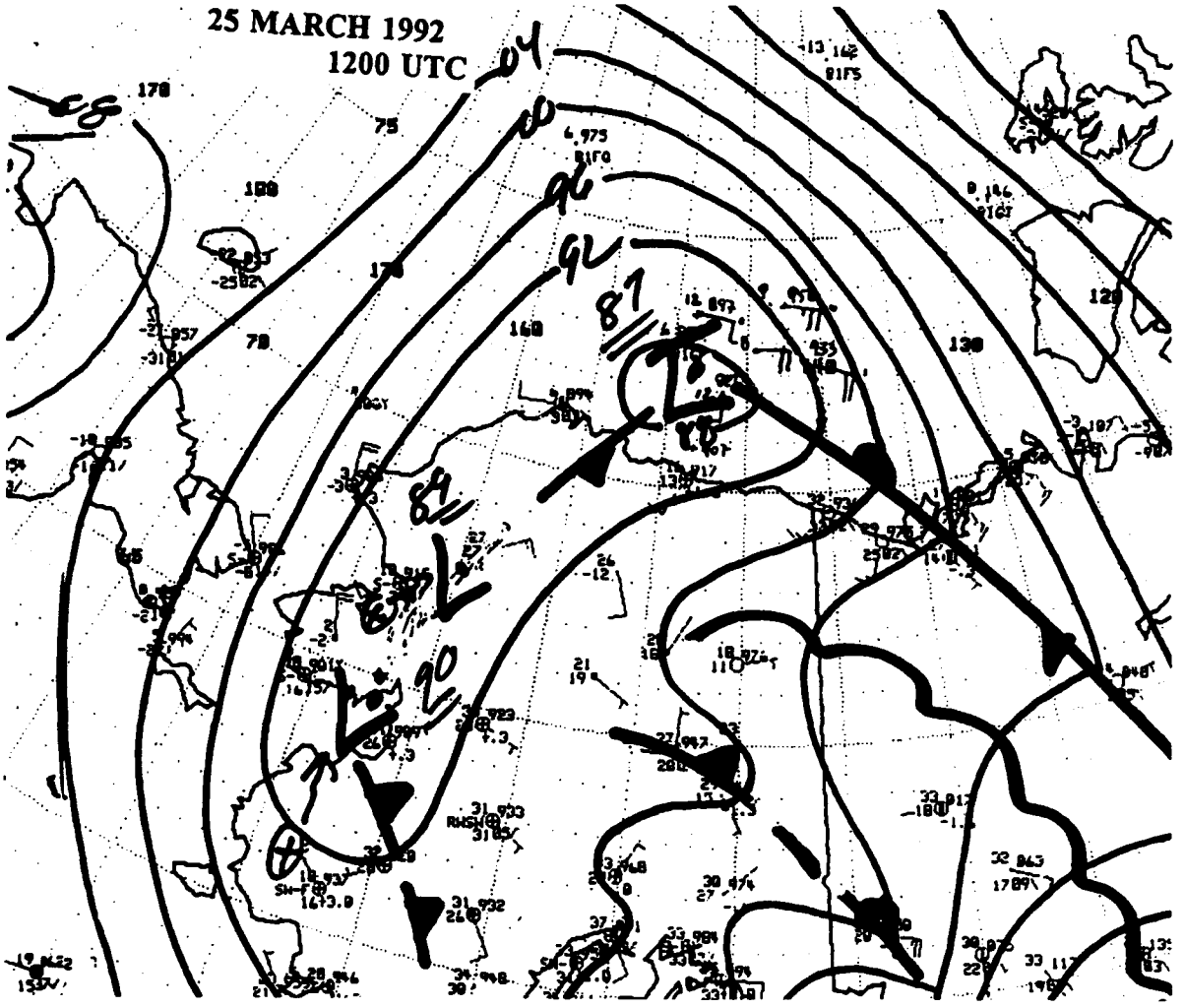

FIG 9. NWS (Anchorage) surface analysis. 25 March 1992, 1200 UTC.

since been superimposed on the analysis). However, DMSP and NOAA satellite data gave clear evidence of a low center formation in the region much earlier (shortly after 25/0000 UTC).

Fig 10 is a NOAA infrared satellite image showing clear evidence of the low formation on 25 March at 0532 UTC. This image was, in fact, sent by facsimile to Deadhorse with the caption, as shown, indicating "LOW MVG THRU ICE CAMP AREA". Development and movement of this low was not classical. It appeared to form in the northern lee of the Brooks Range and then move rapidly north-northwestward passing west of the ice camp location in the space of only a few hours. A secondary low is also apparent in this image forming just north of Barrow, Alaska.

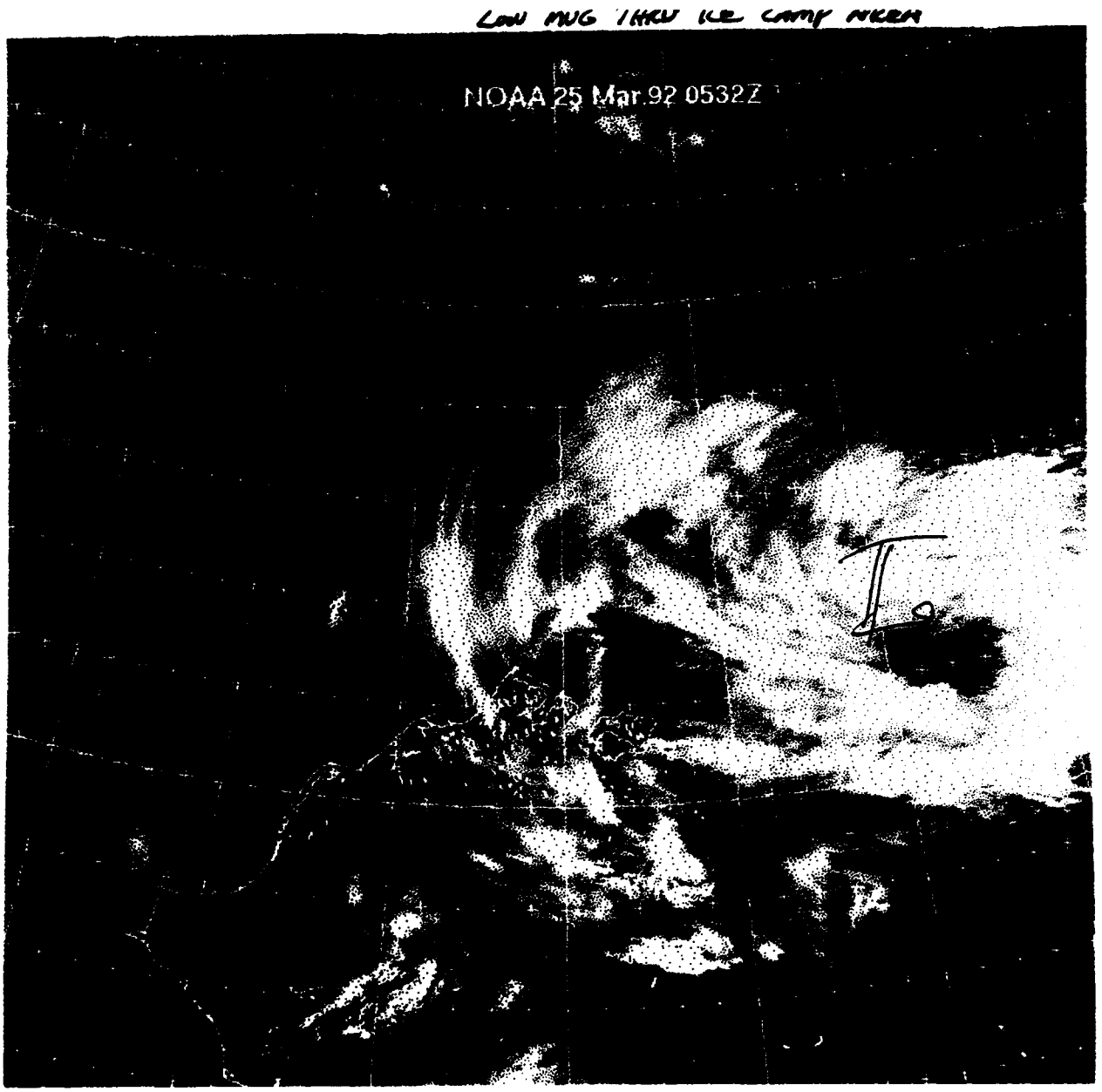

FIG 10. NOAA infrared (Ch4) data. 25 March 1992, 0532 UTC.

The low pressure system continued its northward movement throughout the 25th of March. Buoy winds remained southerly during this period. A NOAA infrared image transmitted to Deadhorse based on a 1606 UTC observation (Fig 11) noted "Many New Major Lead Openings" in the region between Deadhorse and the ice camp. The low center in this image is implied near 74.5°N, 151.5°W.

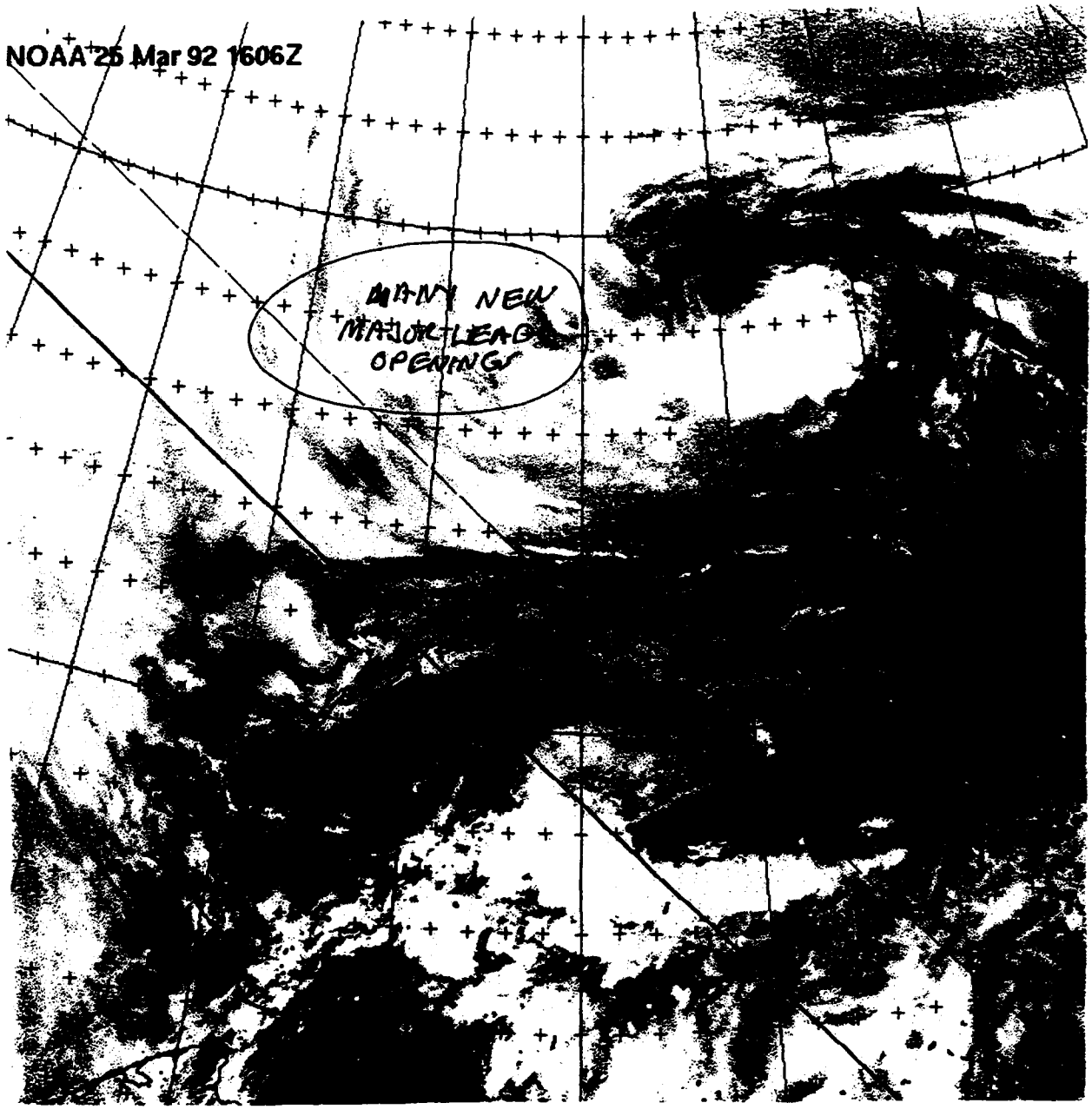

FIG 11. NOAA infrared (Ch4) data. 25 March 1992, 1606 UTC.

The NWS surface analysis on the following day, 26 March at 0600 UTC (Fig 12), shows buoy winds shifting to westerly south of the low center (the low center analyzed independently of the buoy reports which were later superimposed). By 1800 UTC the 26 March surface analysis (not shown) reveals northerly winds at all locations except one which reported calm. The low center at this time had moved north-northeastward to near 77°N, 143°W.

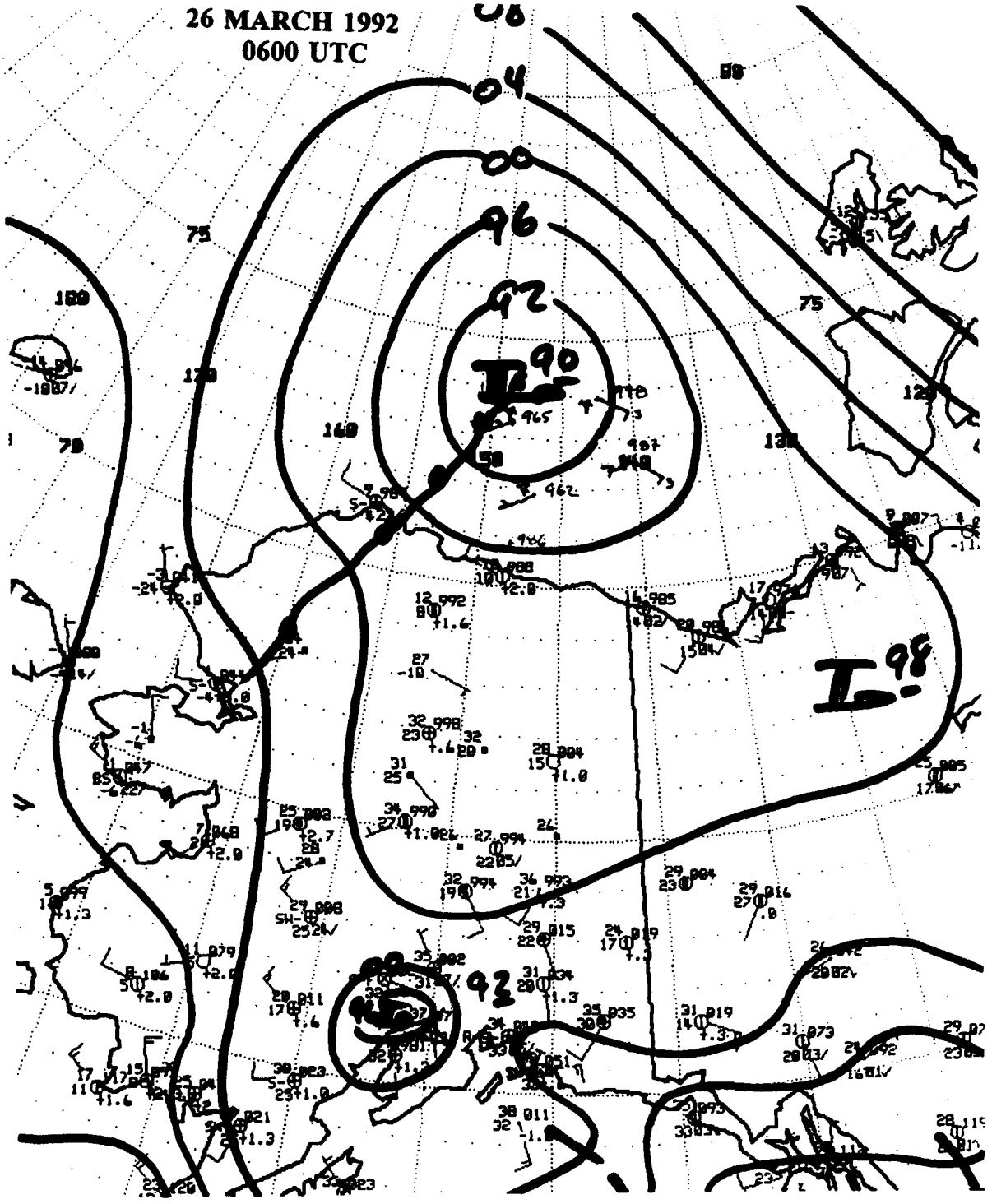

FIG 12. NWS (Anchorage) surface analysis. 26 March 1992, 0600 UTC.

The buoys changed direction almost immediately with the wind reversal even though wind speeds were quite light. Fig 13 shows the track of buoy 7101 from 24 to 28 March 1992. The sudden northwestward excursion of the buoy commencing with the strengthening east-southeasterly winds early on 24 March is notable, as well as the reversal in direction starting on the 26th of March. The northwest movement of the ice in east-southeasterly flow is consistent with the generally accepted observation that ice tends to move in a direction 30-40° to the right of the surface wind direction.

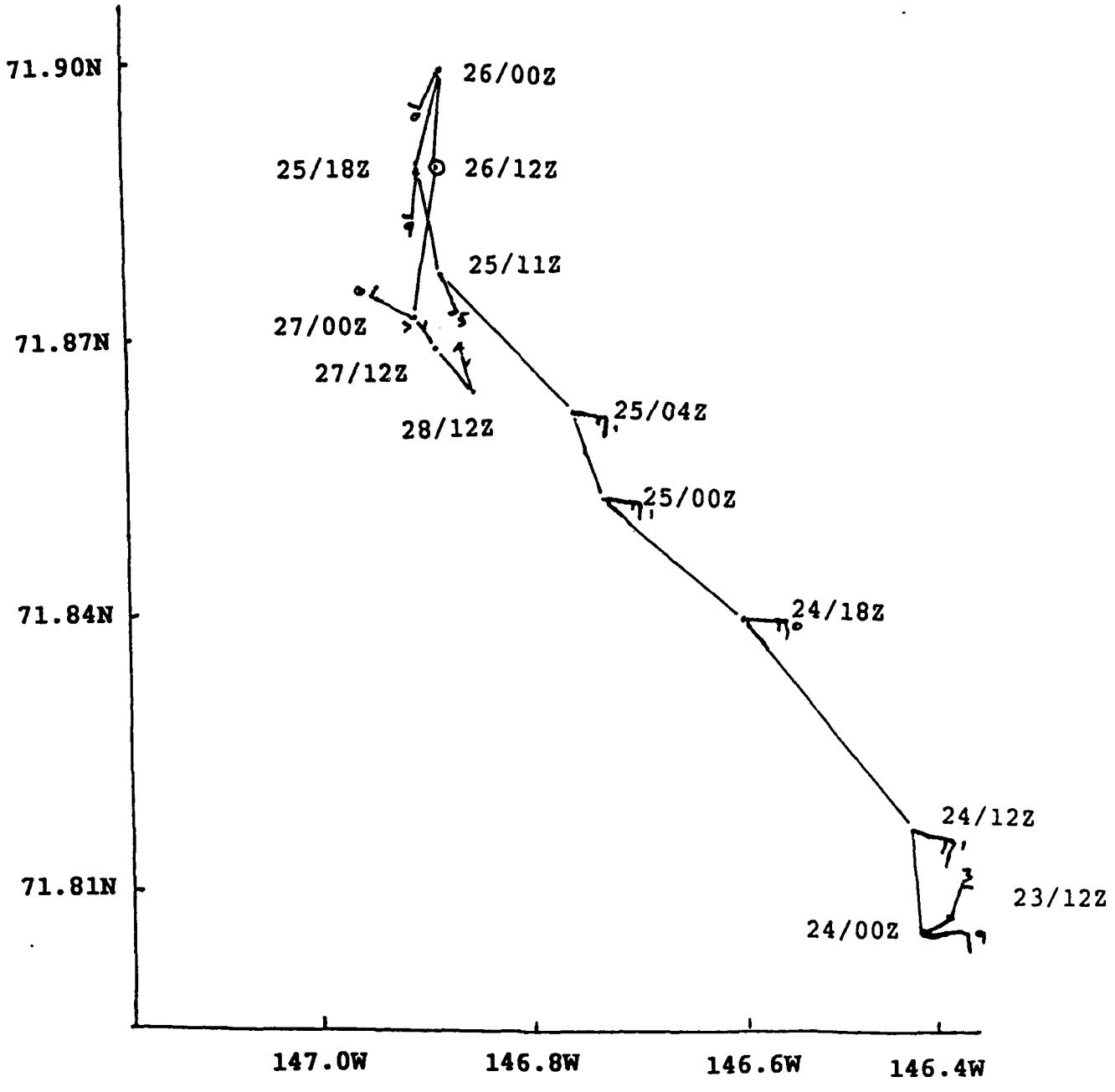

FIG 13. Track of buoy 7101 from 24 to 28 March 1992.

The next available SAR image over the area was on 27 March at 2129 UTC (Fig 14). This image reveals that the main wind driven lead to the north has largely closed to a maximum width of only 1 or 2 km and appears to be largely refrozen. This conclusion is based on the fact that winds were nearly calm over the area at this time; open water under such conditions should appear black; nevertheless the lead is moderately reflective. A newly formed thin ice condition could explain the increase in reflectivity. The fact that even higher reflectivity, such as appears in figure 6, is not observed also suggests that frost flower development or rafting was not a prevalent condition within the lead at this time.

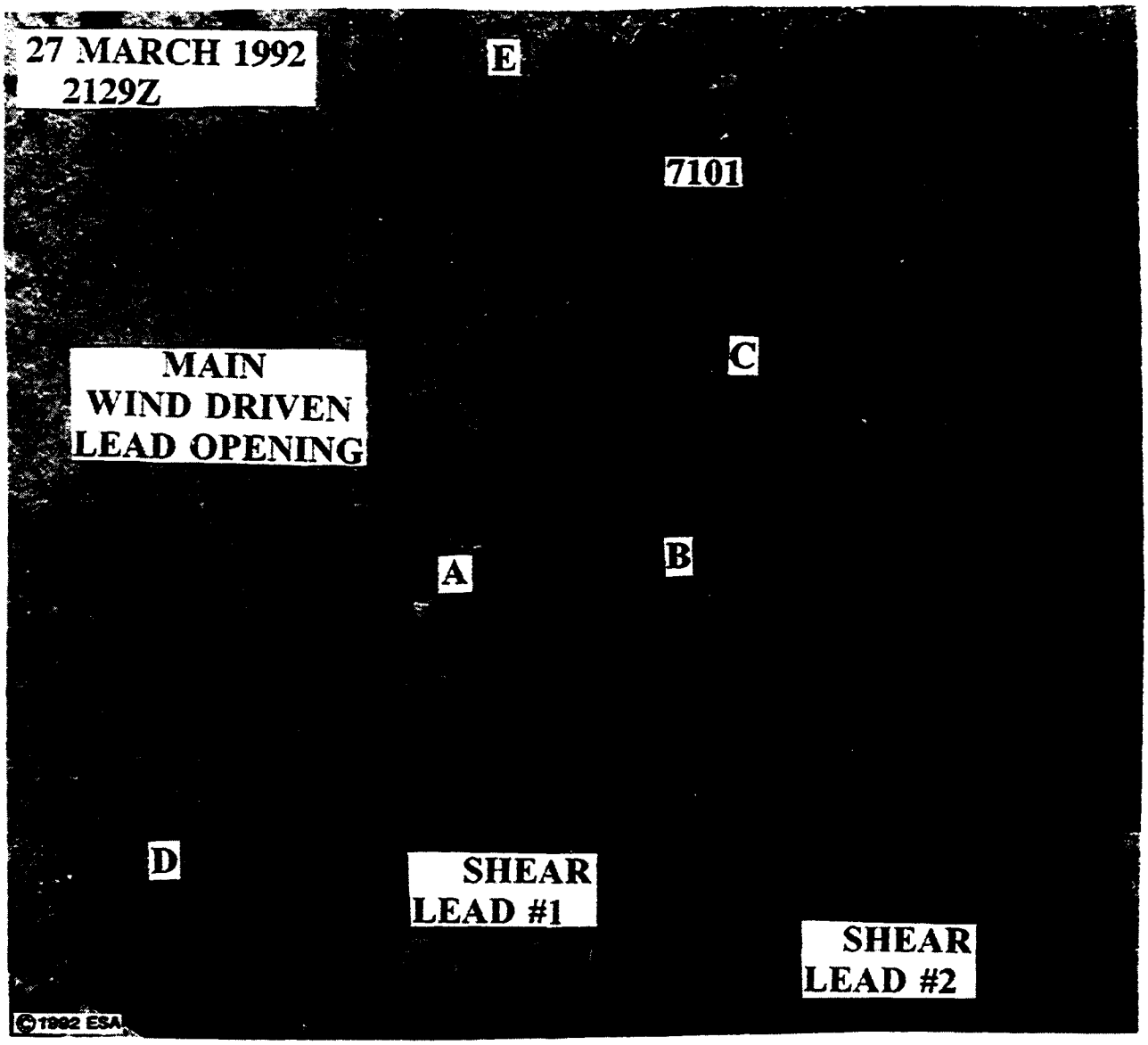

FIG 14. SAR data. 27 March 1992, 2129 UTC.
©1992 ESA; used by permission.

In comparing this image with that of Fig 1, which shows the ice area before lead formation, it can be seen that the ice floes to the north have not come back precisely to their positions before the break. They have shifted somewhat to the west relative to the position of floes A and D. Conversely, ice floes on the south side of shear lead #1 and shear lead #2 have shifted eastward in relative position by almost 10 km. A detailed description of the absolute and relative motions involved is certainly warranted but beyond the scope of this present study.

IMPORTANT CONCLUSIONS

1. SAR data are extremely useful in monitoring the opening and closing of lead formations and especially the effect of storms on lead formation.

2. Lead formation can be detected under clear sky conditions in DMSP and NOAA satellite data.

3. Ice streamers can sometimes be detected within leads in SAR data. Such features can provide useful information on wind direction existing in such areas.

4. During the process of lead formation highly reflective SAR signals may be attributed to a number of causes, not necessarily mutually exclusive. These include:

a. Bragg scattering producing a strong SAR signal due to reflection from capillary wave action in a moderate to high wind speed condition over open water.

b. Rafting of ice floes and ridging of ice along the edges of leads.

c. Frost flower formation over a refrozen lead.

5. Lead formation can occur very rapidly following the onset of sustained winds of 10-15 kts or greater.

6. Leads can close as rapidly as they open following a reversal in wind direction.

7. Most important, low pressure systems moving over the Beaufort can be responsible for opening significant leads. Opening of the lead can be observed in southerly flow on the east side of the low. Closing of the lead can be anticipated when the low moves eastward or northward to permit northerly or northwesterly flow into the area.

THIS PAGE DELIBERATELY LEFT BLANK

5. SCREAMING EAGLES OF THE NORTH. 29 - 31 MARCH 1992.

Easterly waves in tropical latitudes can frequently be identified in satellite imagery by cloud patterns taking the shape of an "inverted-V" cloud formation (Frank, 1969), or as they are called by forecasters in the Pacific, "screaming eagles" (Fett, et al, 1979).

This study documents a northwesterly moving disturbance over the southern Beaufort Sea that resembled the "inverted-V" and "screaming eagle" cloud formations of tropical latitudes - hence the term "screaming eagles of the north".

29 March 1992

The NWS (Anchorage) surface analysis on this date for 1800 UTC (Fig 1) revealed an inverted trough extending northward through central Alaska, approaching Barter Island on Alaska's North Slope.

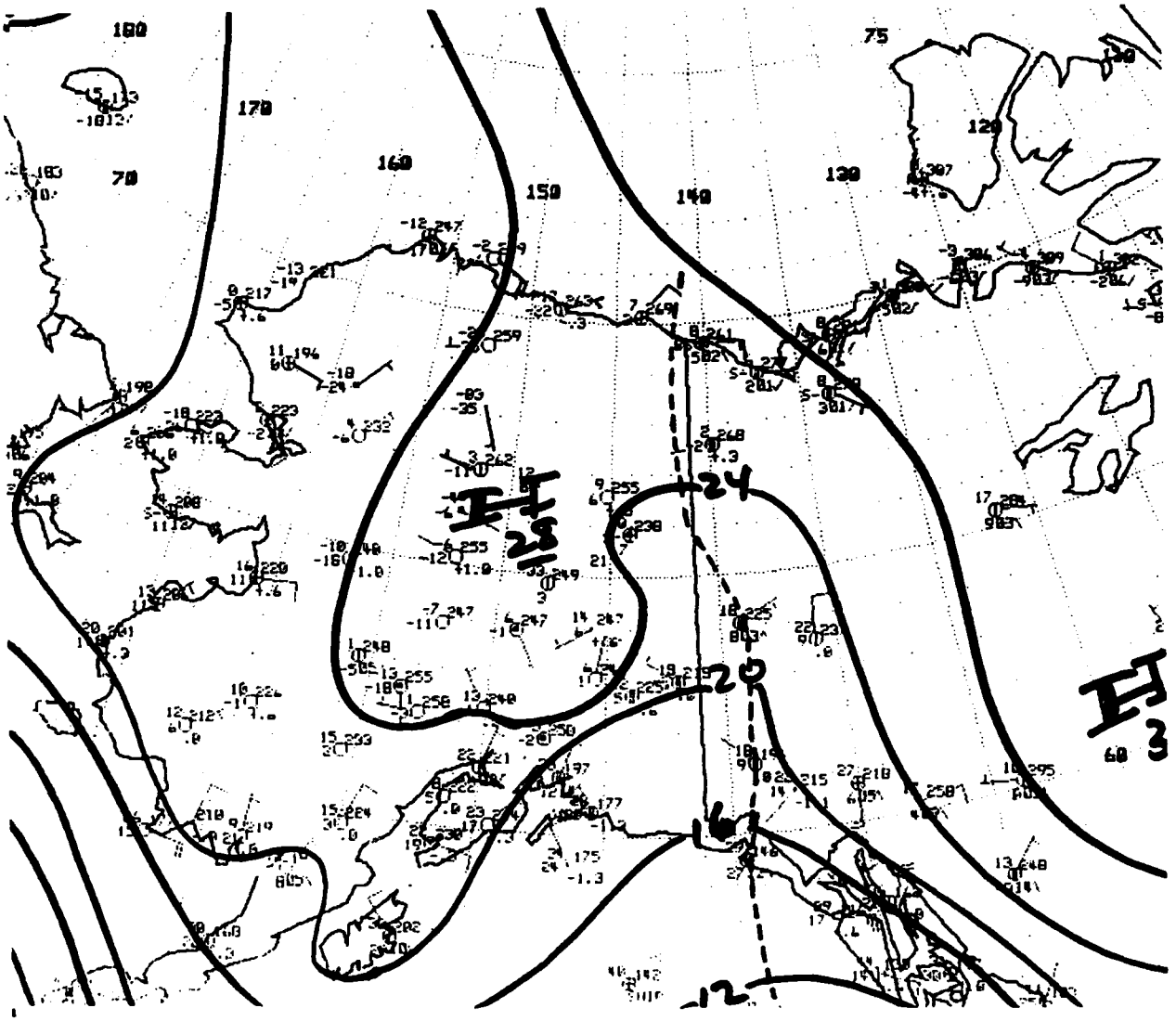

FIG 1. NWS surface analysis. 29 March 1992, 1800 UTC.

A DMSP visible image acquired on 29 March at 1942 UTC (Fig 2) reveals a disturbance in that region bearing a striking resemblance to "screaming eagle" cloud formations often observed in tropical latitudes. The "wing-like" flare of clouds turning anticyclonically northward over the Beaufort Sea is part of the distinctive signature of such disturbances.

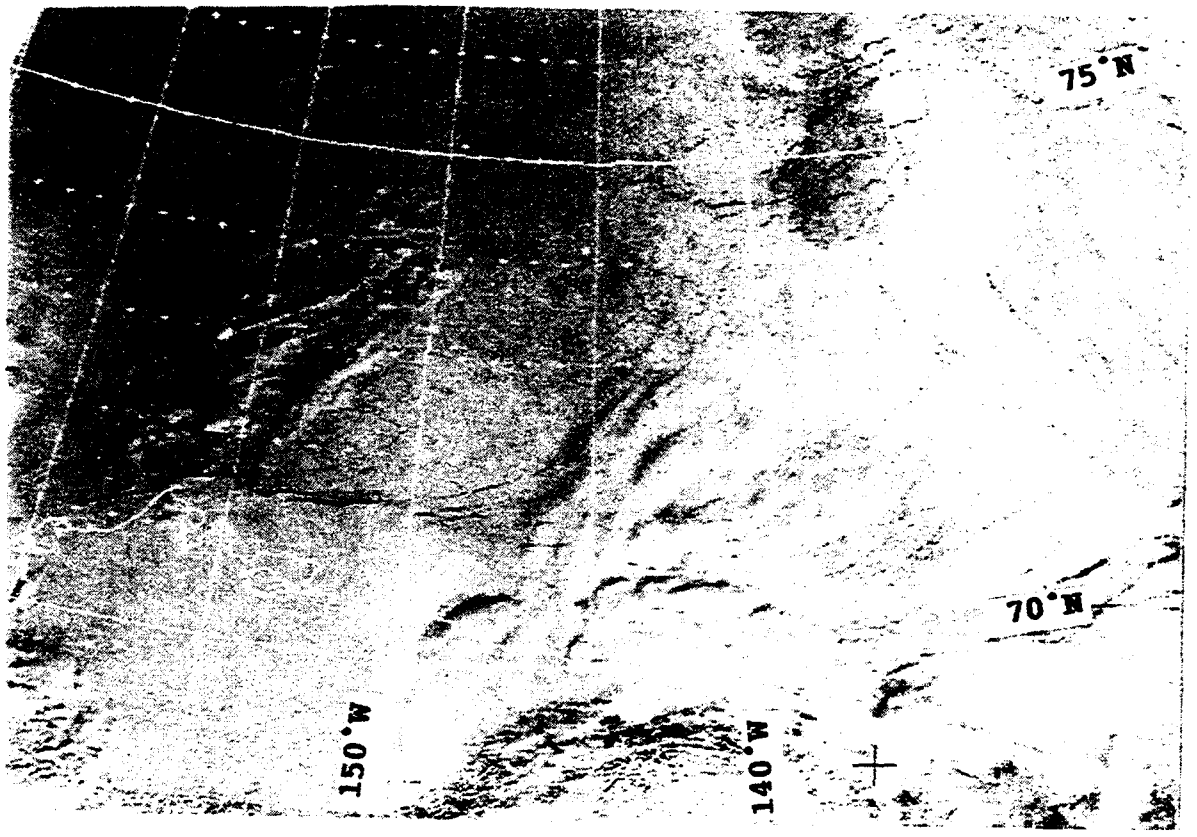

FIG 2. DMSP visible data. 29 March 1992, 1942 UTC.

The "inverted-V" aspect of the cloud formation is more clearly revealed in a NOAA infrared (Ch4) view obtained a few hours later at 2333 UTC (Fig 3). In this image two branches of the cloud formation form an inverted-V shape just north of Barter Island.

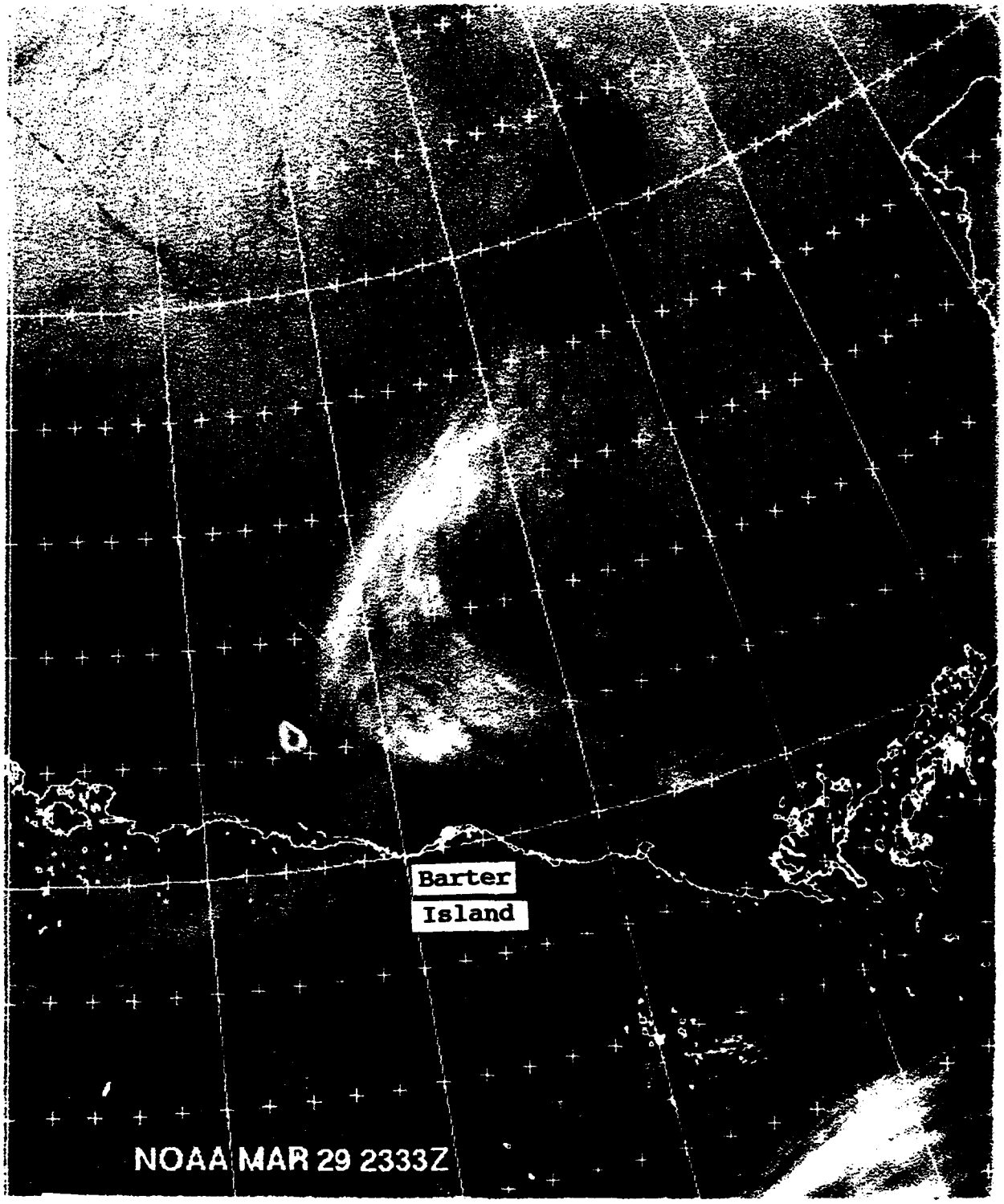

FIG 3. NOAA infrared (Ch4) data. 29 March 1992, 2333 UTC.

30 March 1992

A dramatic DMSP 1/3 nm visible image of the system acquired on 30 March, 0204 UTC,(Fig 4), compliments the NOAA infrared view of Fig 3. Small details of features in the ice pack are revealed in this image. In particular, note that the "tadpole" ice feature just north of the Leadex ice camp can be discerned (See Section 2 for a discussion of this feature).

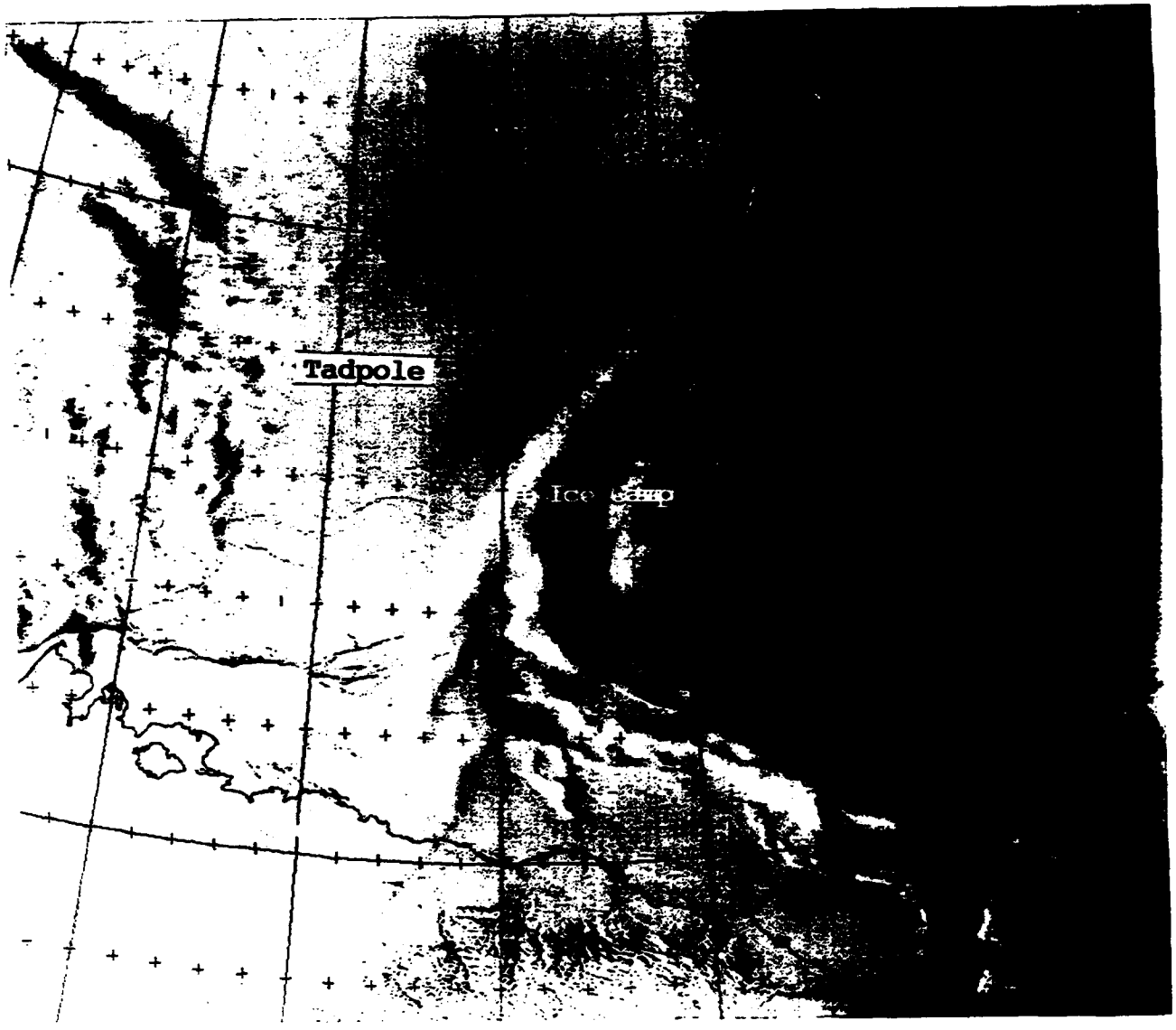

FIG 4. DMSP visible (1/3 nm resolution) data. 30 March 1992, 0204 UTC.

The relatively sharp leading edge of the inverted-V cloud formation has the appearance of a cloud form being stretched in the deformation zone or col region of wind flow at that level. This suggestion is verified by the Navy's SOCMM 700 mb analysis (Fig 5) for 30 March 0000 UTC, which shows a deformation zone in the exact location of the system's leading edge. The cloud band is stretched north and south in response to the deformation pattern. Vorticity is maximized in this analysis south of the col region between Barter Island (near 144°W) and Prudhoe Bay (near 148°W).

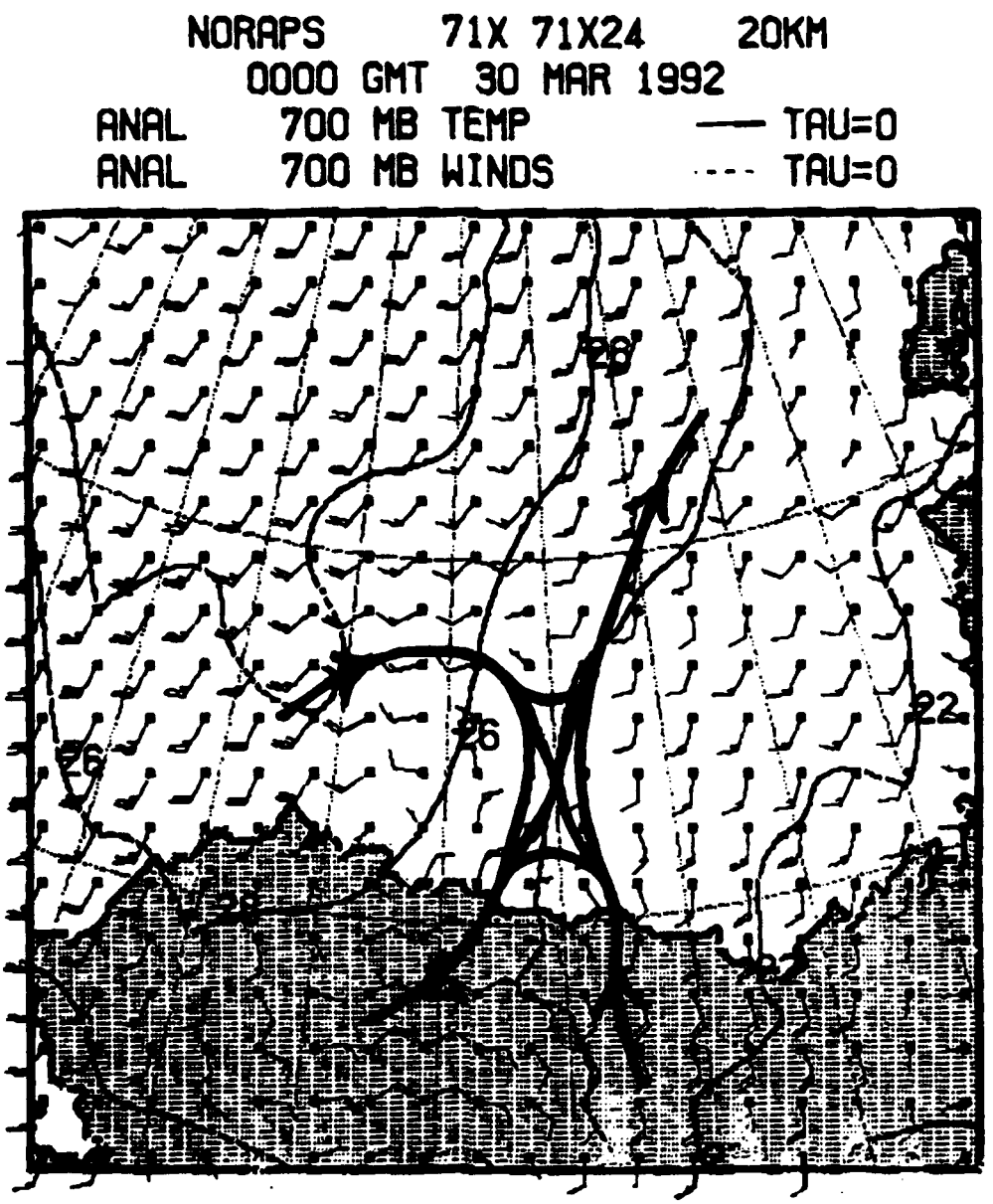

FIG 5. Navy Second Order Closure Mesoscale Model (SOCMM) 700 MB analysis. 30 March 1992, 0000 UTC.

The corresponding SOCMM 925 mb analysis (Fig 6) reveals a streamline trough or line of maximized vorticity along 147°W leading southward toward the Brooks Range. Note the anticyclonic circulation center near 75°N, 138°W. Waves in the tropics begin turning northward when they reach the western edge of such an anticyclonic cell in response to the prevailing southerly flow which acts as a steering current.

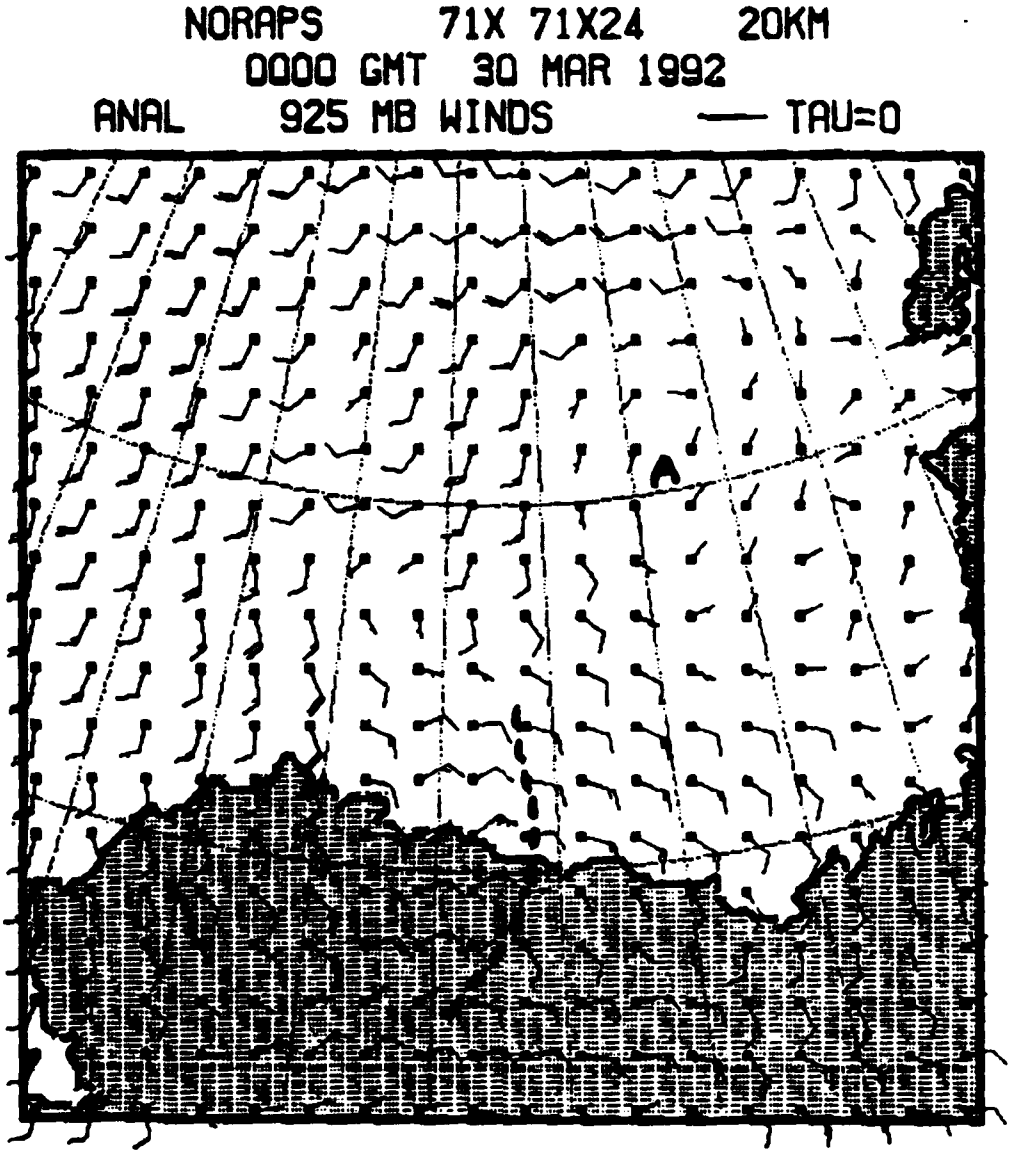

FIG 6. Navy SOCMM 925 mb analysis. 30 March 1992, 0000 UTC.

The next satellite view of the system occurred on 30 March at 0538 UTC (Fig 7). This DMSP infrared view shows the system retaining its appearance (in weakened form) as an inverted-V cloud formation. However, cold cloud development between 72° to 73°N along 140°W, to the east of the leading edge of the formation, is suspicious in the light of satellite views to follow, and may represent some incipient local cyclonic development.

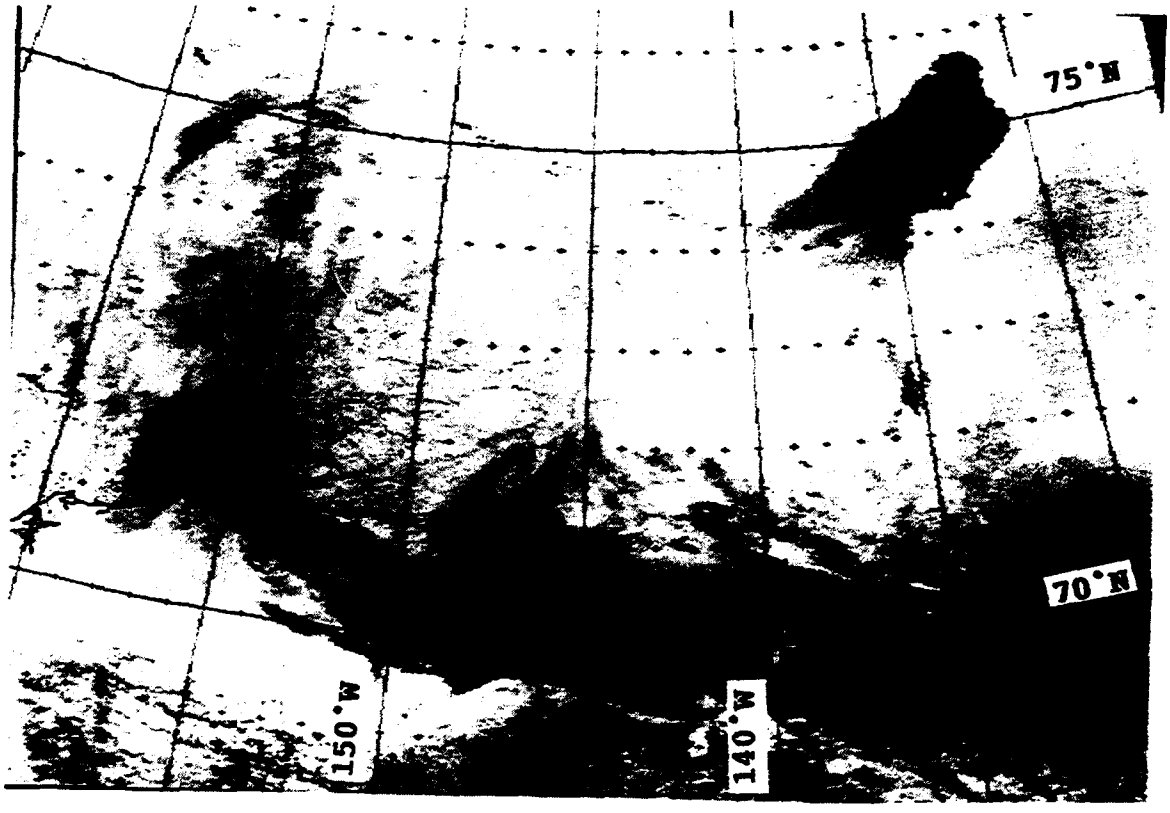

FIG 7. DMSP infrared data. 30 March 1992, 0538 UTC.

The NWS (Anchorage) surface analysis for 30 March at 0600 UTC (Fig 8)(about the same time as Fig 7) has been reanalyzed in the region of interest to reflect buoy and ice camp data not available at the original time of the analysis. The analysis shows that the wave trough has still not passed Barter Island, contrary to the implications of the SOCMM 925 mb analysis (Fig 6) six hours earlier. Buoy data in advance of the trough also substantiate the lack of further westward translation of the system.

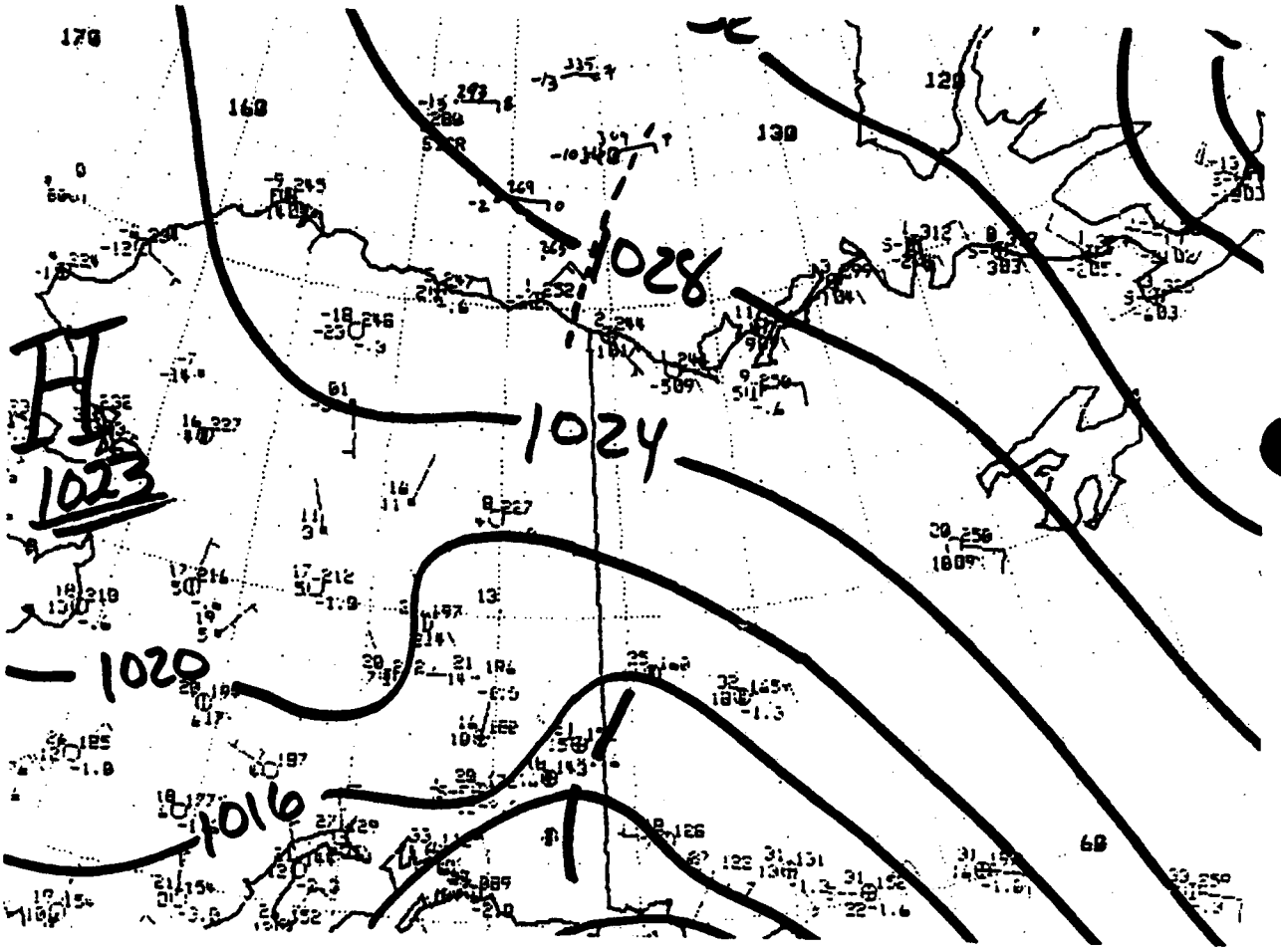

FIG 8. NWS (Anchorage) surface analysis. 30 March 1992, 0600 UTC.

The next available satellite view of the system was not obtained until about 8 hours later. This NOAA-11 infrared (Ch4) view (Fig 9) shows a comma-shaped feature just northeast of the ice camp on 30 March at 1327 UTC. This feature, although small, is the dominant feature of the central Beaufort Sea. The implication, based on preceding evidence, is that the system moved northward from incipient development as discussed in Fig 7 during the 8 hour interval between views. Extensive low level cloudiness appears south of the disturbance, evidence of a moisture flux into the southeasterly current which has been sweeping across the southern Beaufort Sea. There is also a suggestion of minor wave, inverted-V cloud formations, just north of the North Slope near 141.5°W and 151.5°W.

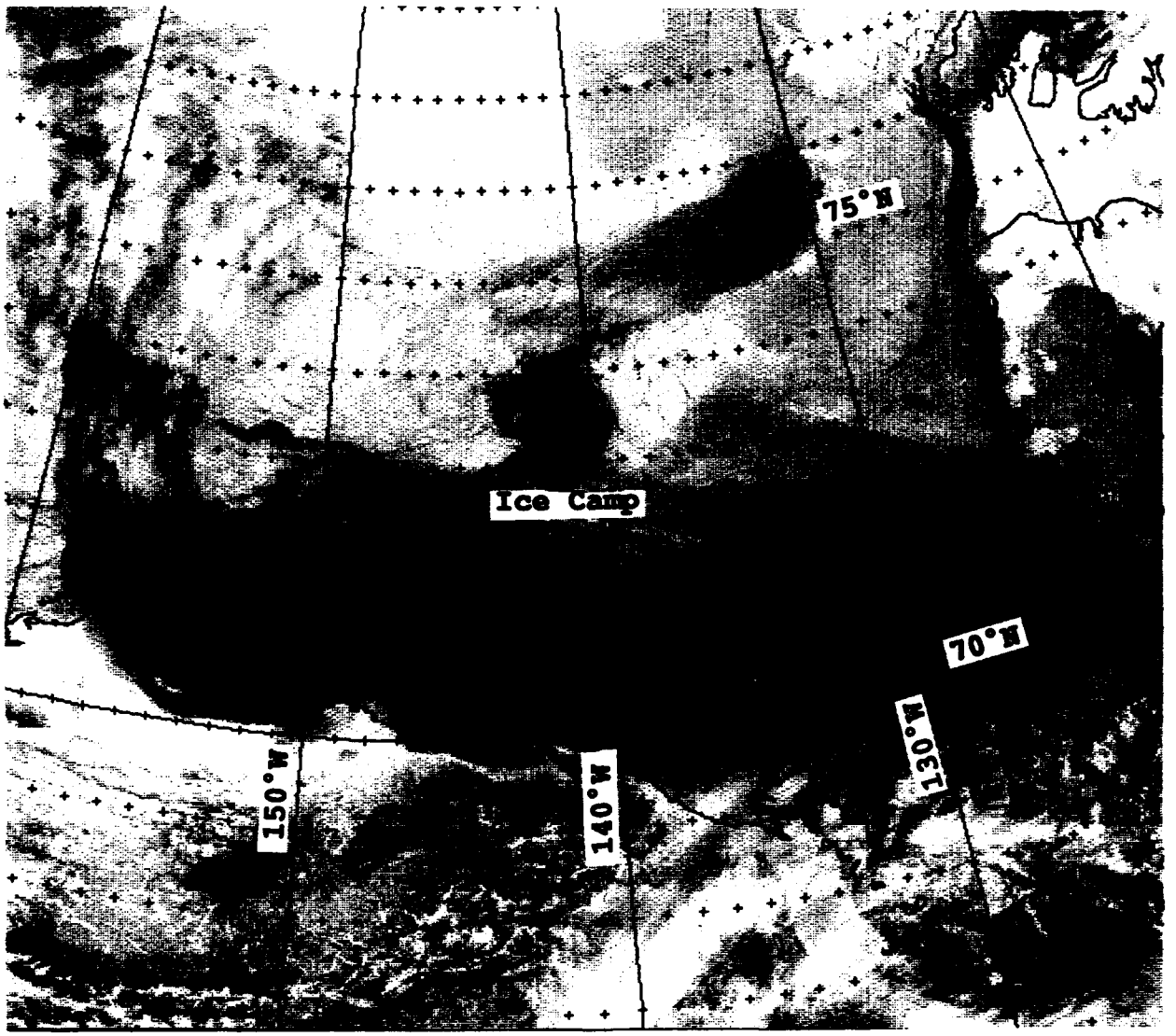

FIG 9. NOAA-11 infrared (Ch4) data. 30 March 1992, 1327 UTC.

The NWS (Anchorage) surface analysis for 30 March at 1200 UTC (Fig 10) again has been reanalyzed based on buoy reports to reveal probable trough location at this time. Density of observations is too sparse to provide information concerning the minor waves to the south.

The trough is seen to be approaching Deadhorse, with the comma-shaped disturbance at the northern end. The station, in fact, showed evidence of trough passage between 1300 and 1400 UTC, when winds shifted from 060° at 8 kts (1300 UTC) to 100° at 9 kts (1400 UTC).

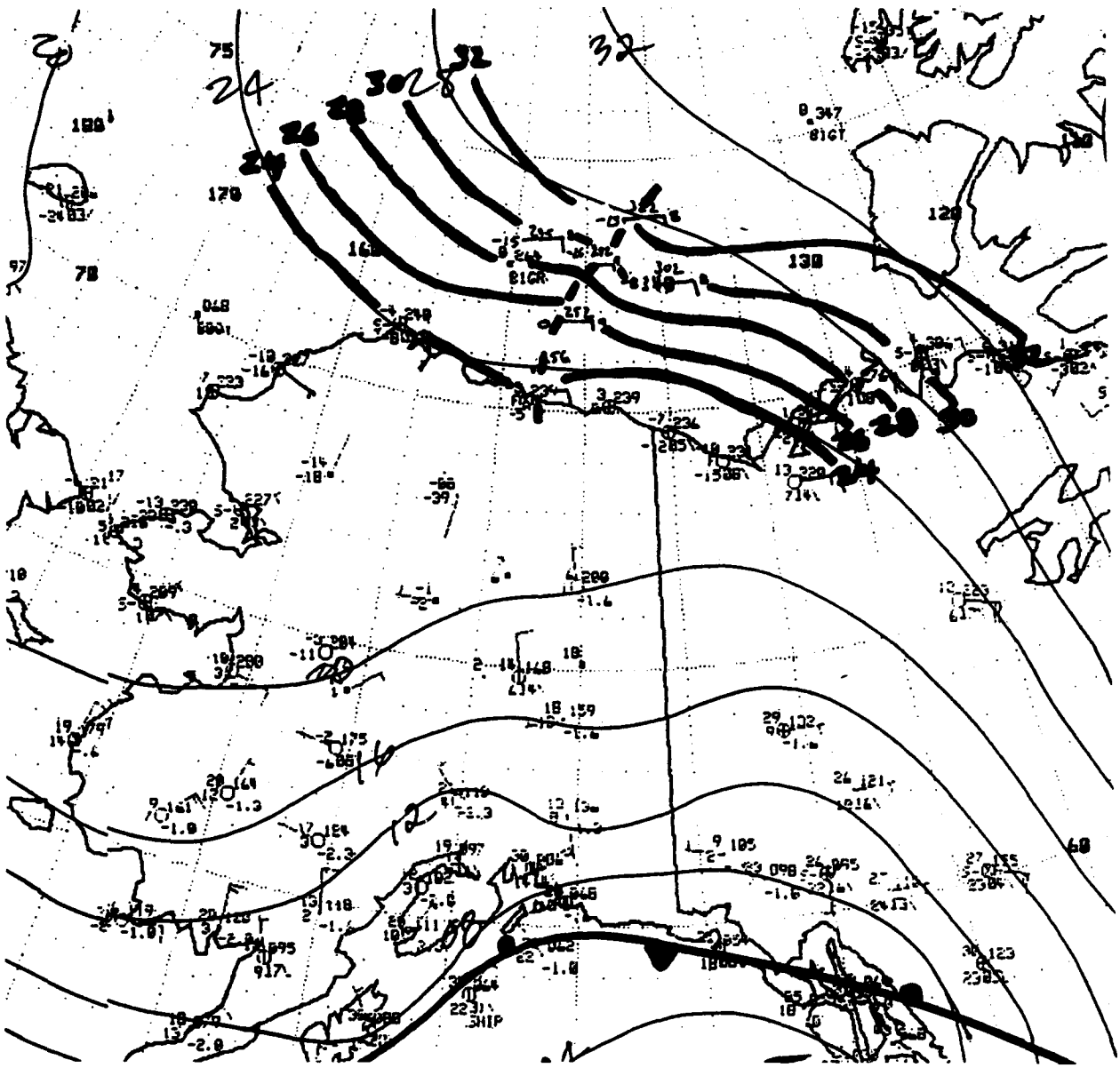

FIG 10. NWS (Anchorage) surface analysis. 30 March 1992, 1200 UTC.

The feature is much more pronounced, however, on the SOCMM 700 mb analysis (Fig 11). If one relates the trough position shown on this analysis to the position of the comma-shaped feature shown in Fig 9 it will be seen that the trough lies precisely along the western edge of the disturbance in the manner of an easterly wave.

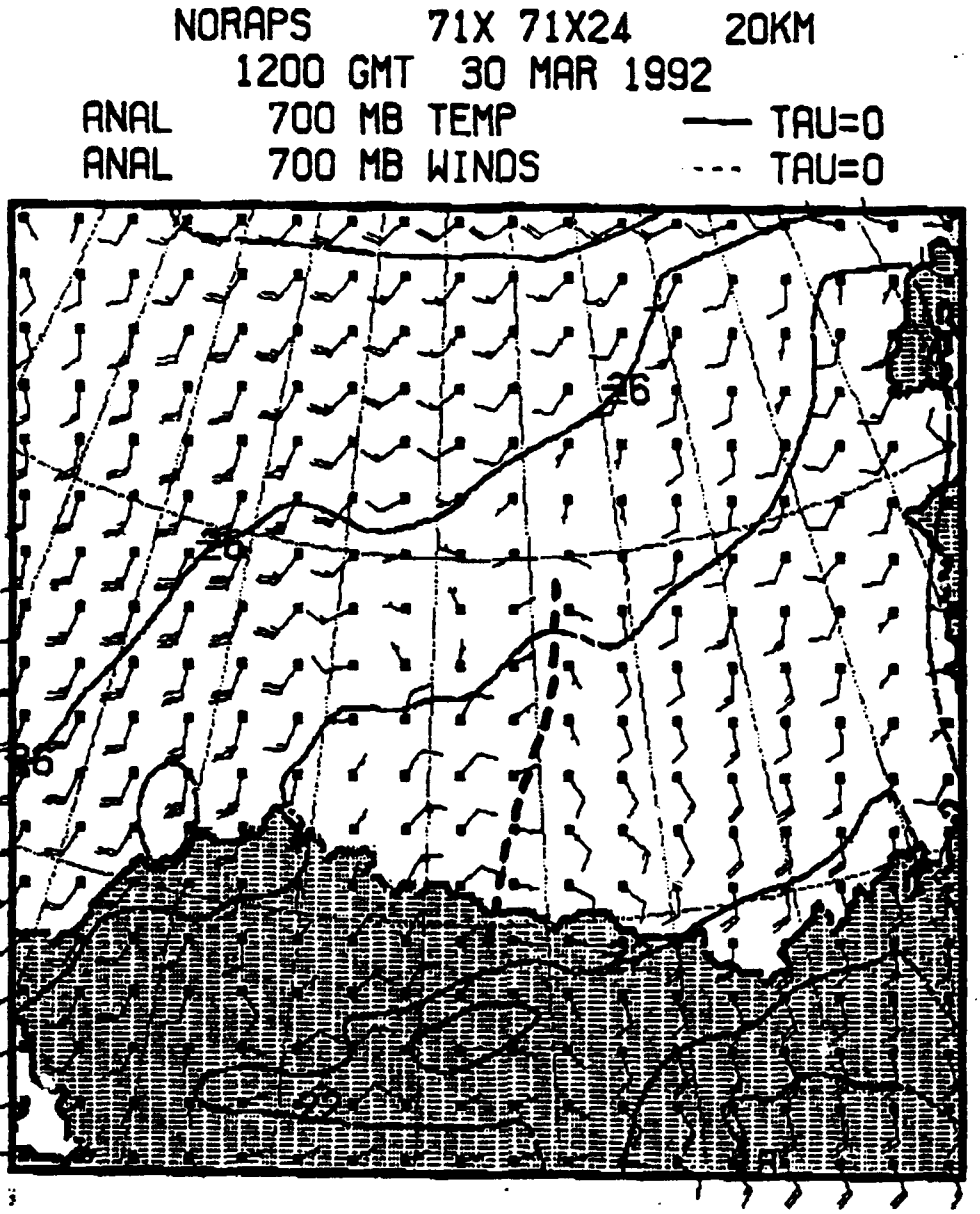

FIG 11. Navy SOCMM 700 mb analysis. 30 March 1992, 1200 UTC.

The system started moving more westerly at this time and is shown in NOAA infrared (Ch4) imagery almost due north of the ice camp on 30 March at 1506 UTC (Fig 12).

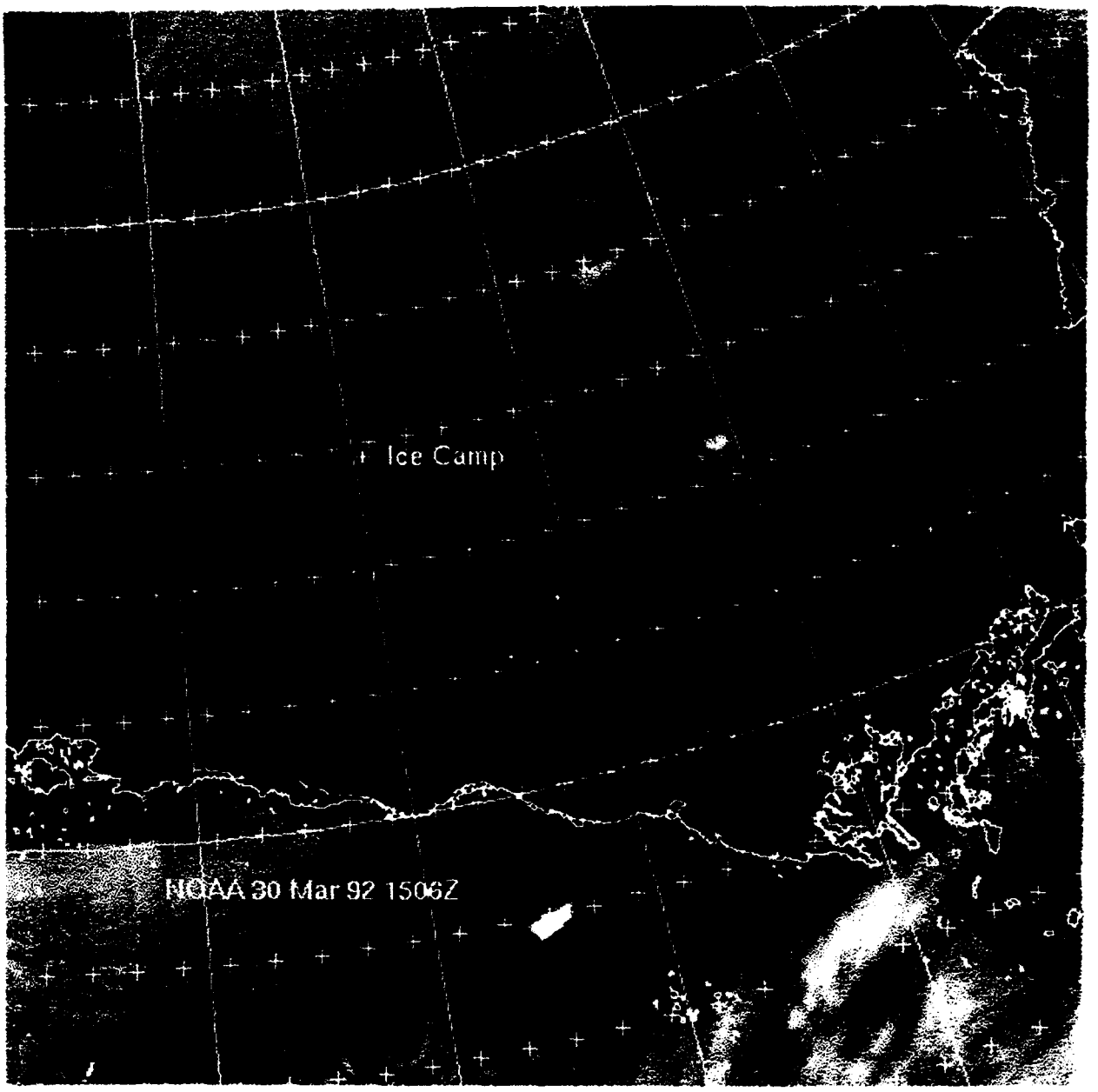

FIG 12. NOAA infrared (Ch4) data. 30 March 1992, 1506 UTC.

About 2 1/2 hours later (1748 UTC) DMSP IR data (Fig 13) reveal the system, now NW of the ice camp. The comma-shape has now "closed in" and the system has assumed an apparent circular shape defined by low and mid-level cloud forms.

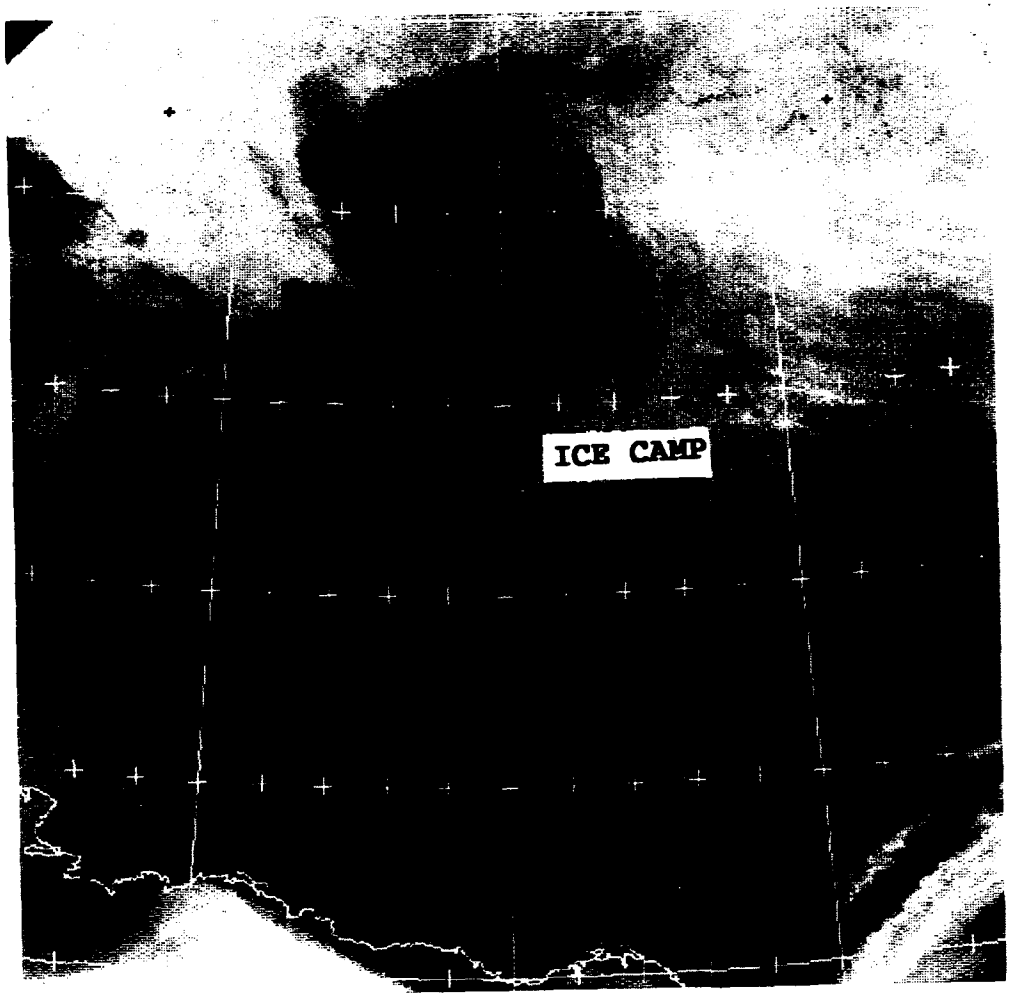

FIG 13. DMSP infrared data. 30 March 1992, 1748 UTC.

Corresponding visible imagery (Fig 14) however, show convective bands on the southeastern side of the system which extend to higher elevations.

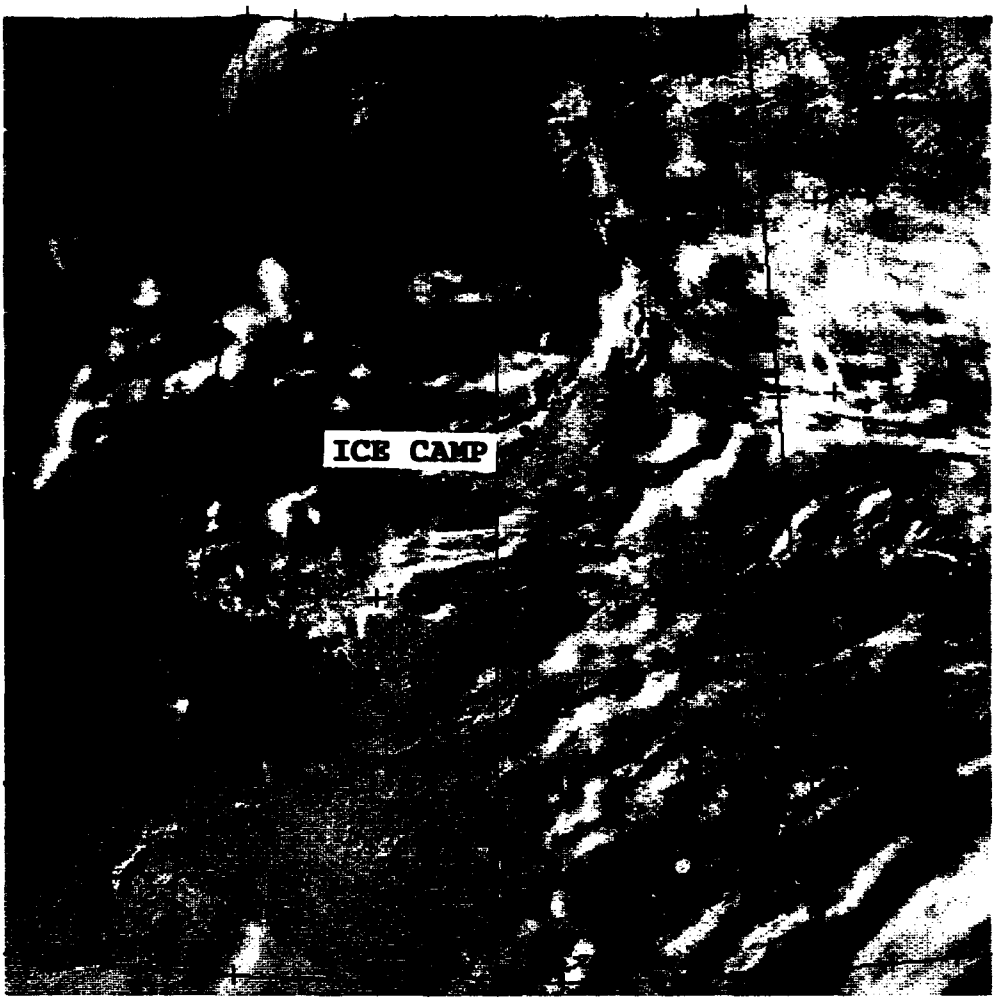

FIG 14. DMSP visible data. 30 March 1992, 1748 UTC.

The NWS (Anchorage) surface analysis for 30 March at 1800 UTC is shown in Fig 15. The disturbance passed through the ice camp and buoy array with only minor perturbations in wind direction and speed recorded at the surface. The pressure pattern, however, provides consistent verification for such passage, as do wind shifts and pressure indications at staions along the North Slope.

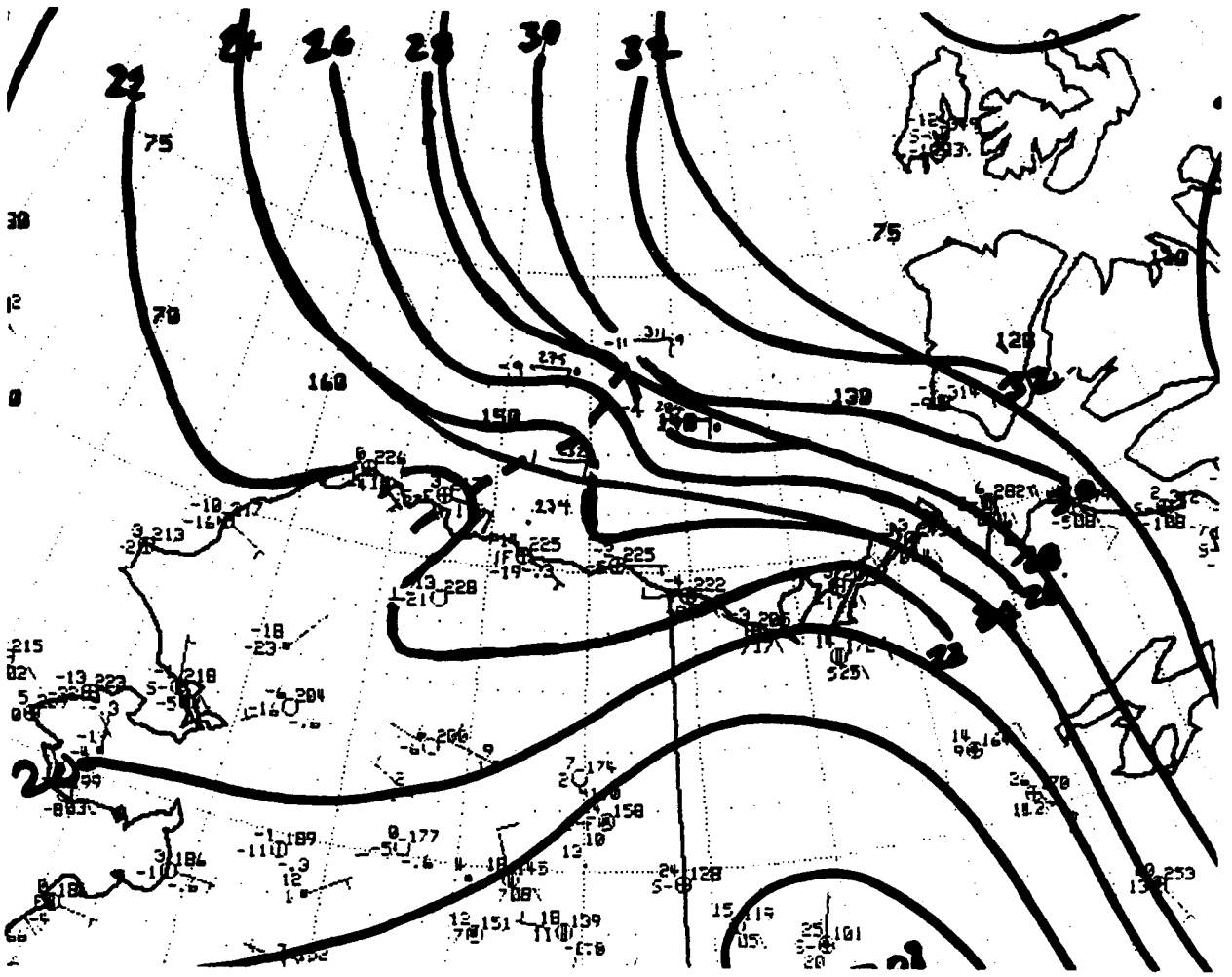

FIG 15. NWS (Anchorage) surface analysis. 30 March 1992, 1800 UTC.

Fig 16 is a time cross section for Deadhorse, Alaska. Although wind shifts, based on rawinsonde data at the surface, are light and inconclusive, a pronounced effect is observed from 700 to 500 mbs. This, again, is similar to easterly wave structure which is typified by more pronounced effects at mid-levels.

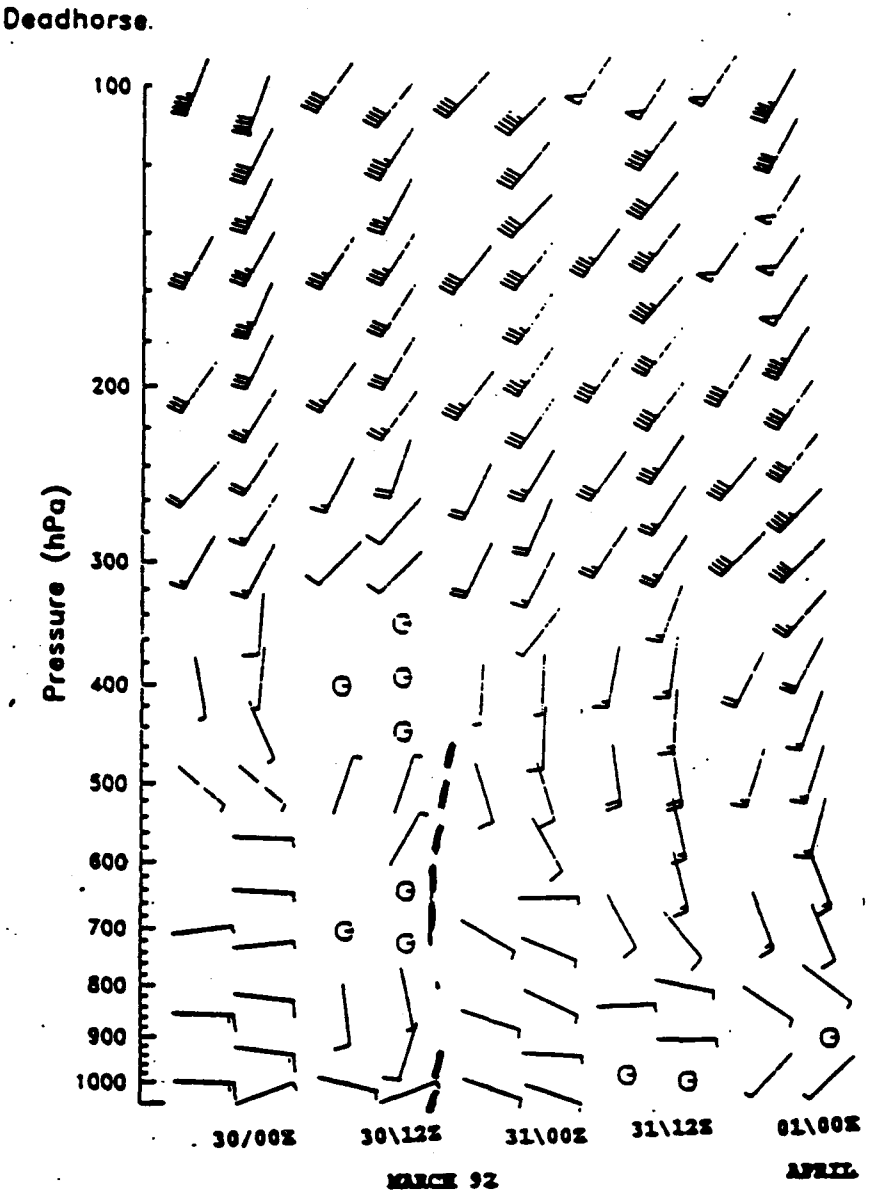

FIG 16. A time cross section for Deadhorse, Alaska. 30 March-1 April 1992. Mandatory and significant level winds are shown for each time period. 0 indicates calm.

DMSP visible views of the system were obtained on 30 March at 1912 UTC (Fig 17) and 2052 UTC (Fig 18). These views show a continued NNW movement of the system around a high pressure cell centered just west of Prince Patrick Island at the 925 mb level (see Fig 22).

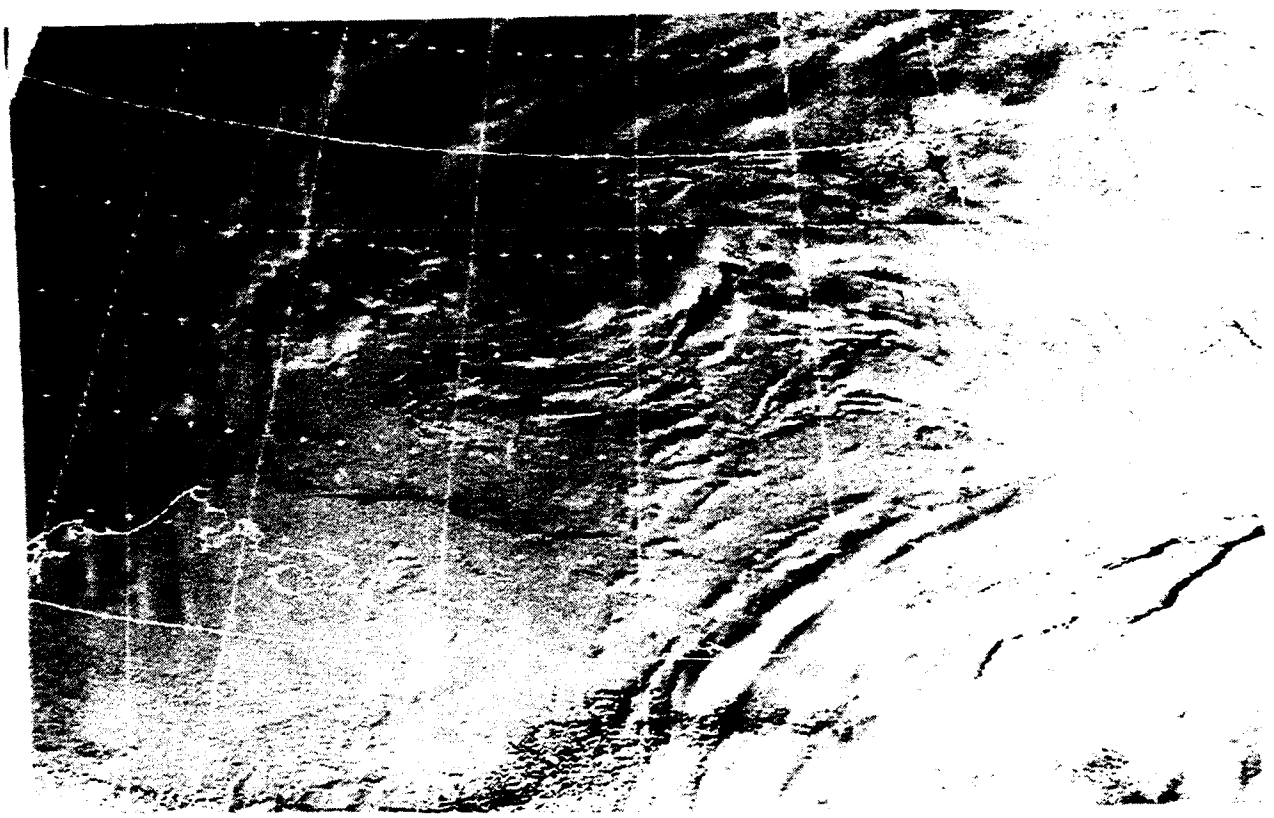

FIG 17. DMSP visible data. 30 March 1992, 1912 UTC.

The satellite data are consistent in showing very suppressed low level cloudiness basically over and west of the trough axis on the west side of the system, with convective cloud forms east of the trough axis. This, again, is similar to easterly wave structure which exhibits low level divergence and descending motion ahead of the trough axis and low level convergence and ascending motion to the rear (Riehl, 1954). Similarly, the depth of the moist layer is lowest west of the trough axis in this example and reaches a maximum height east of the trough axis in the region of the convective cloud bands in the manner of an easterly wave.

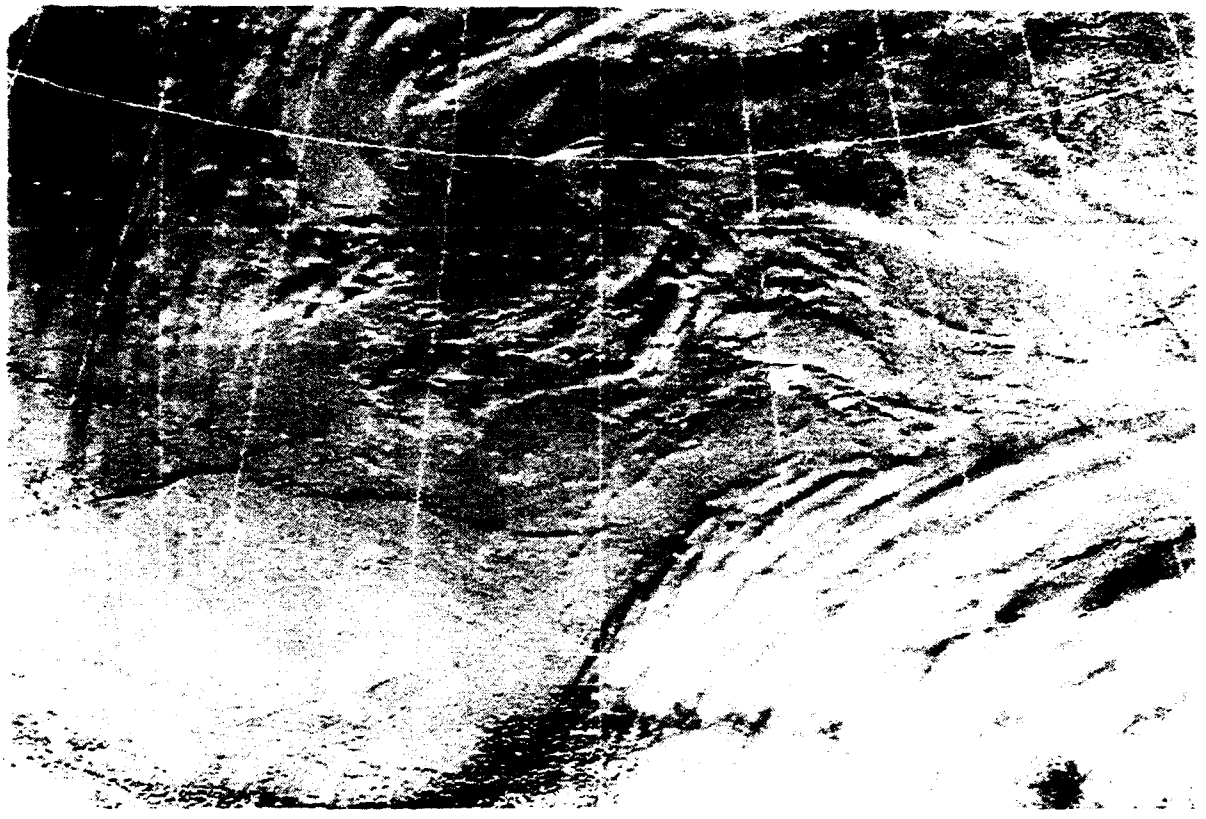

FIG 18. DMSP visible data. 30 March 1992, 2052 UTC.

A NOAA-11 visible (Ch2) view of the system at 2148 UTC is shown in Fig 19. The image continues to show major convective activity to the east, evident as banded cloudiness leading toward the system center, where very suppressed low cloudiness is apparent. The "screaming eagle" appearance of the system is most evident in this image, with the head and beak at the top of the comma shape near 74.5°N, 151.5°W. The legs and talons reach southward and westward past the ice camp along 72°N and the wings sweep northeastward past 76°N.

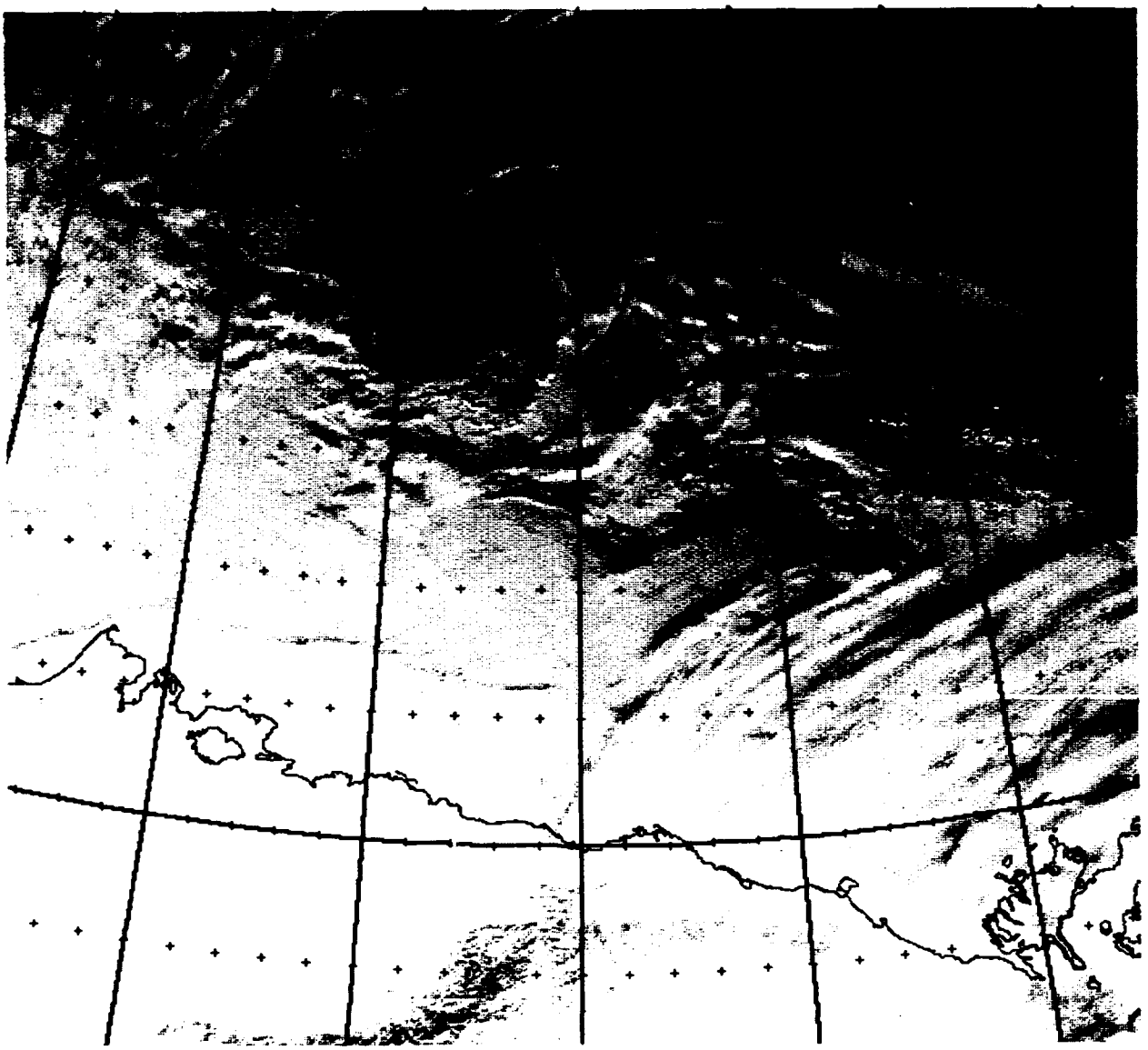

FIG 19. NOAA-11 visible data. 30 March 1992, 2148 UTC.

The companion infrared (Ch4) NOAA view at 2443 UTC is shown in Fig 20. In this image the warm (low level) oval shape of clouds west of the trough axis is clearly revealed.

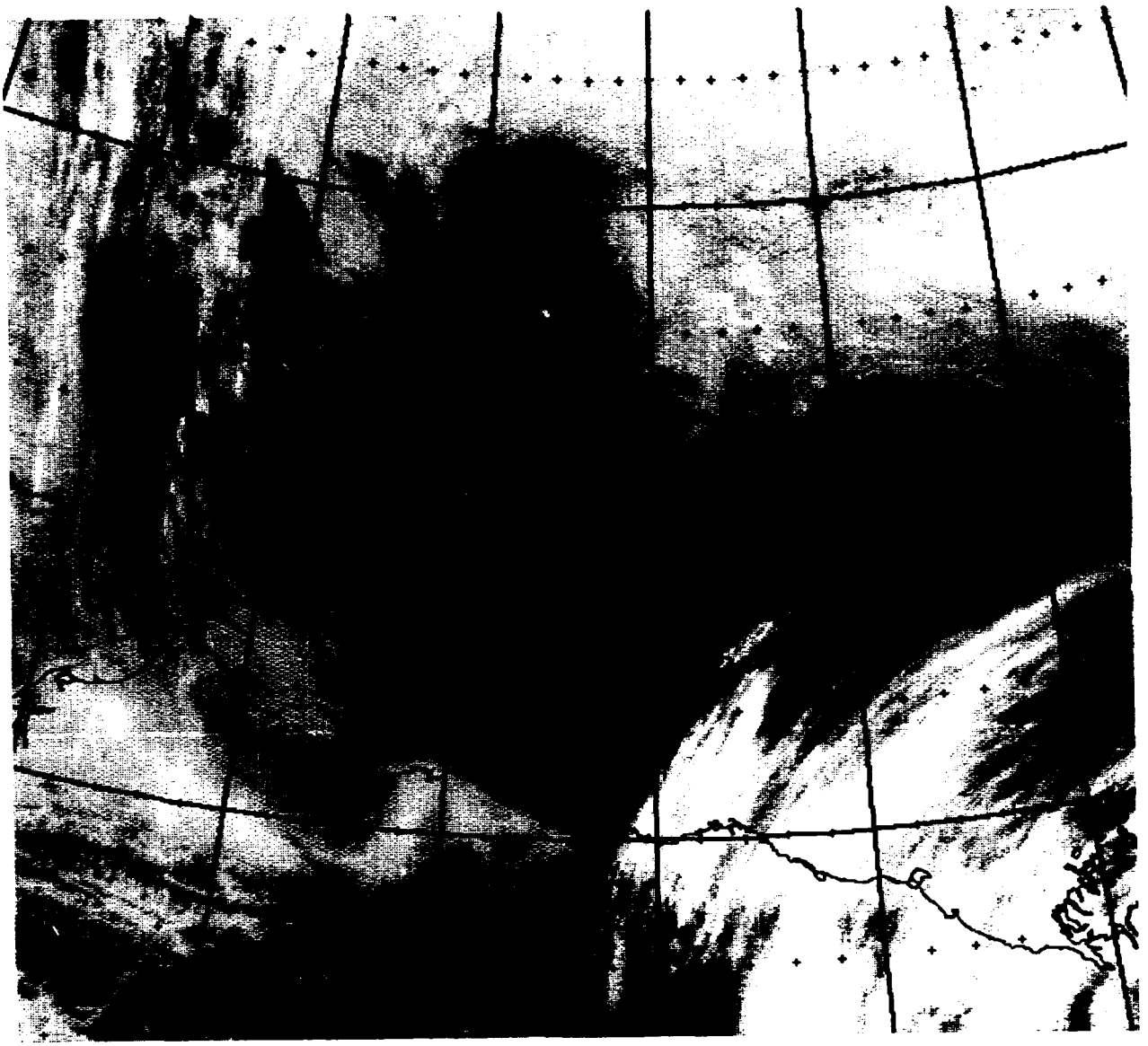

FIG 20. NOAA infrared (Ch4) data. 30 March 1992, 2143 UTC.

A NOAA-11 channel 3 view concurrent with the channel 2 and channel 4 views at 2148 UTC is shown in Fig 21. This daytime (1348 Alaskan Standard Time (AST)) channel 3 view is responsive to both visible and infrared radiation. Hence, cloud top temperatures cannot be reliably inferred at this time and the distinction between cold, bright, clouds and warm. bright, clouds is largely lost. What is remarkable about this image is the apparent delineation of two minor waves south of the screaming eagle feature near 72°N, 148°W and 72°N, 155°W. The wave along 148°W is almost due north of Deadhorse. It is of interest then that weather observations from this station indicated northeasterly flow at about 10 kts until 1300 UTC on 30 March. At 1500 UTC winds then shifted to southeasterly at about 4 kts. Winds were calm at the

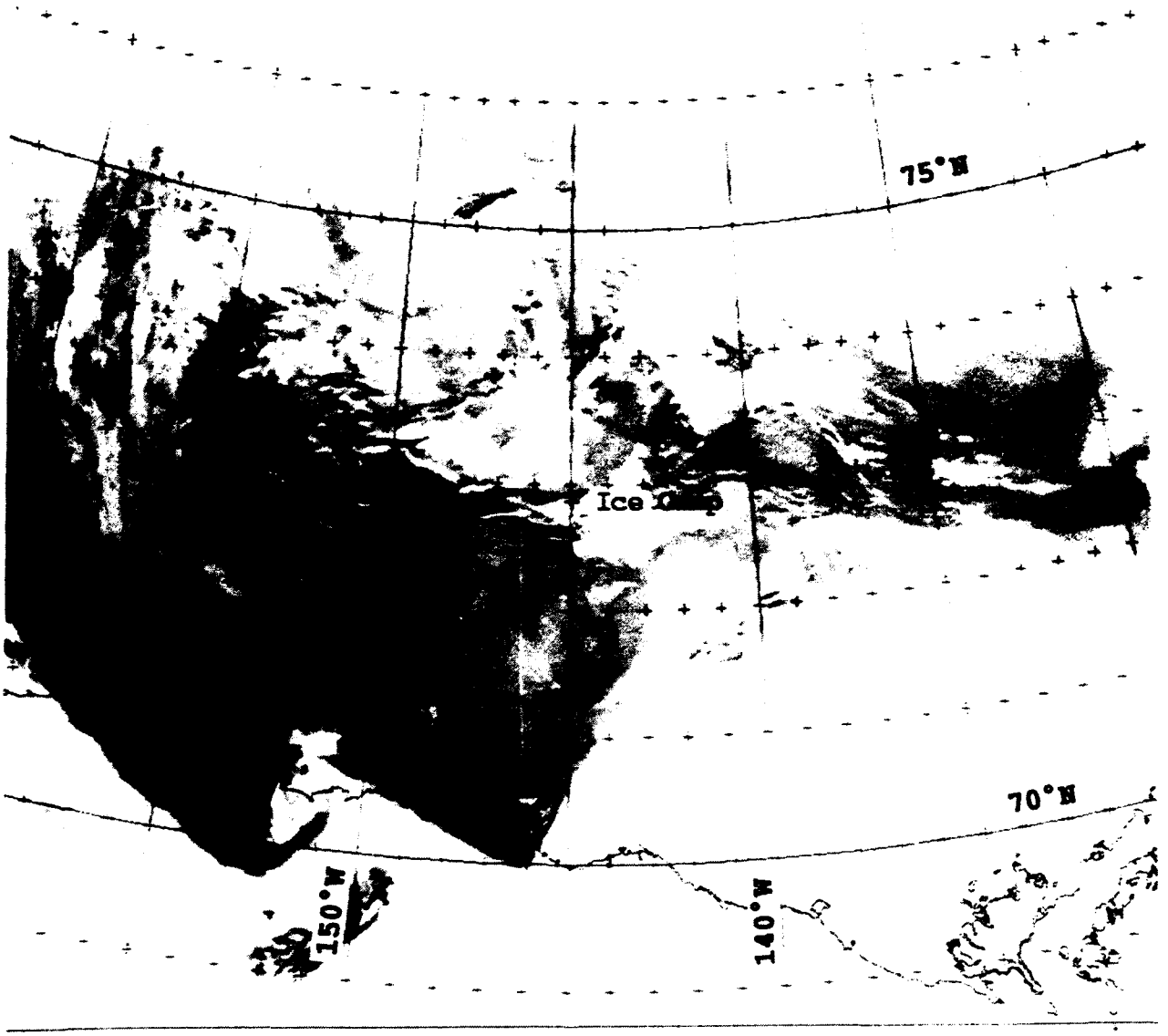

FIG 21. NOAA-11 infrared (Ch3) data. 30 March 1992, 2148 UTC.

time of satellite acquisition (2148 UTC), and then became southeasterly and shifted to southwesterly by 0900 UTC on 31 March. The pattern of wind shifts indicated passage of a low center to the north as implied by the satellite. The superior ability of channel 3 as opposed to channel 4 to resolve such disturbances is facilitated by the added visible light reflection and scattering this channel is susceptible to during daylight hours.

31 March 1992

A minor streamline trough is also indicated in that region on the SOCMM 925 mb analysis for 31 March at 0000 UTC (Fig 22).

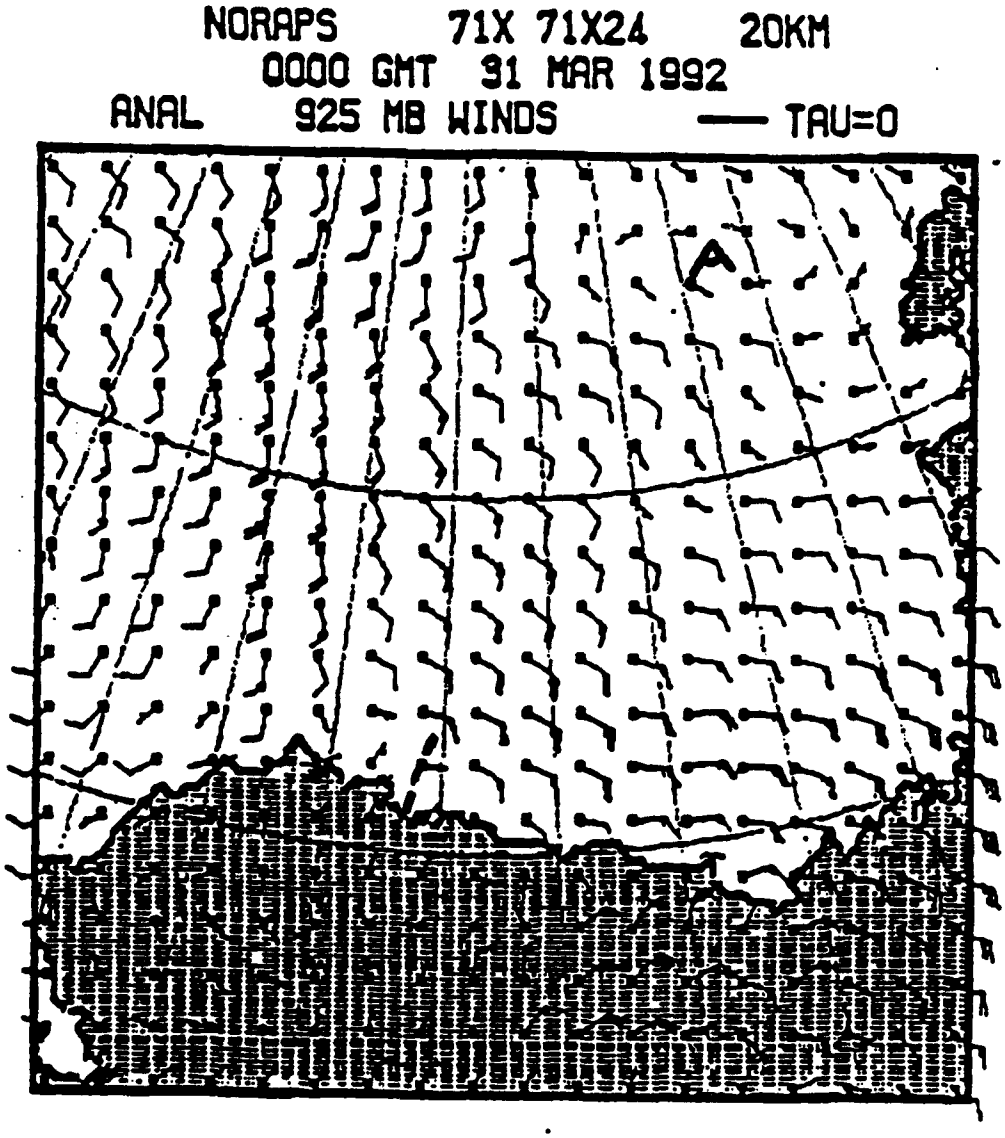

FIG 22. Navy SOCMM 925 mb analysis. 31 March 1992, 1200 UTC.

A final DMSP infrared view of the screaming eagle disturbance on 31 March at 0205 UTC (Fig 25) shows the system well to the northwest moving out of the Leadex region.

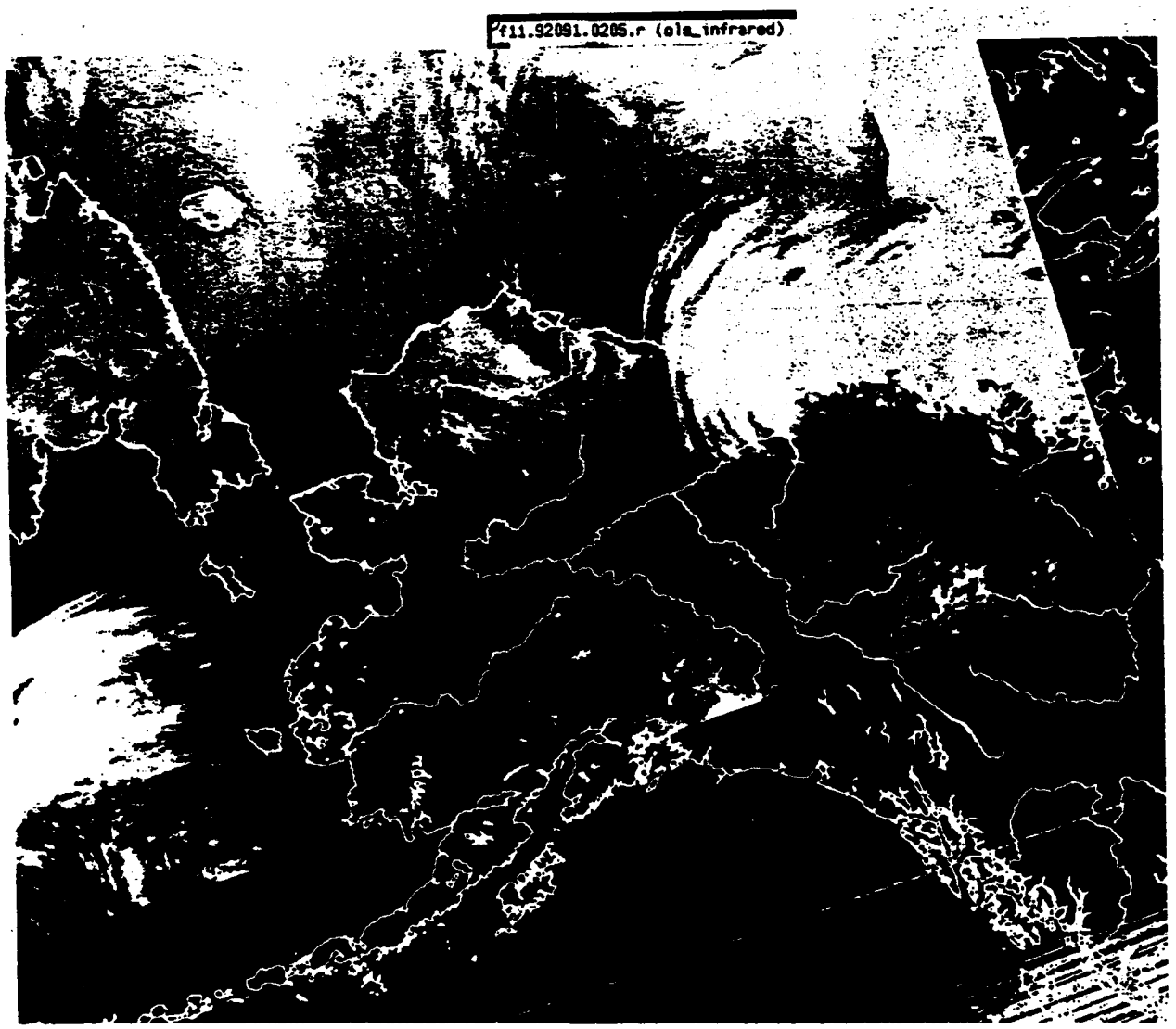

FIG 23. DMSP infrared data. 31 March 1992, 0205 UTC.

IMPORTANT CONCLUSIONS

1. An important category of mesoscale disturbances has a characteristic movement from westerly to northwesterly across the southern Beaufort Sea.

2. Such systems appear to move around the periphery of a high pressure cell in the Beaufort Sea similar to classical easterly wave movement around the Bermuda High in the Atlantic.

3. The cloud formation associated with such disturbances resembles the tropical "inverted-V" pattern, sometimes referred to as a "screaming eagle".

4. The disturbances have a structure similar to easterly waves being most intense in the mid-troposphere with a tendency toward subsidence west of the associated trough axis and convergence and upward vertical motion to the east of the trough axis.

5. The vertical motion pattern favors low cloudiness and a strong low level inversion west of the trough axis and convective cloudiness and no low level inversion east of the trough axis.

6. NOAA channel 3 infrared data acquired during daylight hours are useful in delineating mesoscale waves and vortices not particularly well delineated in other channels.

REFERENCES

1. Frank, N. L., 1969: The inverted-V cloud pattern - an easterly wave, Monthly Weather Review, 97, No. 2, 130-140.

2. Fett, R. W., R. E. Nagle, and W. F. Mitchell, 1973: The low level structure of weak tropical waves, Environmental Prediction Research Facility* Tech. Paper No. 3-73, Monterey CA., 93943-5006, 26 pp.

3. Riehl, H., 1954: Tropical meteorology, McGraw-Hill Book Co. Inc., NY, 392 pp.

*Now the Naval Research Laboratory, Marine Meteorology Division, Monterey CA 93943-5502.

6. UNIQUE CLOUD STREAKS AND WATER PLUME CLOUD EFFECTS OBSERVED DURING STRONG NORTHEASTERLY FLOW OVER THE BEAUFORT SEA. 14 - 20 APRIL 1992

The Leadex ice camp experienced its strongest wind event during the period 14-20 April 1992. From 16 to 19 April northeast winds blew at sustained speeds of more than 20 kts without let up (Fig 1). At least one of the buoys (ice stations) around the ice camp reported sustained winds of 30 kts early on 16 April, while, on 17 April, North Slope locations reported gusts to as high as 54 kts. The northeast winds were caused by a strong pressure gradient over the Beaufort Sea between a high pressure center north of 80°N and low pressure over northern Alaska.

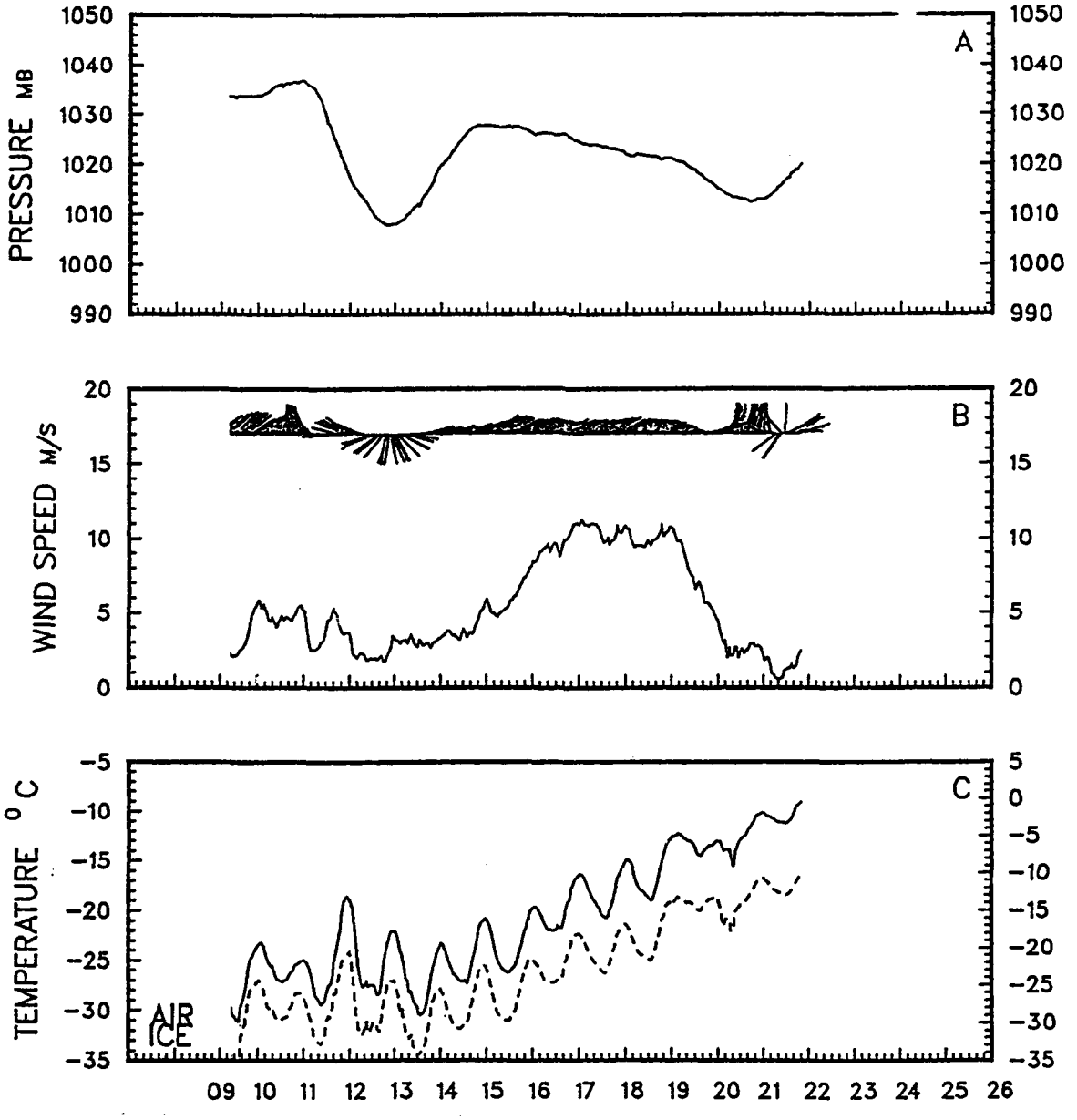

FIG 1. Leadex ice camp time series, 9-21 April 1992. Ice camp position, 9 April - 72.9°N, 145.8°W; 20 April - 72.9°N, 148°W.

During the period of strong northeast winds unique NE-SW oriented streaks appeared in DMSP and NOAA infrared (IR) data over the southern Beaufort, and into the Chukchi and East Siberian Seas. In a given cross section the streaks displayed a consistent pattern of alternately warm and then cool, in terms of thermal structure. However, lengthwise there was some evidence of warm streaks changing to cool and vice versa. Of particular note was preservation of the streaks appearance without essential change in width and to some extent intensity (opacity) along much of their length, which approached distances of about 600 km.

Many of the streaks could be traced as warm thermal features leading back to sections on leads, which apparently opened and permitted plume development, as heat and moisture escaped into the frigid air passing over the lead opening. However most of the streaks had origins not that well defined given the resolution limits of the satellite sensors (about 2 nm). In some regions cool streaks seemed to obscure underlying ice features even more than the warm streaks. The nature of the composition of the streak pattern is also somewhat ambivalent. The streaks could consist of water droplets, ice crystals, water vapor, or a combination of all three. Whatever the composition, the concentration was so thin that, in satellite infrared data, outlines of frozen lead and ice floe patterns could be detected through the streak pattern. The total effect suggested a partially obscuring layer of warm and cool modulations. The regularity of spacing, which ranged from 10-18 km (warm streak to warm streak), and lack of lateral spreading downstream, has suggested the possibility of gravity wave impulses superimposed over the region. Such impulses could have been induced by vertical wind shear, which significantly increased from the surface through the inversion layer. Little or no evidence of the streaks could be discerned in satellite visual data because of the thinness or transparency of the structures and difficulty in resolving them against the relatively bright ice and snow background. Additionally, satellite visible data are notorious for lack of sensitivity in revealing thin cirrus or ice crystal clouds that may be very evident in satellite IR data (Fett, et al, 1977).

Soundings from the ice camp during this period indicated potential for cloud development only in the boundary layer near the surface. Northeast winds in alignment with the streak pattern also existed only near the surface, veering very rapidly to easterly above this level. Winds were very strong during the peak period of the event (16-17 April) creating a slightly elevated low level turbulence inversion at the ice camp. The multitude of lead openings, generally spaced in a fractured manner, rather than along continuous lines, provided a moisture source for continuous replenishment of the obscuring layer.

The existence of cloud streaks (thermal streaks) as they appear in satellite infrared data was first described in a paper by Byers and Stringer (1992). They distinguished between two types of streaks, the first appearing plume-like, having "apparent sources at areas of low ice concentration or open water". A typical

spacing for this type was found to be roughly 6 km. The second type displayed "alternately warm and cool bands of continuous cloud cover" and "no easily identifiable point source". The second type had a wave length of 15 to 30 km in width and displayed stronger curvature. Byers and Stringer examined "roll vortex" theory and came to the conclusion that the first type of streak having a wavelength of about 5 km was likely to occur as a roll vortex. The second type, however, had too long a wavelength to correspond to a roll vortex, and its exact nature remained in question.

The streaks seen in the present investigation appear to be more similar to the second type, having a spacing between warm streaks varying from 10-18 km. An important difference, however, is that many of the streaks can be traced to specific leads where open water apparently exists. The moisture field in which the streaks are embedded is downwind from prominent lead formations. The streaks are aligned with low level flow and show curvature and changes in direction in conformity with changing low level streamline indications. High low-level wind speeds in the region seem essential for the production of these features.

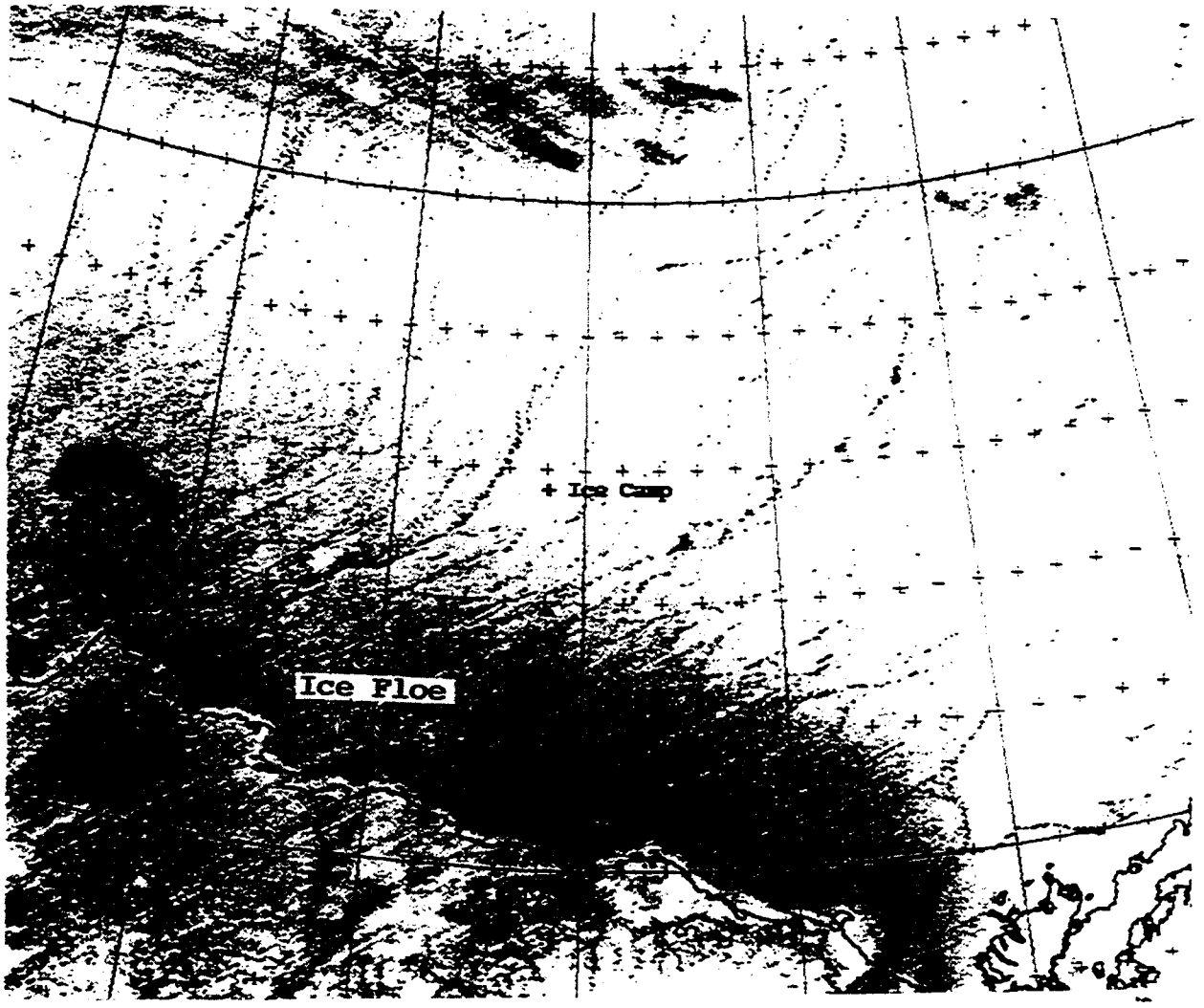

FIG 2. DMSP infrared (TS) data. 14 April 1992, 0431 UTC.

14 April 1992

DMSP data at 0431 UTC (Fig 2) show the region south of the ice camp while winds were still light and there was no significant cloud cover over the ice immediately north of the North Slope. In this image NE-SW oriented lines are an effect of the image creation process and are not atmospheric in nature - note that they appear over land as well as sea and in the upper part as well as the lower part of the image. It is important to point this out because some of the images to follow contain the NE-SW oriented cloud lines or streaks, as described above, that are on cursory inspection, similar in appearance to the streaks noted on this image. Some leads and outlines of ice floes are evident in Fig 2. We wish to focus on those features south of the ice camp from 70°-72°N for comparison with later views.

One such view is shown in DMSP IR data acquired at 1349 UTC (Fig 3). In this image a series of alternating thin, dark lines, and wider, cold rows, appears south of an ice floe, apparent in

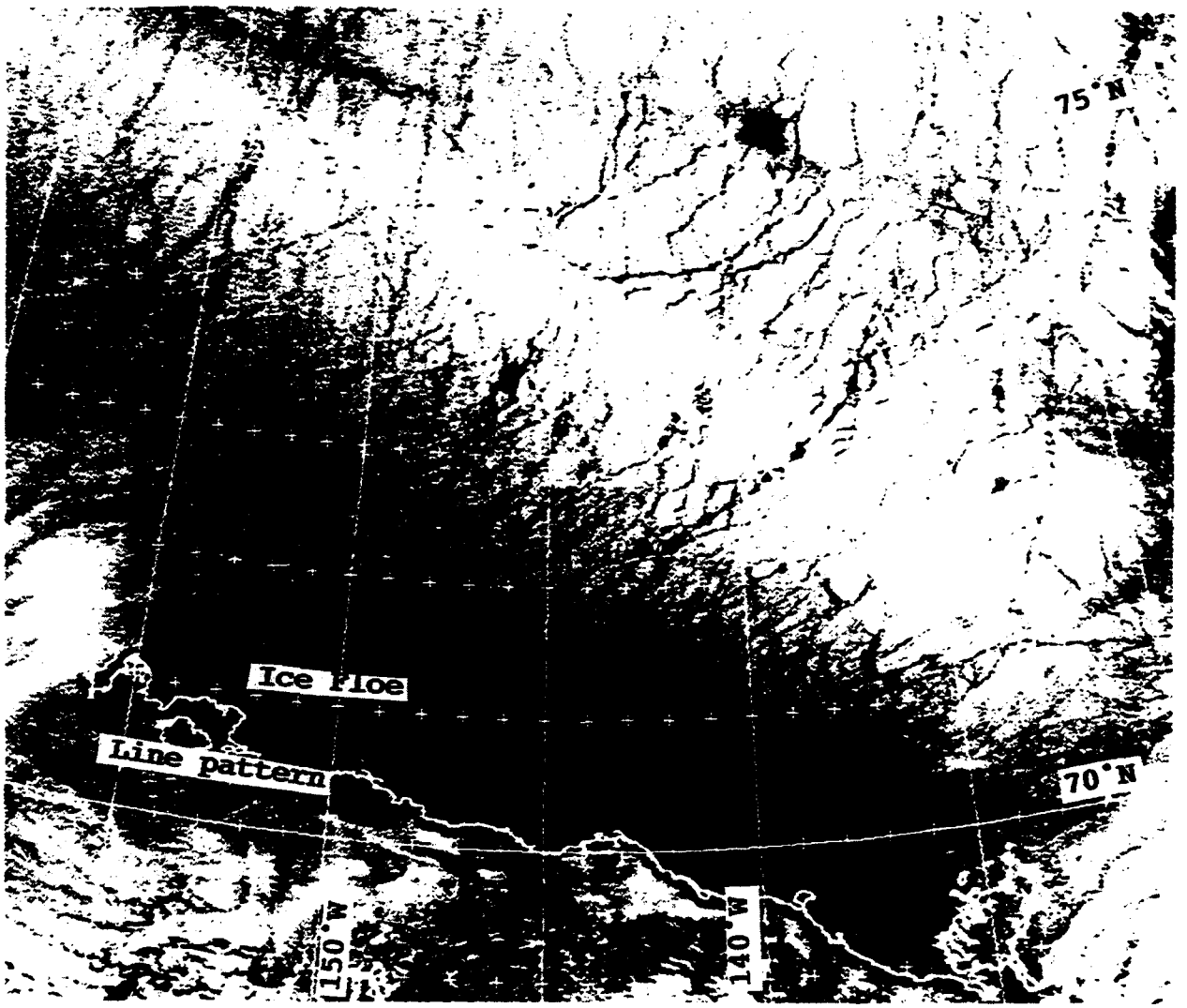

FIG 3. DMSP infrared (TS) data. 14 April 1992, 1349 UTC.

both images near 71.2°N, 147°W. The streaks are oriented in an ENE-WSW direction and have effectively obscured detection of many of the ice features apparent in the earlier view (Fig 2).

The suggestion of such streaks persisted in NOAA Ch4 IR data (Fig 4) acquired at 1529 UTC. The fact that these streaks should appear as observed, from a completely different satellite system, adds validity to the suggestion that they are real and represent ENE-WSW oriented rows of cloud droplets, water vapor, or ice crystals, with intervening clearer areas, extending over that region. Spacing of the streaks is on the order of 10 km in both images.

A careful comparison of Figs 3 and 4 with Fig 2 show differences in the appearance of these streaks as opposed to the spurious streaks in Fig 2. The latter streaks are very thin, closely spaced, and are absolutely straight, extending across the entire image, persisting over land and topographical barriers, as well as at sea. The thermal streaks of Figs 3 and 4 (and in the examples to follow) are wider in nature and have a broader spacing. They originate only at sea, and can be traced only occasionally a short distance onshore.

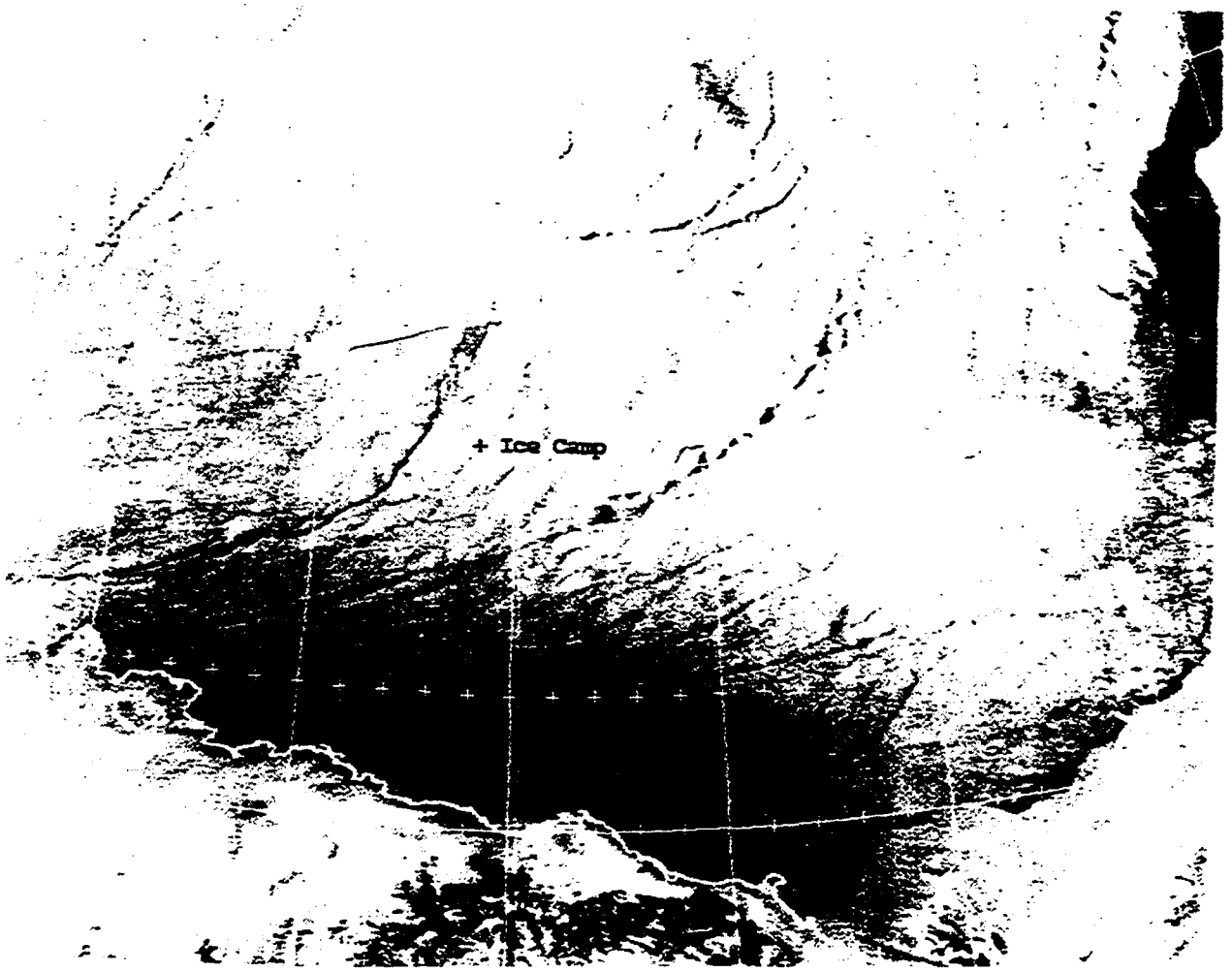

FIG 4. NOAA AVHRR infrared (Ch4) data. 14 April 1992, 1529 UTC.

Deadhorse, Alaska (near 70.3°N, 148.5°W) was in the region of the streak pattern suggested in Figs 3 and 4, and there is some evidence that these features pass onshore near that location. Interestingly, both Deadhorse and Prudhoe Bay weather reports indicate clear skies and good visibilities during the period of the satellite images shown. The 1200 UTC sounding from Deadhorse (Fig 5), taken shortly before the acquired imagery of Figures 3 and 4 on 14 April, shows the strong surface based inversion existing at this time.

Relative humidity high enough to support cloud formation exists only under this inversion below 2000 ft, with much drier conditions aloft. It is possible that the streaks consisted of ice particles, or were very thin, of insufficient concentration to be recorded as significant cloud formations covering more than 1/8 of the sky. A review of satellite visible imagery shows no evidence of cloud lines. This serves to reinforce this possibility.

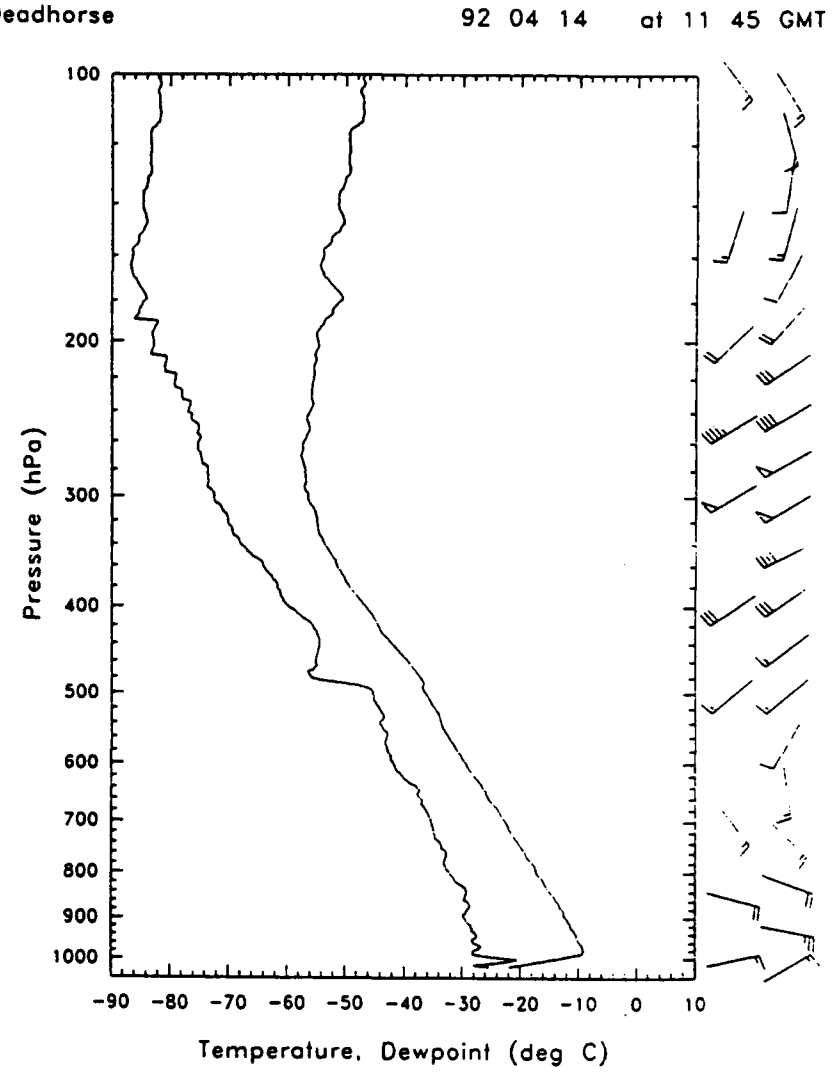

FIG 5. Deadhorse, Alaska, rawinsonde data. 14 April 1992, 1145 UTC.

15 April 1992

NOAA IR (Ch4) data (Fig 6) show that the cloud line (streak) effect continues to persist on this date, being more developed north of 71°N. Leads can faintly be discerned through the low level obscuration in which the streaks are embedded. Even the ice floe, pointed out earlier near 71.2°N, 147°W, can be detected.

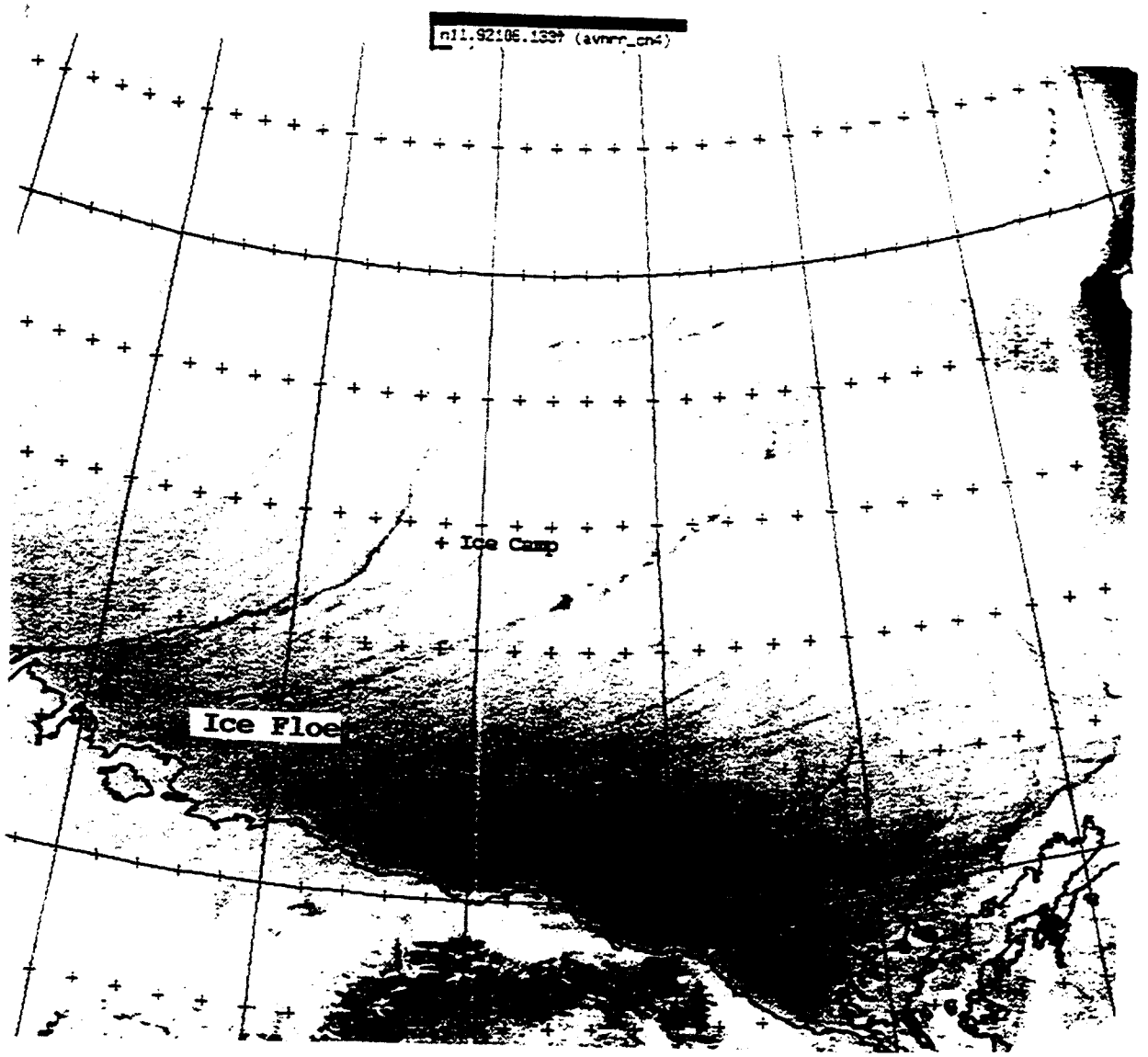

FIG 6. NOAA AVHRR infrared (Ch4) data. 15 April 1992, 1339 UTC.

Prudhoe Bay and Deadhorse continue reporting clear skies but with blowing snow in the 15 kt wind speeds prevailing at the time of the NOAA data. Fig 7 is the NWS (Anchorage) surface analysis for 1200 UTC revealing the 15-20 kt winds south of 72°N along the North Slope. Gator (near 73N, 150W), and Leadex (near 72.8N, 146.5W), also report clear skies in observations taken at 1500 UTC. Sounding data (not shown) continue to indicate a low level inversion in moist conditions with cloud potential only below 1500 ft.

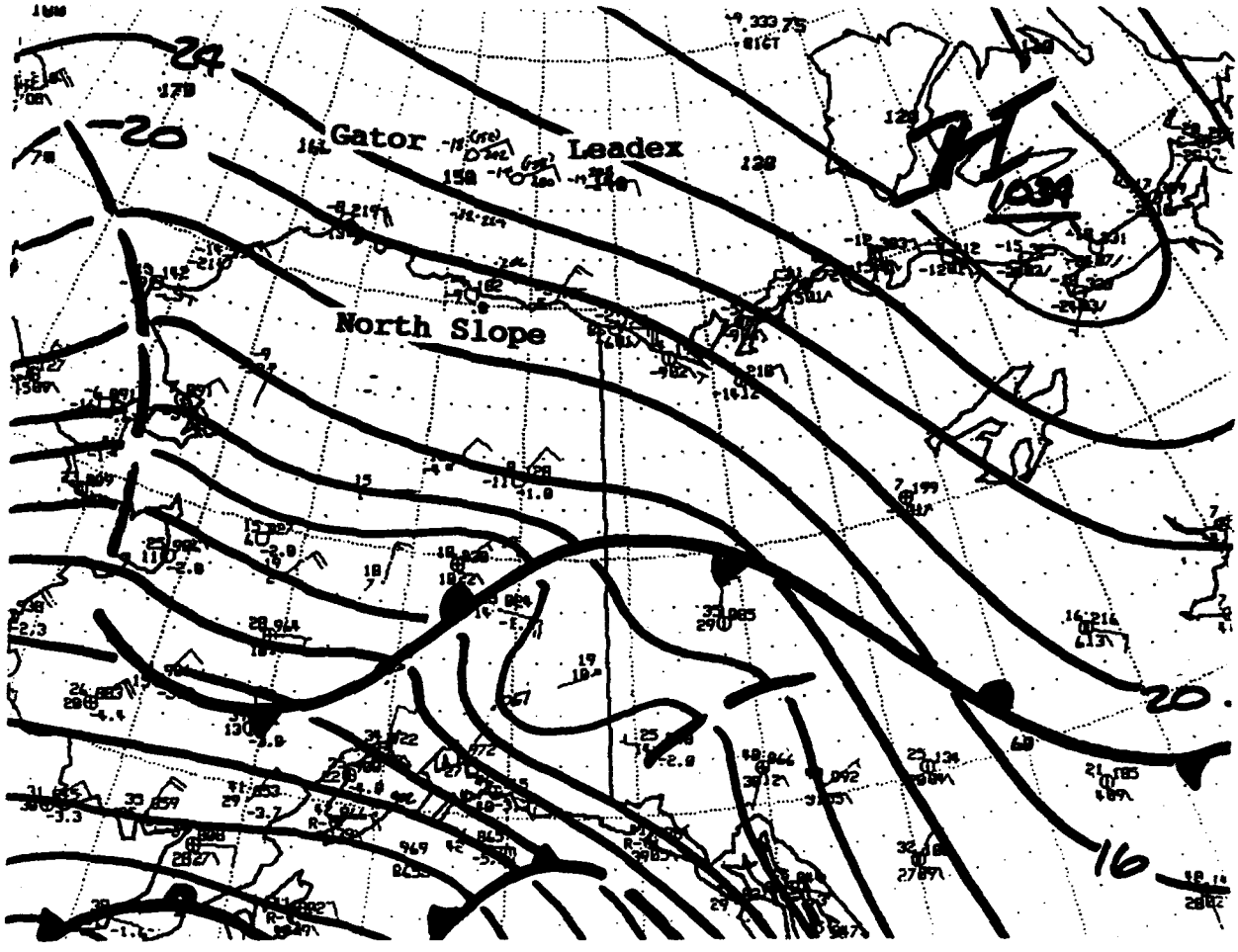

FIG 7. National Weather Service (NWS), Anchorage, Alaska, surface analysis. 15 April 1992, 1200 UTC.

16 April 1992

By 0000 UTC on this date wind speeds had increased to more than 20 kts with gusts to near 30 kts at most North Slope locations. Ice camp and buoy winds south of 73.5°N attained values of 15-20 kts. Sky conditions were reported as obscured at both Deadhorse and Prudhoe Bay with visibility restricted to about 4 miles in blowing snow.

Fig 8 shows the NWS (Anchorage) surface analysis for 16 April at 0000 UTC. Note sustained winds of 35 kts reported by the Kenmore Oil Rig (station reporting pressure of 168 east of Barrow). Actual location of this rig is 71.2°N, 155.1°W. Anemometer height is 150 ft.

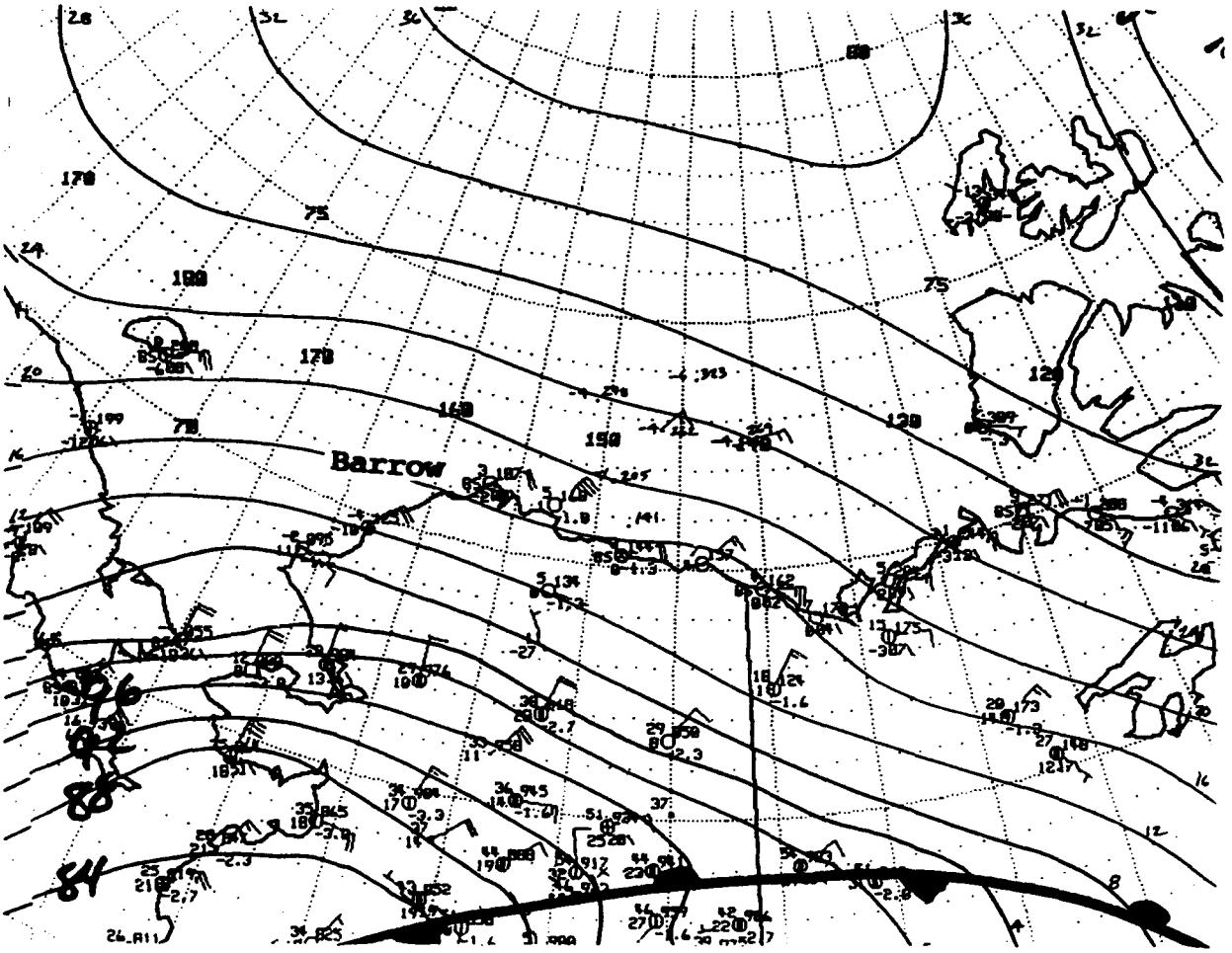

FIG 8. NWS (Anchorage) surface analysis. 16 April 1992, 0000 UTC.

A DMSP infrared image acquired at 0027 UTC (Fig 9) continues to show evidence of thin obscured conditions over the region south of the ice camp, but only slight traces of the cloud streak pattern. The large floe near 71.2°N, 147°W is still apparent in this image. The force of the onshore winds is compressing the ice south of the ice camp thereby inhibiting the production of lead openings in that region.

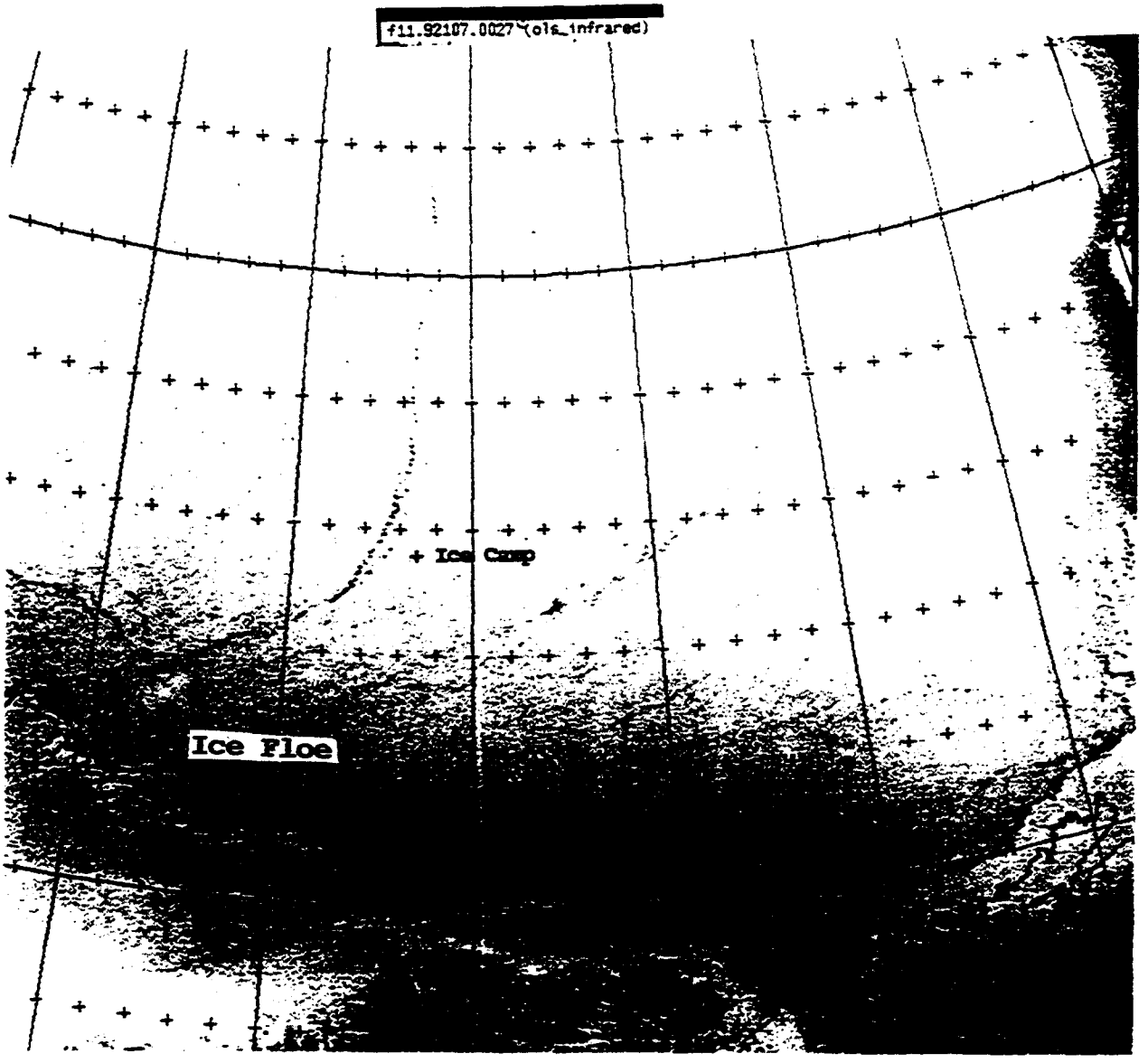

FIG 9. DMSP infrared (TS) data. 16 April 1992, 0027 UTC.

By 1200 UTC on 16 April visibility at Deadhorse had dropped to 1/2 mile under obscured sky conditions in blowing snow. Reported winds were from 060° at 21 kts gusting to 29 kts. The NWS (Anchorage) surface analysis (Fig 10) shows reports at that time. Added to the NWS reports are surface observations from ice camp "Gator" (73.1°N, 150.8°W) and Leadex (72.8°N, 146.6°W) as well as some ice station (buoy) data. Note that the pressure gradient was stronger than shown on this analysis (NWS did not have real time assess to the buoy data).

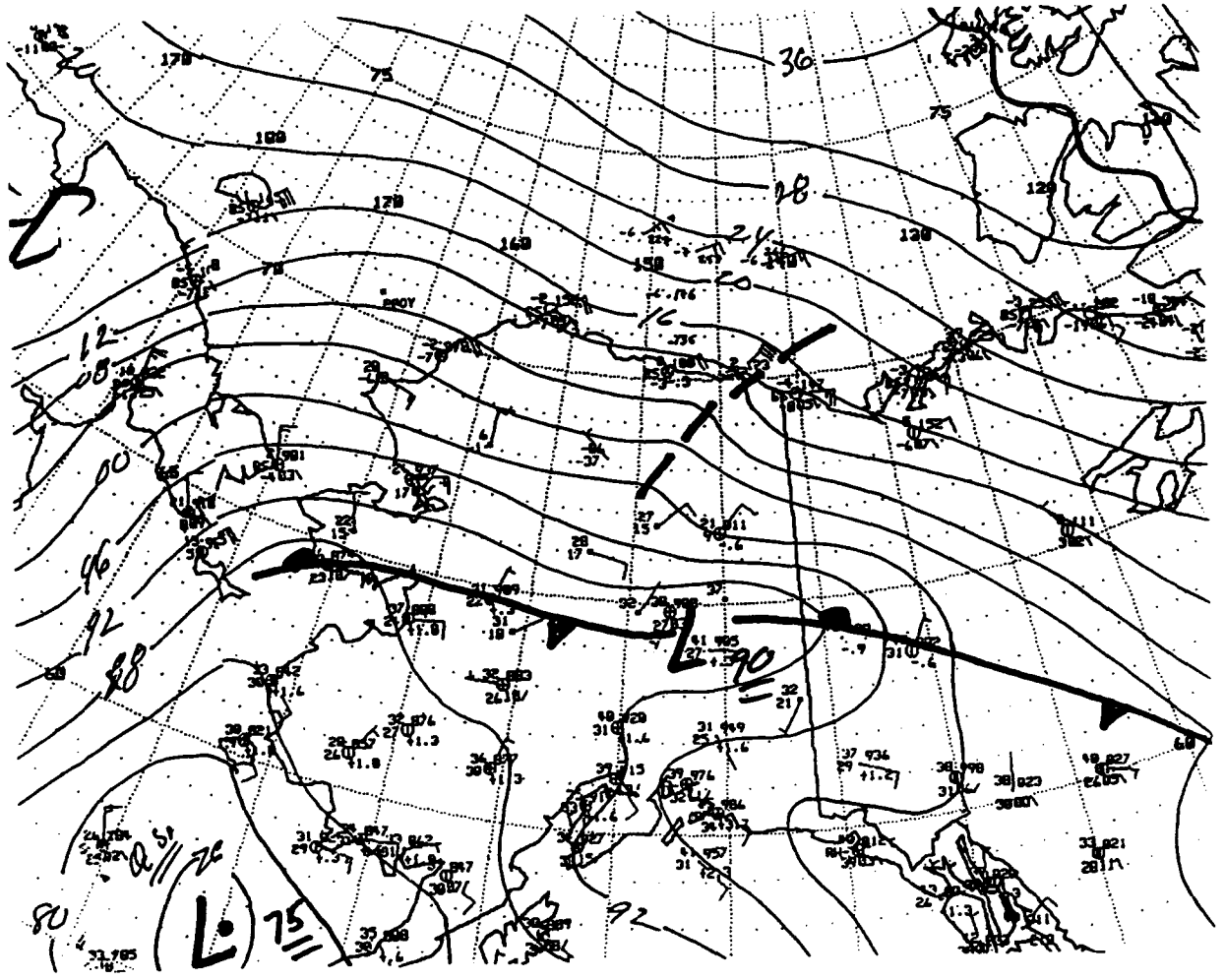

FIG 10. NWS (Anchorage) surface analysis. 16 April 1992, 1200 UTC.

A remarkable set of data was obtained at 1505 UTC by the NOAA-11 satellite system. The AVHRR channel 4 view is shown in Fig 11. NE-SW oriented streaks associated with cloud lines or plumes originate from the region near Banks Island westward along 74°-75°N. It is apparent in this image that the cloud obscuration is quite thin since the outlines of many lead and ice floe features are easily seen through the obscuration. Note evidence of plumes extending westsouthwestward from individual leads in the region immediately west of Banks Island (72°-74°N, 130°-135°W). Other leads in the north-central portion of the image also show evidence of plume generation starting at the lead location. The generation of such plumes from obvious leads substantiates the concept of lead openings serving as point sources of moisture responsible for many of the streaks in this image. The plumes in the region west of Banks Island appear very similar to an earlier depiction of plumes shown emanating from leads in the Lincoln Sea (Kozo, et al, 1992). The warm nature of the plumes indicates development capped by a low level (near-surface based) inversion. The streaks in this region appear warmer than the ice surface over which they pass. Further downstream, where winds were stronger, an elevated inversion over a mixed layer could result in the streaks apparently reversing tonality, to appear cooler than the ice surface over which they pass, so that a "warm" edge effect is created. This is difficult

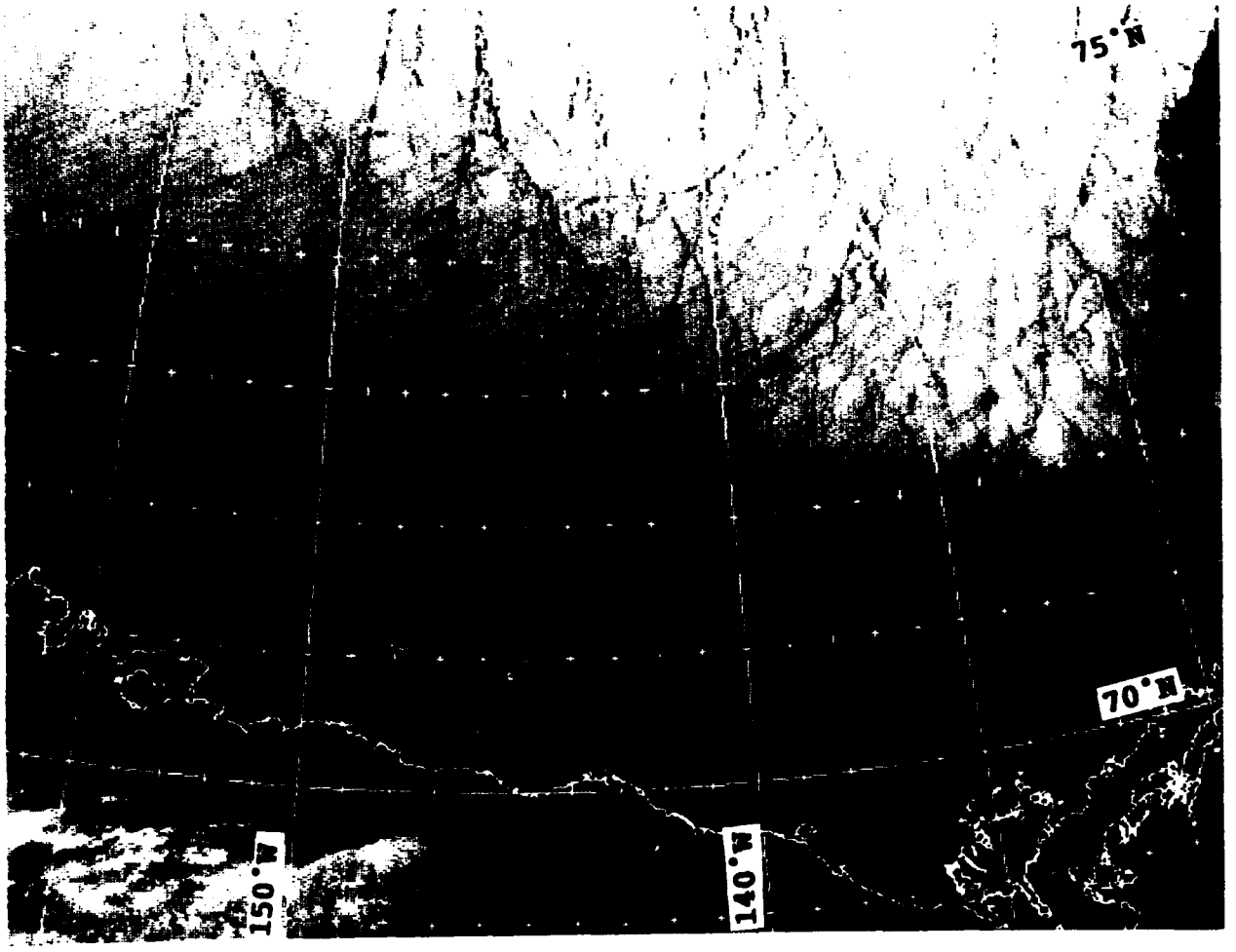

FIG 11. NOAA-11 AVHRR infrared (Ch4) data. 16 April 1992. 1200 UTC.

to establish, but there are subtle indications of the "cool" streaks obscuring the underlying ice features and leads which suggest that possibility. As indicated earlier a gravity wave mechanism, induced through vertical wind shear, may also (or alternately) be involved.

The sudden generation of hundreds of lead openings attests to the increase in surface stress induced by the strong winds over the region at this time. It will be noted that the streaks are evident mainly north of about 72°N; the area to the south of this latitude seems completely obscured. It is possible that this obscuration was caused by blowing snow (reported at the time by Deadhorse and other North Slope locations).

A simultaneous view of the area as depicted in NOAA daytime channel 3 data is shown in Fig 12. Channel 3 daytime data are unique in that the channel responds at this time, not only to long wave infrared radiation, but also to scattered and reflected solar radiation. The effect of this difference can be seen immediately

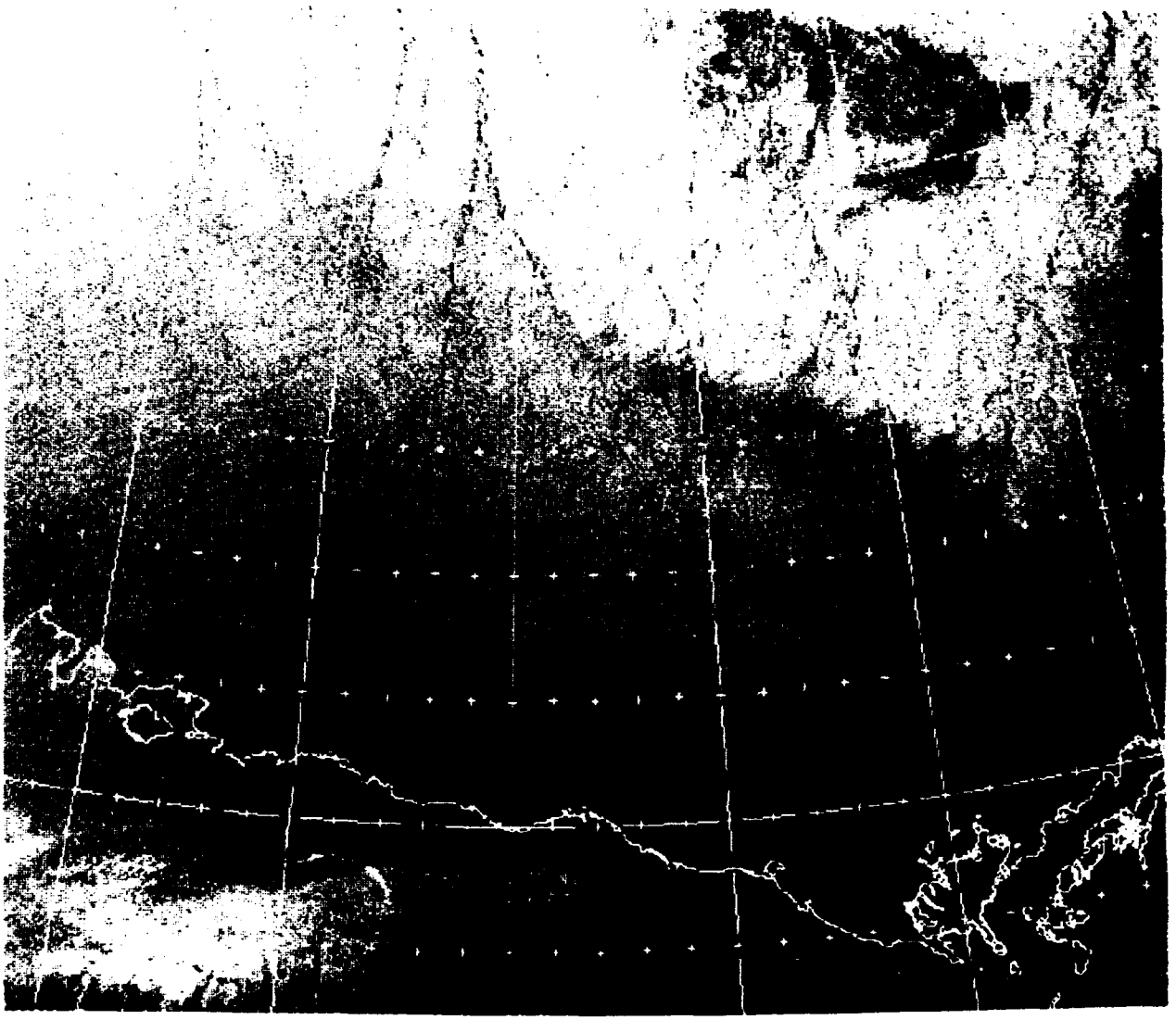

FIG 12. NOAA-11 AVHRR infrared (Ch3) data. 16 April 1992, 1505 UTC.

in 3 locations when comparing this figure with the IR depiction of Fig 11. (1) Low cloudiness showing a weak vortex with center near 76°N, 138.5°W is revealed in this image. The channel 4 view (Fig 11) shows nothing in this region. (2) A sharp "zig-zag" diagonal extending from near 72°N, 130°W, to 74°N, 144°W, is very apparent in this image. The diagonal seems to indicate the source region for the field of clouds which extends downstream (SW) from this feature. This sharp demarkation is not apparent in the channel 4 view (Fig 11). (3) A bright cloud streak passing eastward over the region near Point Barrow in the channel 4 data is barely perceptible as a warm streak in the channel 3 data.

The differences between these two channels can be accentuated by taking "pixel-by-pixel" difference between the two channels and displaying this as a Ch3-Ch4 "difference" image (Fig 13). In this image in the three areas where differences are large the features are enhanced; in the areas where differences are small little or no change can be detected.

FIG 13. NOAA-11 AVHRR infrared (Ch3-Ch4) difference data. 16 April 1992, 1505 UTC.

When the question is posed as to why these 3 particular features are accentuated, the answer lies in the added effect of solar scattering and reflection to which channel 3 is responsive during daylight hours. Water droplet clouds are more highly reflective than ice crystal clouds. From this we can deduce that the "white" plumes emanating from the "zig-zag" diagonal lead opening are water droplet plumes. The field of clouds downstream from this plume, as revealed in the channel 4 (Fig 11) and channel 3 (Fig 12) data, apparently consist of ice particles, or are too thin to yield much of a difference response between the two channels. Similarly we can deduce that the cloud vortex to the northeast is a water droplet feature, as is the plume passing over the Point Barrow area. It is of great interest and it appears logical that the water cloud plume should appear immediately adjacent to the major "zig-zag" lead opening and diffuse downstream, as is shown in Fig 13. Water droplet formation should be greatest and cloud opacity greatest in this region. At the same time note that channel 3 is unresponsive to the warm plumes emanating from the leads northeast of the "zig-zag" fracture in the region north of 73°N between 130°-135°W. These plumes were well-delineated in channel 4 (Fig 11). The most plausible rationale for this difference would be that those plumes were very thin and created little additional reflected or scattered solar energy to the channel 3 sensor.

The sudden formation of the "zig-zag" lead opening is of great interest. Fig 14 is the Navy mesoscale model (SOCMM) 10 m wind analysis for 16 April at 1200 UTC. The model shows that winds increase from about 15 kts near 74°N to as high as 40 kts close to the North Slope. The lead "zig-zag" feature is occurring in the region of speed divergence between relatively light winds to the northeast and gale force winds to the southwest.

Such speed divergence implies great surface stress, being essentially proportional to the square of the velocity, effectively "pulling" the ice apart at its weakest locations, thereby creating the "zig-zag" lead fracture.

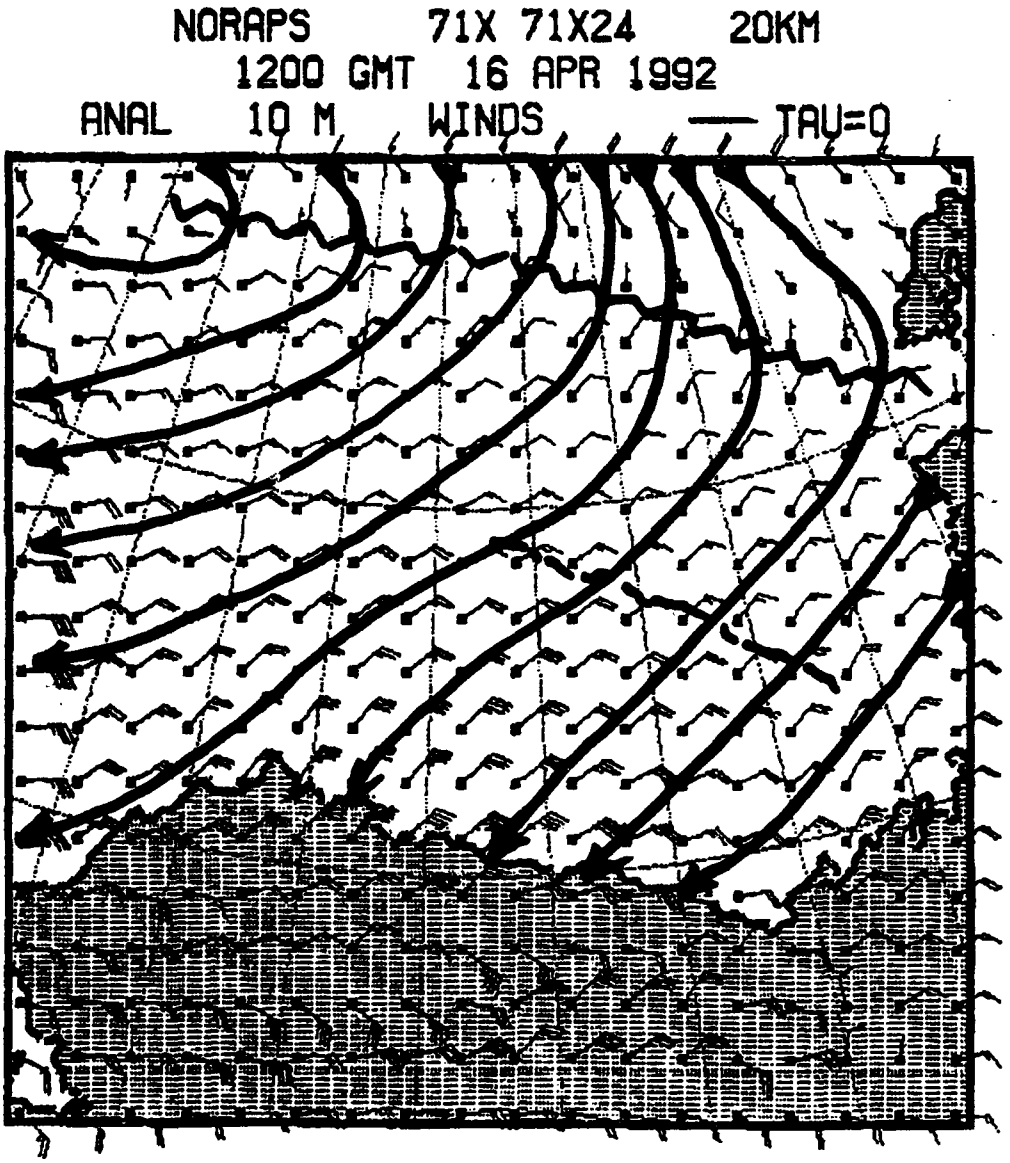

FIG 14. Navy Mesoscale Second Order Closure Model (SOCMM) 10 m wind analysis. 16 April 1992. 1200 UTC.

The streak pattern shows up especially well in infrared (Ch4) data captured by NOAA-10 AT 1911 UTC (Fig 15). The pattern is well defined in the region NW of Barrow, but traces can be seen over the entire Beaufort Sea. The lead extending north-south in the left-center portion of the image (between 145°-150°W) shows evidence of several warm streaks emanating from what appears to be open water along the lead.

These streaks may well extend even further northeast of the lead feature (there seems to be some suggestion of this in the image) but they become much more evident to the southwest. It is possible that the streaks incorporate and are occasionally enhanced by additional moisture as they pass over subsequent lead openings in their southwesterly trajectories.

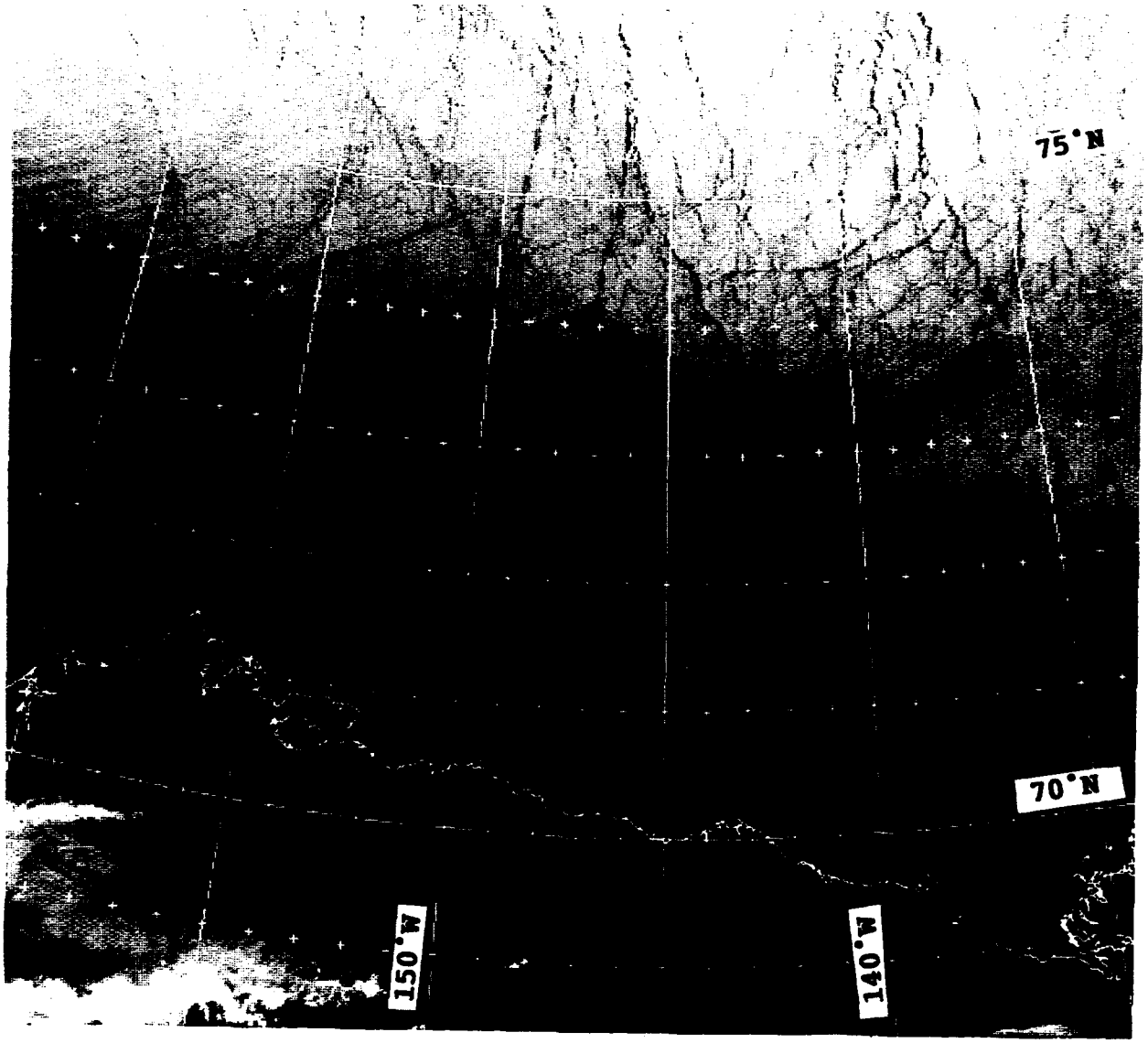

FIG 15. NOAA-10 AVHRR infrared (CH4) data. 16 April 1992, 1911 UTC.

One point is of interest and well exemplified in this image. It will be noticed that a temperature change from cooler (light gray) to warmer (darker gray) occurs along many of the streaks in the western portion of the image. There are several possible explanations for this change but the fact that the ice temperature warms by about 5°C going from 75°N to 70°N is perhaps dominant. The warmer temperature sensed based on this effect would be caused by absorption and then re-transmission of radiation from the underlying ice surface by the overlying thin obscuration.

North of the Mackenzie River delta area, in the lower right portion of the image, the streaks are aligned in an east-west direction. They then turn to essentially a northeast-southwest alignment over the central Beaufort. The streaks to the west show a slight tendency to curve anticyclonically from the top-center to the left side of the image.

A streamline analysis of the 16 April 1800 UTC surface analysis (Fig 16) shows consistent evidence of surface streamline alignment with the streak pattern. Note that all North Slope wind indications are basically easterly, shifting to northeast over the ice camp and buoy region. Even the slight anticyclonic turning of the winds to the west is supported by this analysis.

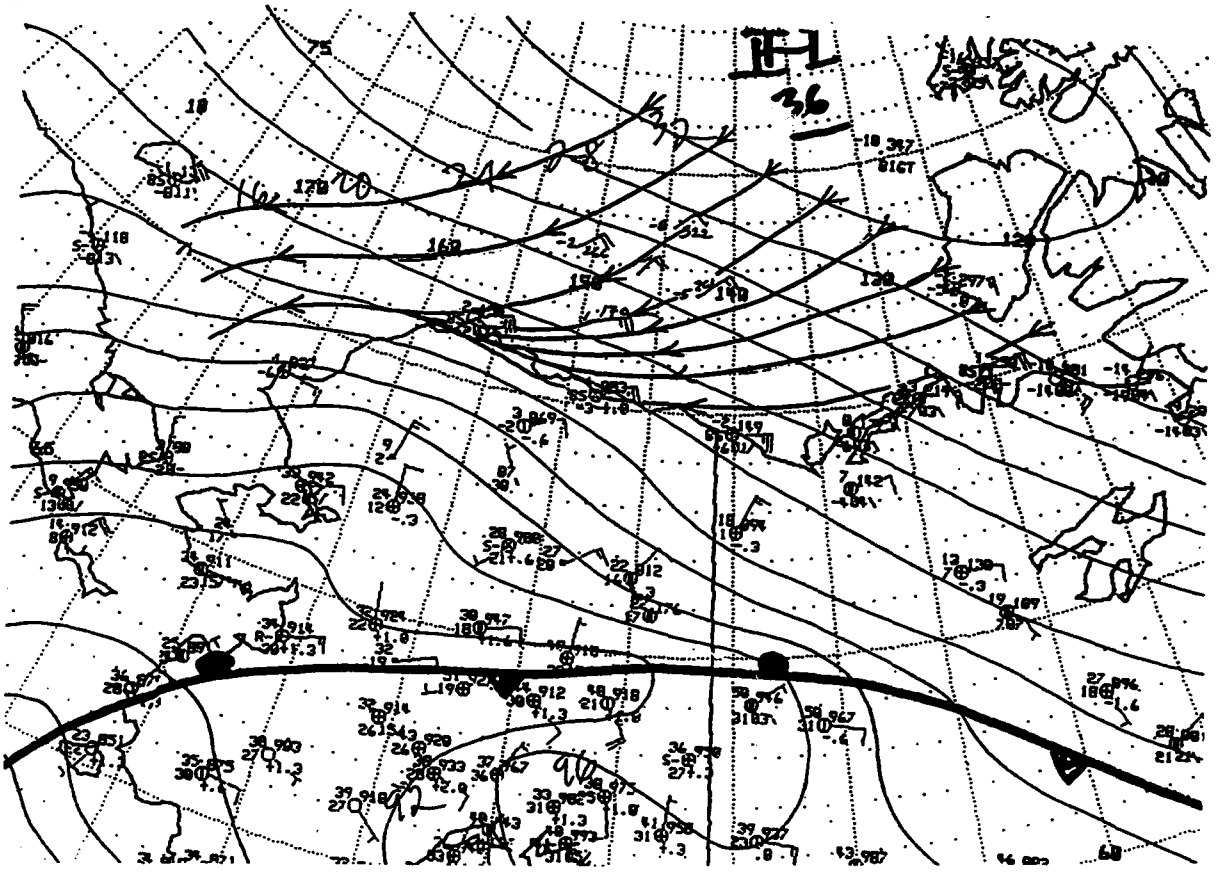

FIG 16. NWS (Anchorage) surface analysis. 16 April 1992, 1800 UTC. Surface streamlines have been superimposed on this analysis over the Beaufort Sea.

17 April 1992

Strong northeasterly wind flow persisted over the Beaufort Sea on this date. The streak pattern also persisted as shown on NOAA-11 infrared (Ch4) data acquired at 1313 UTC (Fig 17).

The Leadex ice camp was well within the streak pattern region at this time. Sounding data at 2001 UTC revealed a very shallow mixed layer about 170 m in depth. Winds veered within the mixed layer from 064° at 22 kts at the surface, to 087° at 44 kts at a height of only 27 m. Since the streaks maintain a northeast-southwest alignment the implication is that they are a "very near the surface" phenomenon, with the most likely cause being a combination of ice crystals and blowing snow.

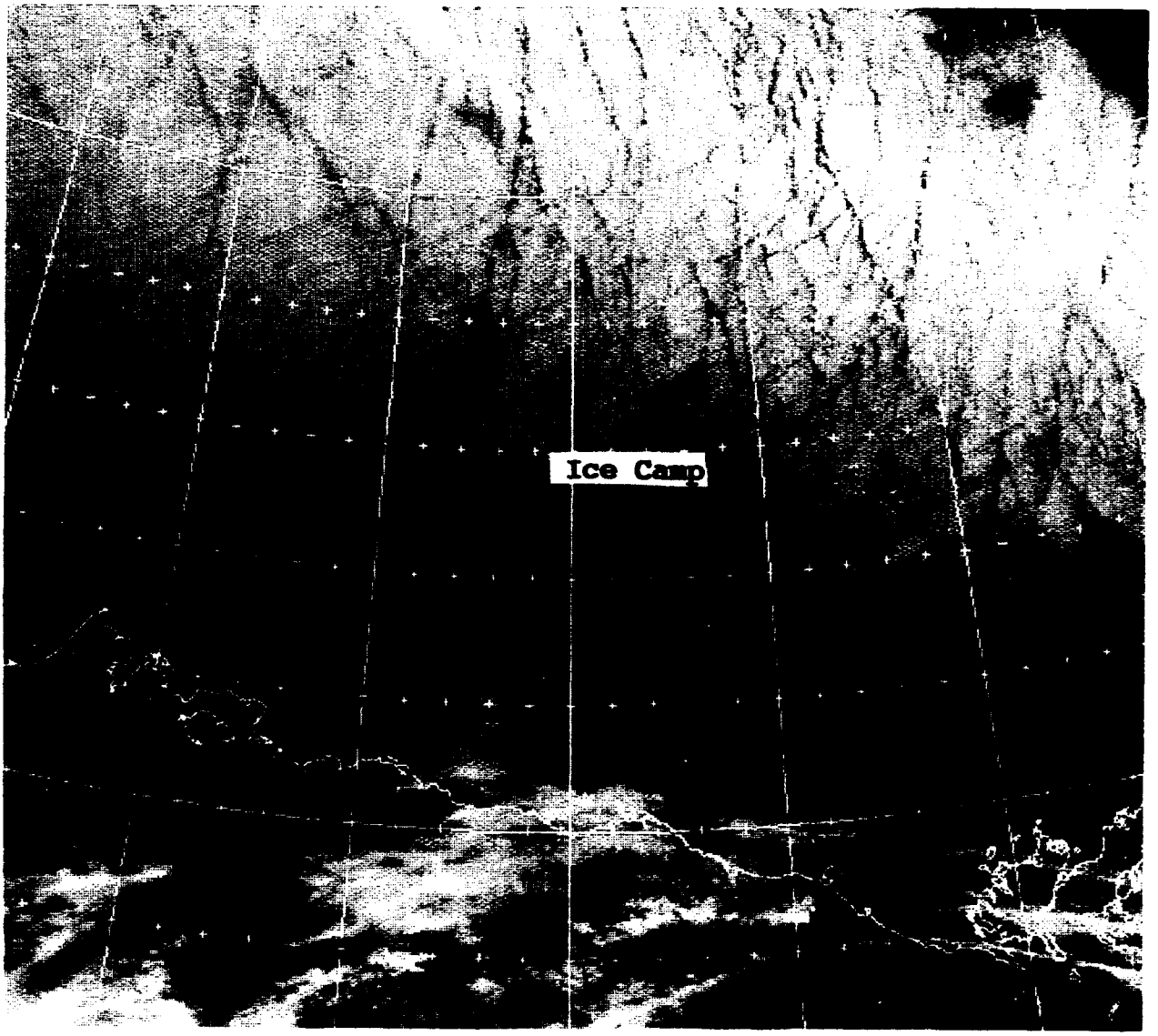

FIG 17. NOAA-11 AVHRR infrared (CH4) data. 17 April 1992, 1313 UTC.

An additional NOAA-11 infrared (Ch4) image (Fig 18) was received at 1540 UTC. The pattern can be detected from the Mackenzie River delta area well to the WNW toward Wrangel Island. Occasional enhancements of the warm streak pattern can be detected where the streaks intersect lead formations. This is especially evident in the eastern half of the image.

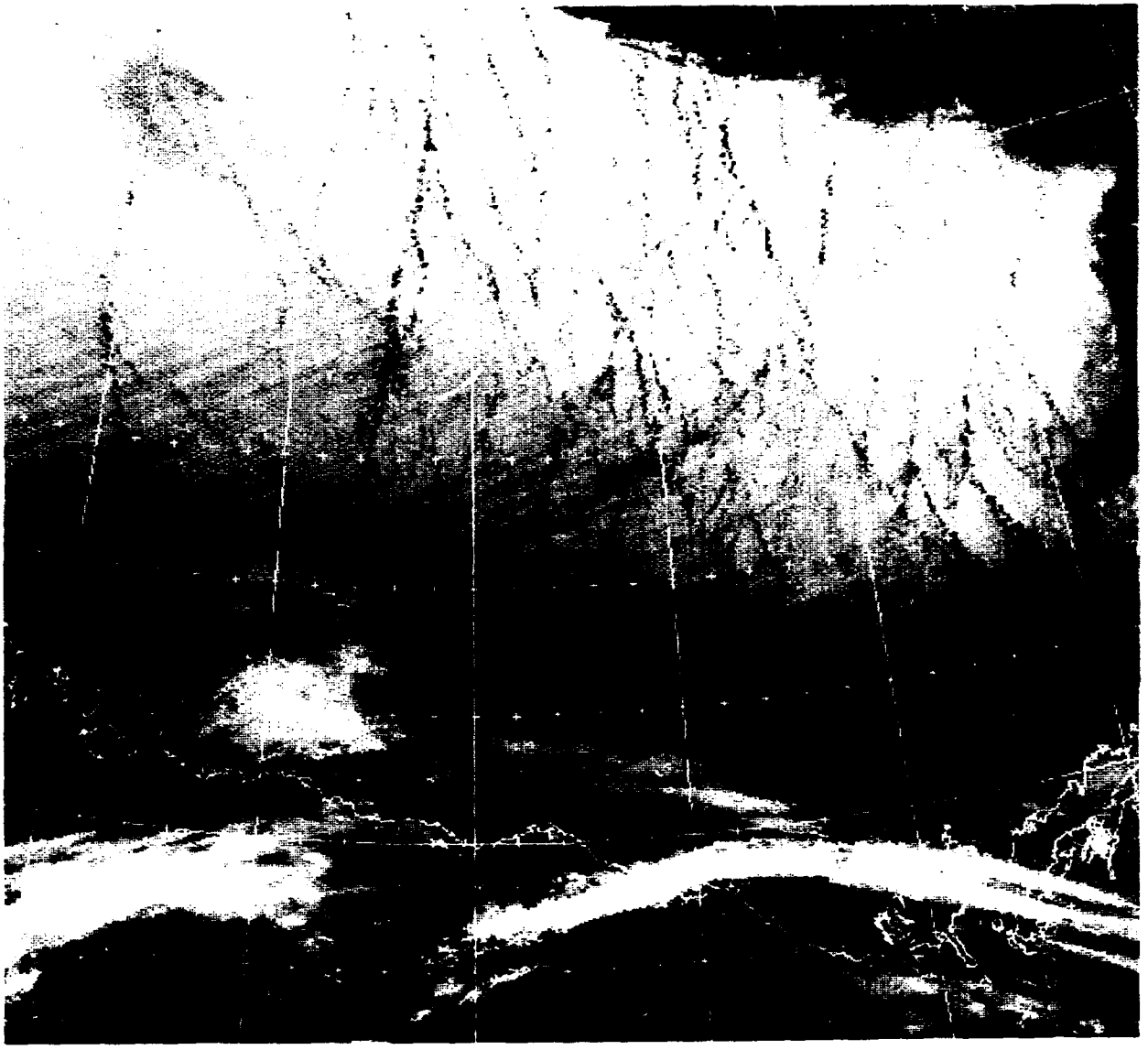

FIG 18. NOAA-11 AVHRR infrared (CH4) data. 17 April 1992, 1540 UTC.

Note again the tendency toward a more easterly alignment north of the Mackenzie River delta area, becoming more northeast-southwest aligned in the central and western portion of the image. There is also a tendency for the streaks to curve slightly anticyclonically downstream. This same alignment and anticyclonic flow tendency is shown in the mesoscale model 10 m wind analysis for 17 April at 1200 UTC (Fig 19).

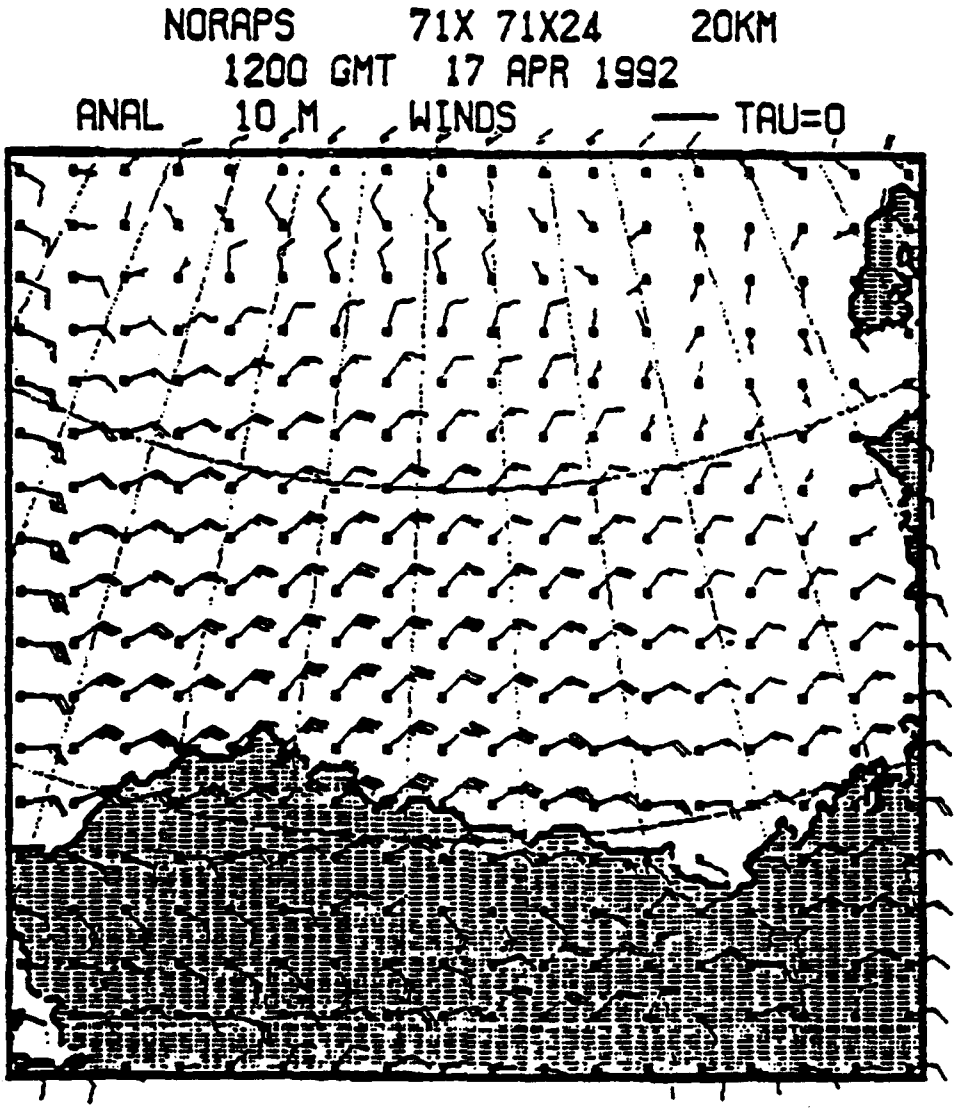

FIG 19. Navy SOCMM 10 m wind analysis. 17 April 1992, 1200 UTC.

NOAA-10 obtained an image over the region on 17 April at 2027 UTC (Fig 20). Westerly moving, short wave disturbances, were beginning to enter the southern Beaufort at this time. However, the strong northeasterly flow remained evident along with the streak pattern to the north.

One interesting development shown on this image is the pronounced low level cloud plume extending west-northwestward from an apparent point source on the polynya near Banks Island. Although surface winds were northeasterly in that region, winds at 925 mb up to 700 mbs turned westerly. It is possible that this plume broke through the low level inversion because of a greater open water area in that region, involving considerably more heat exchange, and was then advected WNW by the higher level wind flow.

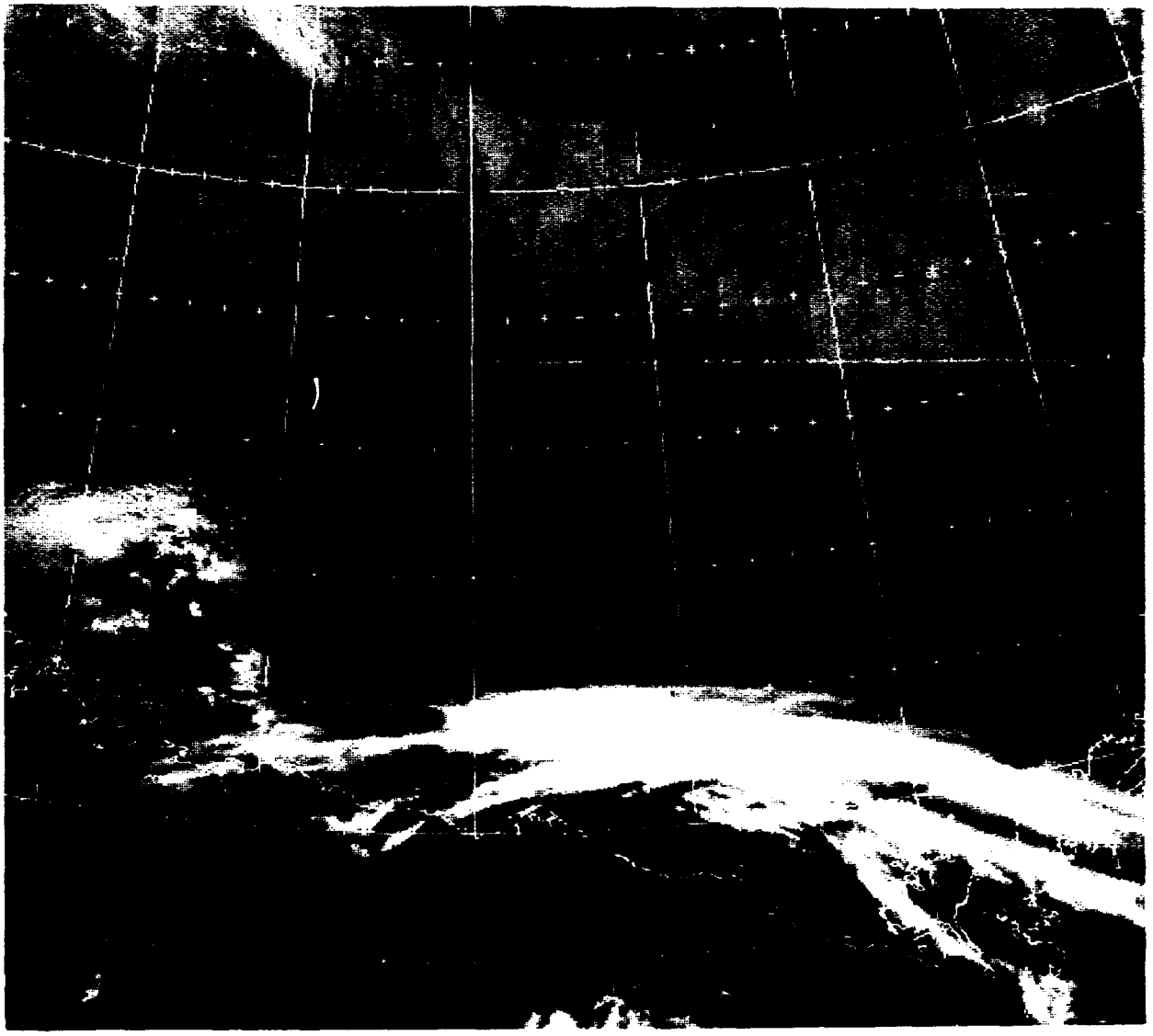

FIG 20. NOAA-10 AVHRR infrared (CH4) data. 17 April 1992, 2027 UTC.

18 April 1993

A final NOAA-11 infrared (Ch4) image acquired on this date at 1622 UTC is shown in Fig 21. This was about the last of the streak patterns observed as northeasterly wind speeds over the region began to diminish late on the 18th and during the 19th of April (See Fig 1). The image does illustrate in a very subtle fashion one important final point. If each of the prominent leads are examined, especially those extending from southeast to northwest, starting near the Banks Island area, and then progressing westward, it will be seen that warm gray shades, implying cloud or ice crystal development, are formed over and downwind of each lead extension.

The notable lead extending northwestward from near 73°N, 145°W separates an apparent clear area to the east from the streak pattern and warm gray shade obscuration to the west in exactly this manner.

These observations strongly suggest that regions of open water in leads are indeed point sources for many of the the streak patterns observed. A full understanding of causes for variations in the pattern, however, requires further investigation.

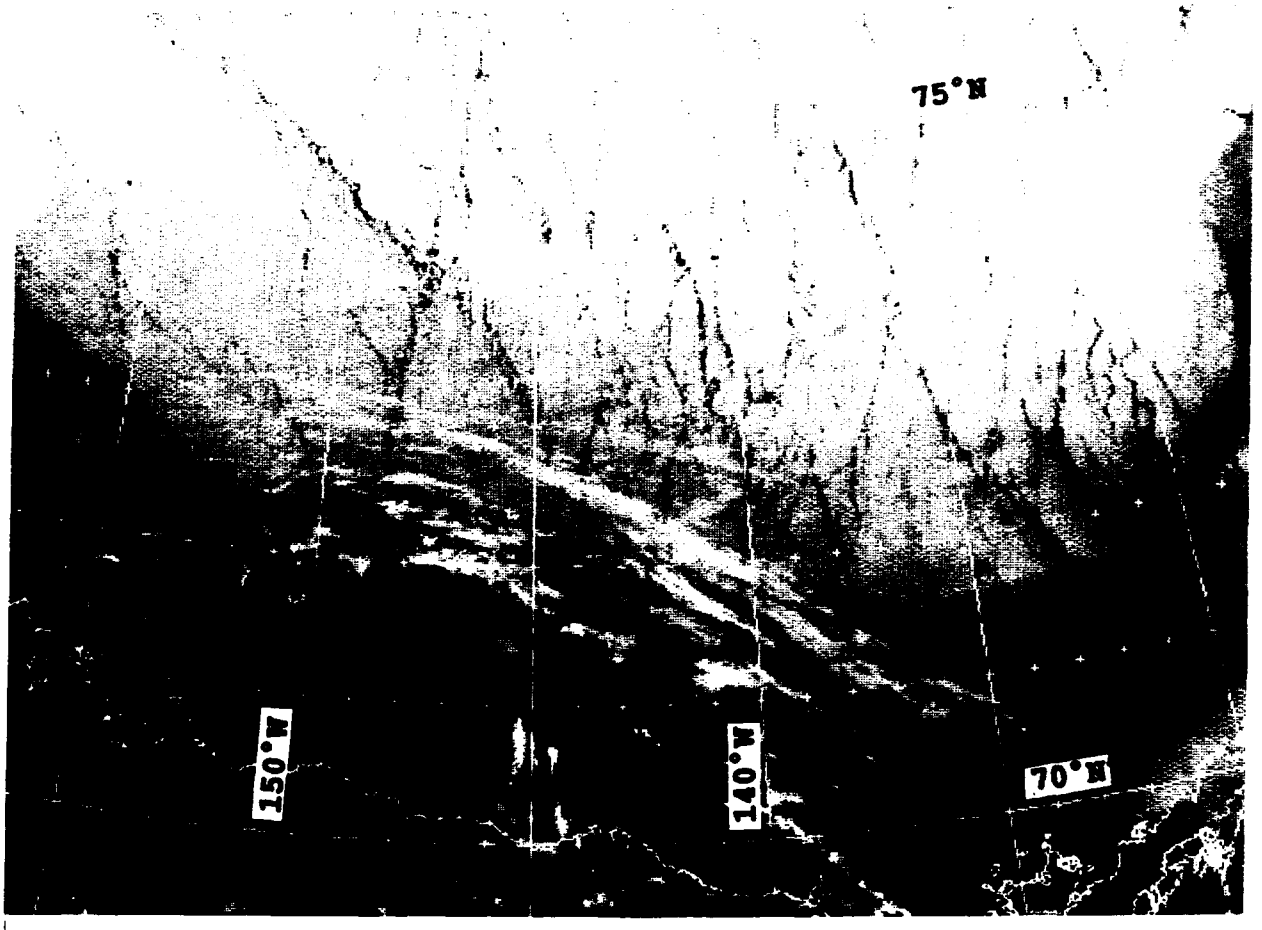

FIG 21. NOAA-11 AVHRR infrared (Ch4) data. 18 April 1992, 1622 UTC.

IMPORTANT CONCLUSIONS

1. High wind speed events over the Beaufort Sea can result in fractured lead developments. Such developments can occur in the southeast quadrants of high pressure cells under a strong near surface based inversion, where winds are steady out of the northeast for long distances. Open water regions within the leads can serve as point sources of heat and moisture leading to a field of water droplet or ice crystal cloud streaks, uniquely sensed as thermal streaks in NOAA and DMSP infrared imagery.

2. The thermal streaks are aligned with the low level wind flow, and change alignment as direction shifts.

3. It is likely that the formation of such streaks, over the immense area covered, have a major impact on energy and heat balance relationships in the Arctic.

4. Gravity wave impulses may be superimposed and be a factor in the field of streaks observed; however, firm evidence for such interaction is yet to be established.

5. The "roll vortex" hypothesis for the cloud streak formations can be ruled out, since indicated wave lengths of 10-18 km yield unreasonable aspect ratios, based on existing theory, implying cloud formation at too high an altitude.

6. The cloud streak phenomena presented in this study require additional detailed investigation and "in-situ" measurements before a complete understanding can be achieved.

REFERENCES

Byers, Carl A., and W. J. Stringer, 1992: Unusual cloud forms in the Arctic boundary layer. AMS Proceedings of the Third Conference on Polar Meteorology and Oceanography, Portland, Or., pp 7-10.

DISTRIBUTION LIST

DR STEVEN BURK
NRL CODE 7541
MONTEREY CA 93943-5502

DR ROGER COLONY
POLAR SCIENCE CENTER
APL U OF WASH
1013 NE 40TH ST
SEATTLE WA 98105

DR THOMAS CURTIN
ONR CODE 1125 AR
800 N QUINCY ST BCT 1
ARLINGTON VA 22217-5000

DR KEN DAVIDSON
NPS CODE MR DS
MONTEREY CA 93943

ED DIEMER
NATIONAL WEATHER SERVICE
222 W 7TH AVE #23
ANCHORAGE AK 99513-7575

DTIC DOC PROCESS DIV 2
CODE DTIC FD BLDG 5
CAMERON STATION
ALEXANDRIA VA 22304-6145

DR CHRIS FAIRALL
NOAA WPL CODE R E WP7
325 BROADWAY
BOULDER CO 80303-3328

TED FATHAUER
NATIONAL WEATHER SERVICE
101 12TH AVE ROOM 270
FAIRBANKS AK 99701

GARY HUFFORD
NATIONAL WEATHER SERVICE
222 W 7TH AVE #23
ANCHORAGE AK 99513-7575

GARY HERBERT
NOAA CMDL
325 BROADWAY
BOULDER CO 80303-3328

ROBERT FETT
E19200 FISH HAWK LAKE RD
WATERSMEET MI 49969

DR JOHN JAYNOR
NOAA WPL CODE R E WP7
325 BROADWAY
BOULDER CO 80303-3328

DR ANDREW JESSUP
APL UNIV WASH
1013 NE 40TH ST
SEATTLE WA 98105-6698

JEFF KEY
CIRES U OF COLORADO
CAMPUS BOX 449
BOULDER CO 80309

STUART KNOKE
WILLIAMSON & ASSOC
731 N NORTHLAKE WAY
SEATTLE WA 98103

THOMAS LEE
NRL CODE 7531
MONTEREY CA 93943-5502

DR RON LINDSAY
APL U OF WASHINGTON
1013 NE 40TH ST
SEATTLE WA 98105-6613

DR MARK MERRIFIELD
MARINE PHYSICAL LAB
SCRIPPS OCEANOGRAPHIC INST
SAN DIEGO CA 92093-0213

DR JAMES MORRISON
POLAR SCIENCE CENTER
APL U OF WASH
1013 NE 40TH ST
SEATTLE WA 98105

NAVAL RESEARCH LAB 12
CODE 5227 DOCS SEC
WASHINGTON DC 20375-5320

NAVAL RESEARCH LAB
CODE 1221 CLASSIF MGT
WASHINGTON DC 20375-5320

DR JAMES OVERLAND
PMEL NOAA
1801 FAIRVIEW AVE EAST
SEATTLE WA 98102

STEVE PAYNE
NRL CODE 7530
MONTEREY CA 93943-5502

DR OLA PERSSON
NOAA WPL CODE R E WP7
325 BROADWAY
BOULDER CO 80303-3328

DR DOMINIQUE RUFFIEUX
NOAA WPL CODE R E WP7
325 BROADWAY
BOULDER CO 80303-3328

SAIC 2
550 CAMINO EL ESTERO
MONTEREY CA 94940

DR ROBERT SCHUCHMAN
ERIM BOX 8618
ANN ARBOR MI 48107

DR RUSS SCHNELL
MONA LOA OBSERVATORY
PO BOX 275
HILO HI 96721-0275

SEASPACE
ATTN R BERNSTEIN
9240 TRADE PLACE STE 100
SAN DIEGO CA 92126

PAT SHERIDAN
NOAA ERL CODE R E CG1
325 BROADWAY
BOULDER CO 80303

IRINI SOKOLIK
NASA AMES RES CENTER
MAIL STOP 245-4
MOFFETT FIELD CA 94035-1000

ROBERT STONE
NOAA ERL CODE R E CG1
325 BROADWAY
BOULDER CO 80303

WILLIAM THOMPSON
NRL CODE 7541
MONTEREY CA 93943-5502

DR ALAN WAGGONER
ATMOSPHERIC SCI DEPT
UNIV WASH AK 40
SEATTLE WA 98195

DANIEL WOLFE
NOAA WPL CODE R E WP7
325 BROADWAY
BOULDER CO 80303-3328

DDR&E R&AT E&LS
ATTN ASST FOR ENV SCIENCES
RM 3D129 THE PENTAGON
WASHINGTON DC 20301-3080

DIRECTOR
DEFENSE INTELLIGENCE AGENCY
WASHINGTON DC 20301

NAVRSCHLAB
ATTN DR E HARTWIG
WASHINGTON DC 20375-5320

COMMANDING OFFICER
OFFICE OF NAVAL RESEARCH
PSC 802 BOX 39
FPO AE 09499-0700

NAVRSCHLAB
ATTN 70353
JCSSC MS 39529-5004

NAVRSCHLAB
ATTN DR MOSELY CODE 7300
JCSSC MS 39529-5004

NAVRSCHLAB
ATTN A PRESSMAN CODE 7240
JCSSC MS 39529-5004

OFFICER IN CHARGE
NAVOCEANCOMDET
PSC 486 BOX 1243
FPO AP 96506-1243

US NAVAL ACADEMY
ATTN OCEANOGRAPHY DEPT
121 BLAKE RD
ANNAPOLIS MD 21402-5000

NAVAL WAR COLLEGE
ATTN GEOPHYSICS OFFICER
686 CUSHING RD
NEWPORT RI 02841-1207

COMSPAWARSYSCOM
ATTN PMW 165
WASHINGTON DC 20363-5100

AWS TECHNICAL LIBRARY
859 BUCHANAN ST
SCOTT AFB IL 62225-5118

US ARMY COLD REGION
RESEARCH & ENGINEERING
LAB
ATTN TECHNICAL LIBRARY
HANOVER NH 03755

COMMANDANT 2
US COAST GUARD
WASHINGTON DC 20226

NOAA NESDIS LIAISON
ATTN CODE SC2
NASA JOHNSON SPACE CENTER
HOUSTON TX 77058

DIRECTOR
NATIONAL EARTH SAT SERV
SEL FB 4 S3218
SUITLAND MD 20233

FEDERAL COORD FOR METEORO
SERVS & SUP RSCH OFCM
11426 ROCKVILLE PIKE STE 300
ROCKVILLE MD 20852

DIRECTOR NMC
NWS NOAA
WWB W32 RM 204
WASHINGTON DC 20233

NATIONAL WEATHER SERVICE
WORLD WEATHER BLDG RM 307
5200 AUTH ROAD
CAMP SPRINGS MD 20023

COLORADO STATE UNIVERSITY
ATTN DR WILLIAM GRAY
ATMOSPHERIC SCIENCES DEPT
FT COLLINS CO 80523

UNIVERSITY OF WASHINGTON
ATMOSPHERIC SCIENCES DEPT
SEATTLE WA 98195

LOUISIANA STATE UNIVERSITY
COASTAL STUDIES INSTITUTE
ATTN 0 HUH
BATON ROUGE LA 70803

CHAIRMAN METEOROLOGY DEPT
MCGILL UNIVERSITY
805 SHERBROOKE ST
N MONTREAL QUEBEC
CANADA H3A 2K6

DIRECTOR OF NAVAL
OCEANO & METEOROLOGY
MINISTRY OF DEFENCE
LACON HOUSE THEOBOLD ROAD
LONDON WC IX8RY ENGLAND

EUROPEAN SPACE AGENCY
18 AVENUE EDOUARD BELIN
31055 TOULOUSE CEDEX
FRANCE

EUROPEAN SPACE OPERATIONS
ATTN DR J MORGAN
R BOSCH STR 5 D61 DARMSTADT
FEDERAL REPUBLIC OF
GERMANY